R-09-35

Assessment of potential for glacially induced hydraulic jacking at different depths

Margareta Lönnqvist, Harald Hökmark
Clay Technology AB

August 2010

Svensk Kärnbränslehantering AB
Swedish Nuclear Fuel
and Waste Management Co

Box 250, SE-101 24 Stockholm
Phone +46 8 459 84 00

ISSN 1402-3091
SKB R-09-35

Assessment of potential for glacially induced hydraulic jacking at different depths

Margareta Lönnqvist, Harald Hökmark
Clay Technology AB

August 2010

Summary

Hydraulic jacking is a phenomenon that occurs when the pore pressure in a fracture exceeds both the normal stress acting on it and its tensile strength. It can lead to significant increases in fracture transmissivity, which would have an impact on the flow and transport conditions in the rock in a way that is difficult to assess. Therefore, hydraulic jacking has been put forward as a possible matter of concern for the long-term safety of a KBS-3 nuclear waste repository /SKB 2006b/. The present report aims to investigate and give perspective on the potential and requirements needed to initiate hydraulic jacking of horizontal fractures at different depths and to establish reasonable bounding estimates of the maximum jacking depth for typical Swedish bedrock using data mainly from the Forsmark repository site.

If hydraulic jacking occurs, it is most likely initiated during a glacial period when high pore pressures must be assumed to build up in the rock below the ice sheet. As the ice front is advancing, high pore pressures may be transferred to the ice front by long highly transmissive fractures or build up below an impermeable permafrost layer in front of the ice sheet. During deglaciation a large proportion of the glacially induced pore pressure may be retained by the rock. The present understanding of the stress conditions at the Forsmark site /Glamheden et al. 2007a, Lund et al. 2009/ is that both horizontal stress components will be larger than, or approximately equal to, the vertical one at all times. Therefore, it appears that hydraulic jacking will be of concern primarily for sub-horizontal fractures. Possible indications, in the form of sediment filled sub-horizontal fractures, of hydraulic jacking events occurring during previous glaciations have been found at several Swedish sites to depths of a few tens of metres /*e.g.* Leijon 2005, Hökmark et al. 2006/.

The potential for hydraulic jacking at different depths is investigated by use of combinations of analytical solutions and numerical models without considering any couplings between stress and fluid flow. The following additional assumptions and simplifications are made throughout the report:

- Only 1D and 2D calculations are performed. These simplifications are likely to overestimate the pore pressures (and potential for hydraulic jacking) compared with the 3D reality.
- The ice sheet profile used in all modelling work is given by a generic representation of a steady-state ice /Paterson 1994/ with its maximum height set to 3,000 m.
- The hydrostatic pressure at the ice/bed interface is assumed to be 90% of the height of the ice (or approximately 98% of the mechanical ice load) at all times, although in reality, it will vary over time.
- The vertical stress is assumed to be equal to the weight of the overburden at all times and at all depths.
- The bulk hydraulic conductivity of the rock mass at Forsmark is assumed to be in the range 10^{-11}–10^{-8} m/s depending on depth and the specific storage coefficient is estimated to be about 10^{-7} m^{-1}. For these combinations of parameters, the hydraulic diffusivity is in the range 10^{-4}–10^{-1} m^2/s.

The following estimates of the maximum jacking depth during the glacial phase are made based on the results from the present study:

- **Advancing (or stationary) ice front without permafrost.** In homogeneously fractured rock, hydraulic jacking is unlikely to be initiated at greater depths than about 30 m. In rock with few conductive fractures, fracture lengths of several kilometres are needed for sufficiently high pore pressures to propagate undisturbed to the ice front and initiate hydraulic jacking at depths of a few hundred metres. This observation points to the very specific conditions regarding fractures and background permeability required to initiate jacking at large depths.
- **Advancing ice front in combination with proglacial permafrost.** For the most conservative case considered in this study (a hydraulic diffusivity in the upper 400 m of the rock set to 10^{-1} m^2/s and 10^{-4} m^2/s elsewhere and a permafrost degradation rate of about 0.5–1 m/year), the maximum jacking depth is 350 m. By allowing for seasonal variations in the hydrostatic pressure at the ice/bed interface, the maximum jacking depth may be reduced by 40–50%, *i.e.* to about 200 m. The possible occurrence of open taliks (unfrozen parts of the permafrost) in the near vicinity of the repository region will tend to reduce the pore pressure further.
- **Retreating ice front without permafrost.** If the effects of a slow build-up of pore pressures during the advancement of the ice sheet are approximated by assuming that the pore pressure distribution has reached steady state before its subsequent retreat, the jacking depth is around 50 m for the frontal retreat speed relevant for Forsmark (300 m/year) assuming a uniform hydraulic diffusivity of at least 10^{-2} m^2/s at all depths. Even for faster (up to 500 m/year) frontal retreat speeds, the maximum jacking depth is unlikely to be more than 100 m. Furthermore, the low permeability at larger depths will prevent a vertical transfer of pore pressures upwards and thus contribute to a more effective drainage of the upper part of the system and, consequently, a reduced maximum jacking depth.

The potential for hydraulic jacking is always greatest at shallow depths. Therefore, if jacking occurs at all, it is likely to be initiated near the ground surface. The associated increase in fracture transmissivity will tend to reduce the pore pressures and prevent hydraulic jacking from occurring at larger depths. This is not considered in the estimates of the maximum jacking depths provided above, which therefore should be considered conservative estimates.

Contents

1 Introduction and background

1.1 General

Hydraulic jacking is a phenomenon that occurs when the pore pressure in a fracture exceeds both the normal stress acting on it and the fracture's tensile strength. As a result, the fracture will dilate and under certain circumstances propagate (cf. Figure 1-1). As the jacking process progresses, the fracture surfaces separate and the apertures may become very large /SKB 2006b/ and impact on the flow and transport conditions in the rock. The rock above near-surface horizontal and sub-horizontal fractures can be lifted; otherwise the maximum apertures are limited by the deformation properties of the surrounding rock mass. The increased apertures are likely to remain as long as there are tensile conditions in the fracture /SKB 2006b/. It is generally believed that hydraulic jacking is a reversible process /Hökmark et al. 2006/ as long as there is no shear component or the fracture is filled with solid materials.

If hydraulic jacking occurs, the process is most likely to be initiated during a glacial period, when high pore pressures must be assumed to build up in the rock below the ice sheet. As the ice front is advancing, high pore pressures may be transferred to the ice front by long highly transmissive fractures or build up below an impermeable permafrost layer in front of the ice sheet. During deglaciation a part of the glacially induced pore pressure may be retained by the rock.

1.2 Glacially induced stresses

Hydraulic jacking is first initiated in fractures oriented perpendicular to the least principal stress. Because of the bending of the crust and the associated development of flexural stresses in the upper crust, the horizontal stresses at repository depth develop in a much more complex manner than the vertical stress in response to the slow loading and unloading during a glacial cycle. The glacially induced horizontal stresses depend not only on the elastic properties of the rock beneath the ice but also on how the properties vary with depth and on the behaviour of the viscous mantle under the elastic crust. The present understanding of the state of stress during a glacial phase at the two sites investigated by SKB (Forsmark and Laxemar) /Glamheden et al. 2007a, Hakami et al. 2008, Lund et al. 2009/ is that, at least at the Forsmark site, both horizontal stress components will be larger than, or approximately equal to, the vertical one at all times, cf. Section 3.2. Therefore, it appears that hydraulic jacking will be of concern primarily for sub-horizontal fractures. A schematic view of the evolution of the stress conditions during the glacial phase and principles of hydraulic jacking during a deglaciation is presented in Figure 1-2.

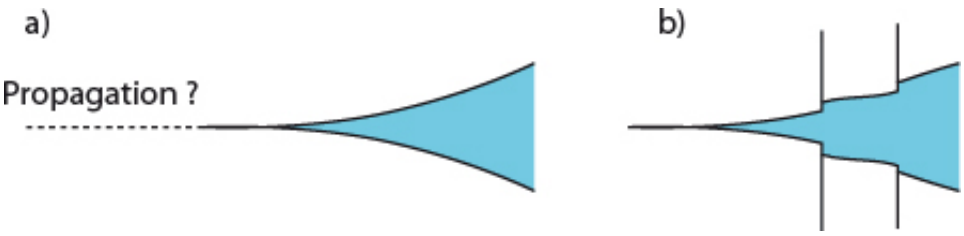

Figure 1-1. *As the pore pressure in a fracture increases, the fracture will dilate (a). For the fracture to propagate (b) more fluid needs to flow into it. Therefore, propagation is partly controlled by permeability /Neuzil 2003/.*

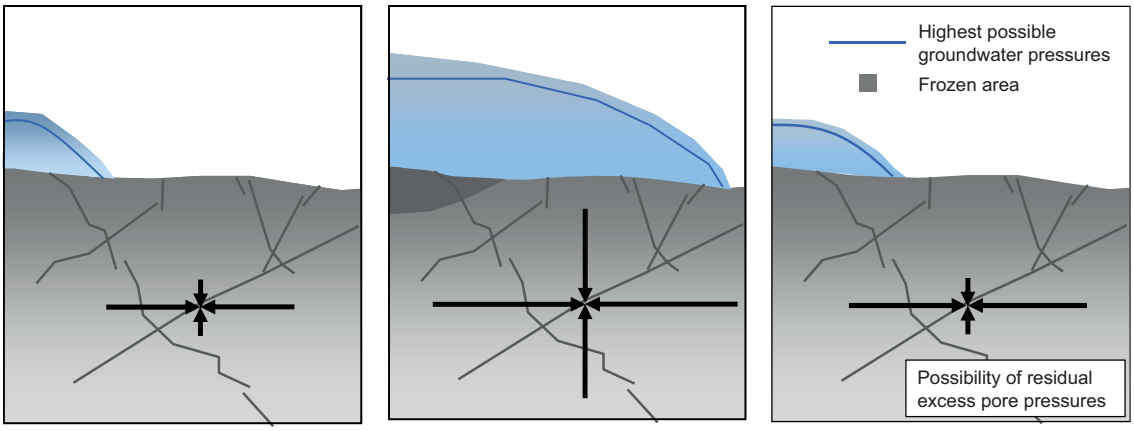

Figure 1-2. *Principles of hydraulic jacking during glaciation, after /Boulton et al. 2001a/. Left: Before the ice sheet reaches the site, the horizontal stresses dominate; in a strike-slip stress regime, e.g. Laxemar /Hakami et al. 2008/, only one horizontal stress component is greater than the vertical stress component. Middle: As the ice sheet covers the site, the stresses and pore pressure increase. Right: When the ice has retreated, the glacially induced vertical stress decreases faster than the glacially induced pore pressure, which may cause sub-horizontal fractures to open.*

1.3 Observations of hydraulic jacking

Shallow sediment-filled structures, which may have been caused by hydraulic jacking events during past glaciations, have been found at several locations in Sweden, see *e.g.* /Hökmark et al. 2006/. An example is Forsmark, where sediment filled sub-horizontal fractures have been observed to depths of a few tens of metres /SKB 2005, 2006c/. Locally, these fractures have apertures in the range 50–82 cm /SKB 2005/, cf. Figure 1-3.

Figure 1-3. *Example of a horizontal sediment-filled fracture, which was exposed at Forsmark during the construction of the nuclear power plant in the 1970s, from /Leijon 2005/.*

1.4 Previous assessments of hydraulic jacking

Hydraulic jacking can theoretically also be initiated at substantially greater depths /*e.g.* Lindblom 1997, Talbot 1999, Hökmark et al. 2006/. Analytical estimates by /Lindblom 1997/ showed that an ice sheet that is 800 m thick can theoretically cause hydraulic jacking at a depth of 500 m outside the ice provided that the hydrostatic pressure at the ice/bed interface is 100% of the height of the ice (or 109% of the mechanical ice load). Similarly (with the same pressure assumption), /Lindblom 1997/ concluded that, at positions beneath the ice sheet but far from the ice front, an ice thickness of 1,000 m can cause jacking at a depth of 60 m. However, in case the hydrostatic pressure at the ice/bed interface is lower than about 90% of the height of the ice (*i.e.* lower than 98% of the mechanical ice load), jacking is not possible beneath the ice sheet. The approach taken by /Lindblom 1997/ overlooks the transient behaviour of the system as well the non-zero, although potentially very small, permeability of the rock that will drain the high pressures. Instead, he argued that most of the pore pressure will either be preserved by the rock or transferred, without significant loss, to the ice front by very long fractures. A similar approach was taken by /Talbot 1999/. Based on previous numerical modelling, /Talbot 1999/ argued that the excess pore pressures behind a retreating ice sheet can lift already loosened blocks the size of up to a third of the ice-thickness, see Figure 1-4. Based on a reconstructed Weichselian ice sheet with a maximum thickness of around 3,500 m in Fennoscandia, he estimated that blocks of the size 500–1,000 m could potentially be lifted. However, estimates of how much the blocks could be lifted would depend on the pressure decrease following the expansion of the fracture. No evidence has yet been found at Forsmark or Laxemar to support the theories of /Lindblom 1997/ and /Talbot 1999/ that jacking has occurred at depths larger than a few tens of meters /SKB 2006b/.

/Hökmark et al. 2006/ summarised the specific conditions that are required in order to initiate hydraulic jacking at large depths into the following points:

- Steep slope of the ice sheet front.
- High water pressure at the ice/bed interface.
- Conductive steeply dipping rock fractures beneath the melting part of the ice.
- Horizontal or gently dipping highly transmissive fractures leading towards a position beyond the ice margin.
- Rock mass with low permeability and few connecting fractures.

As part of the international collaboration projects DECOVALEX III and BENCHPAR, WP4 research teams from Canada, Finland, Scotland and Sweden investigated the potential for hydraulic jacking during a glacial cycle /Chan et al. 2005/. The teams performed numerical hydro-mechanical modelling based on data from the Whiteshell Research Area in Canada. Numerical analyses in both 2D and 3D were carried out. In the 3D models, local topography was taken into account and continental scale coupled THM ice sheet/drainage modelling was performed to provide spatially and temporally varying hydro-mechanical boundary conditions for the transient analyses. Effects due to temperature, salinity, pressure-dependent permeability, permafrost and large-scale isostasy were not considered.

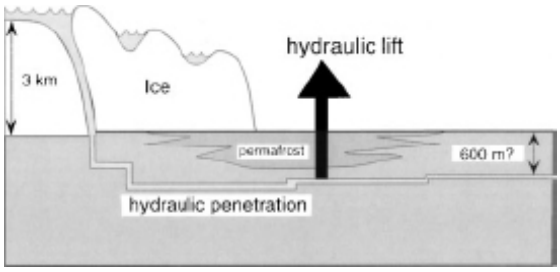

Figure 1-4. *Schematic view of the principles of hydraulic jacking, from /Talbot 1999/.*

The more realistic assumptions made by /Chan et al. 2005/ showed that the transient boundary conditions had a significant impact on the subsurface evolution. Figure 1-5 (right) shows the temporal evolution of the minimum effective stress at the six points in one of the modelled fracture configurations (Figure 1-5, left) as the ice sheet passes over the repository area. Hydraulic jacking occurs when the effective stress becomes tensile. Hydraulic jacking was not observed at any of the investigation points in any of their modelling efforts and the groups' conclusions were that it is unlikely to occur in the repository area. In an additional paper /Vidstrand et al. 2008/ found that the same type of analysis gave effective tensile stresses down to repository depth. However, this was attributed to the simplified representation of the crust without account of the horizontal flexural stress increase following downwarping.

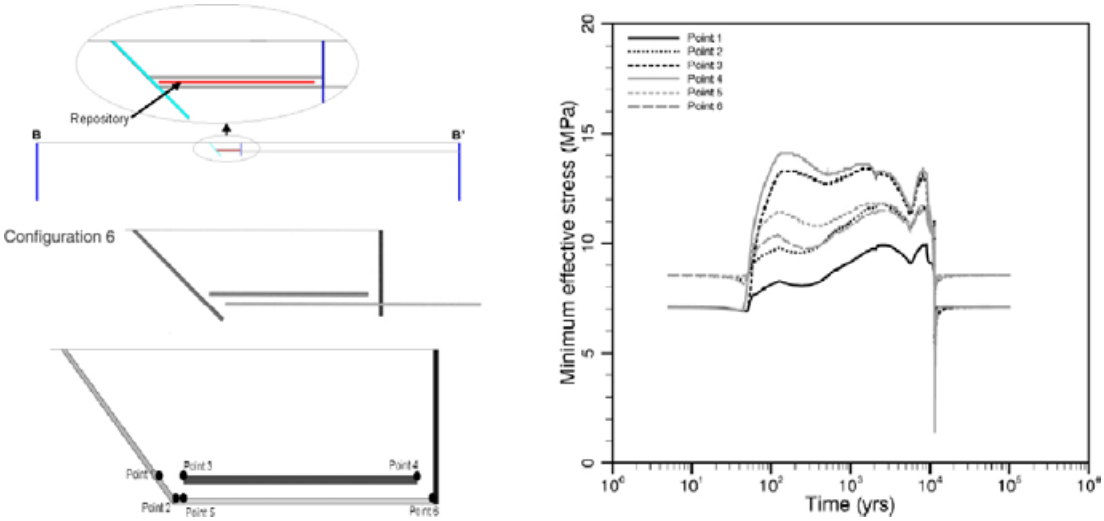

Figure 1-5. *Fracture configuration in DECOVALEX/BENCHMARK modelling and location of history points (left). Temporal development of the minimum effective stress at the history points in Configuration 6 (right). From /Chan et al. 2005/.*

2 Objectives and scope

The objective of this study is to investigate and give perspective on the potential and requirements needed to initiate hydraulic jacking at different depths during the glacial phase and to establish reasonable bounding estimates of the maximum jacking depth for typical Swedish bedrock. It is outside the scope of this report to treat the initiation and propagation of fractures as the jacking process continues. The potential for hydraulic jacking is assessed for the following phases of one glacial advance and retreat cycle by use of a combination of generically designed 2D numerical models and analytical solutions (a summary of the numerical codes and analytical solutions used for each of the conducted analyses is provided in Table 2-1):

- Stationary ice front without permafrost (steady state analyses can be regarded as an upper bound estimate of the pore pressure distribution during the advancement of an ice sheet):
  - High glacially induced pore pressures may be transferred to the ice front, without significant loss, by long highly transmissive fractures in otherwise low permeability rock. This case is investigated for a number of assumptions regarding fracture configurations and their connectivity, fracture transmissivity and rock mass hydraulic conductivity.
  - In homogeneously fractured rock, pore pressures generated close to the ice front region may be transferred short distances and possibly initiate hydraulic jacking at some depth.
- Advancing ice front with permafrost. A permafrost layer can be considered a more or less impermeable layer /*e.g.* Vidstrand 2003/ that restricts drainage to the ground surface and thereby increases the pore pressure outside the ice front, cf. Figure 1-4. This case is investigated for a number of assumptions regarding rock mass hydraulic diffusivity, permafrost depth and degradation rates, seasonal variations in the hydrostatic pressure at the ice/bed interface and inclusion of open taliks (unfrozen parts of the permafrost) within the permafrost body.
- Retreating ice front without permafrost. A large proportion of the glacially induced pore pressure, which has been building up under the ice cover, may be retained by the rock. This case is investigated for a number of assumptions regarding rock mass hydraulic diffusivity, ice front retreat speed and periods of stationary ice front.

Table 2-1. Summary of analyses performed to assess the potential for hydraulic jacking. The analytical solutions and numerical codes used in the assessment are described in detail in Chapter 4.

	Analytical solutions (homogeneous rock model)	Numerical solutions (homogeneous rock model)	Numerical solutions (rock with few conductive fractures)
Advancing ice front			
without permafrost	Steady state and transient analyses, cf. Chapter 6	–	Steady state analyses (UDEC), cf. Chapter 7
with permafrost	Transient analyses (1D only), cf. Chapter 8 and Appendix E	Transient analyses (FLAC/ Code_Bright), cf. Chapter 8	–
Retreating ice front	Transient analyses, cf. Chapter 6	–	–

The following simplifications and general assumptions are made throughout the report:

- Similarly to the approach taken by /Chan et al. 2005/, effects of temperature and salinity are not considered. Furthermore, in order to simplify the problem, the coupling between stress and fluid flow is not taken into account although hydro-mechanical processes in geological media, in general, are governed by intricately coupled mechanisms (*e.g.* /Neuzil 2003/, see also Appendix A).
- The ice sheet is assumed to terminate on land during all phases of the glacial phase. In the reference glacial cycle for the safety assessment SR-Can /SKB 2006a/, the Forsmark and Laxemar sites are situated above sea level with permafrost conditions as the ice sheet advances towards and over them. During the latest major deglaciation, both sites are submerged /SKB 2006a/. However, for the description of the ice sheet and the hydrostatic pressure at the ice/bed interface made here, the difference between mechanical load and glacially induced pore pressure is maximised at the ice margin for the case when the rock is not submerged.
- The ice sheet profile used in this study is given by a generic representation of a steady-state ice along its flow line following /Paterson 1994/, cf. Chapter 3. The ratio between hydrostatic pressure at ice/bed interface and mechanical load is assumed to be uniform along the flow line, *i.e.* the effects of subglacial tunnels are not taken into account.
- Only hydraulic jacking of horizontal fractures is considered. Hydraulic jacking is first initiated in fractures oriented perpendicular to the least principal stress. For the purpose of this study, it is assumed that the vertical stress is the least principal stress at all times and all depths (although this may not be strictly the case at Laxemar, cf. Section 3.2).

3 Ice sheet representation and glacially induced stresses

3.1 General

Glaciers and ice sheets form in places where the winter precipitation, in the form of snow, does not melt away completely in the summer. The present report is only concerned with so-called *warm-based* ice sheets, *i.e.* the ice temperature at the base is at the pressure melting point /SKB 2006a/. This means that there is free water at the ice/bed interface and the ice can slide across the bed.

The projected glacial cycle, for the Forsmark and Laxemar sites, is based on a reconstruction of the Weichselian glaciation /SKB 2006a/. In the reference ice sheet model simulation for the SR-Can safety assessment /SKB 2006a/, the ice thickness about 100,000 years into the glacial cycle, reaches a maximum of 2,900 m at Forsmark and 2,400 m at Laxemar, cf. Figure 3-1. Based on these results, the maximum ice sheet thickness in the present study is set to 3,000 m.

The *accumulation* (growth) and *ablation* (loss) rate of ice sheets and glaciers are determined by a mass balance of ice and snow /SKB 2006a/. The accumulation rate is mainly given by the amount of precipitation, *i.e.* snowfall, whereas the ablation rate is governed by a number of issues, mainly by surface melting of snow and ice or calving of icebergs when the ice sheet terminates at sea. In the Weichselian ice sheet reconstruction /SKB 2006a/, typical values of the speed of the advancing Fennoscandian ice sheet front are of the order of 40–50 m/year. During the last deglaciation, the ice front retreated with a speed of ~200 m/year at what is present day Oskarshamn and ~300 m/year at present day Forsmark /SKB 2006b/.

3.2 Glacially induced stresses

Hydraulic jacking is first initiated in fractures oriented perpendicular to the least principal stress. The present understanding of the evolution of the glacial stresses at the Forsmark and Laxemar sites is that, with the exception of the time period leading up to a glaciation when the forebulge flexure tends to reduce the horizontal stresses, compression increases on all fracture orientations. Figure 3-2 shows the temporal evolution of the glacially induced principal stresses at 500 m depth at Forsmark and Laxemar obtained from 3D ice/crust/mantle analyses by /Lund et al. 2009/.

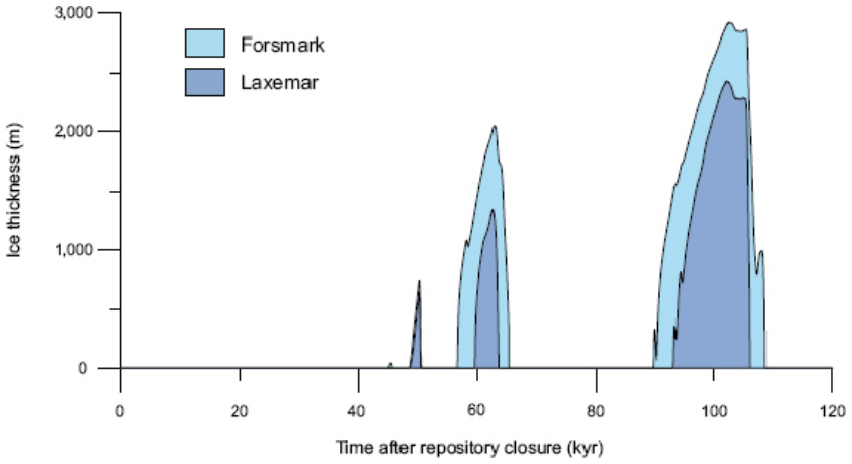

Figure 3-1. *Modelled ice sheet thickness at Forsmark and Laxemar repository sites during the reference glacial cycle. From /SKB 2006a/.*

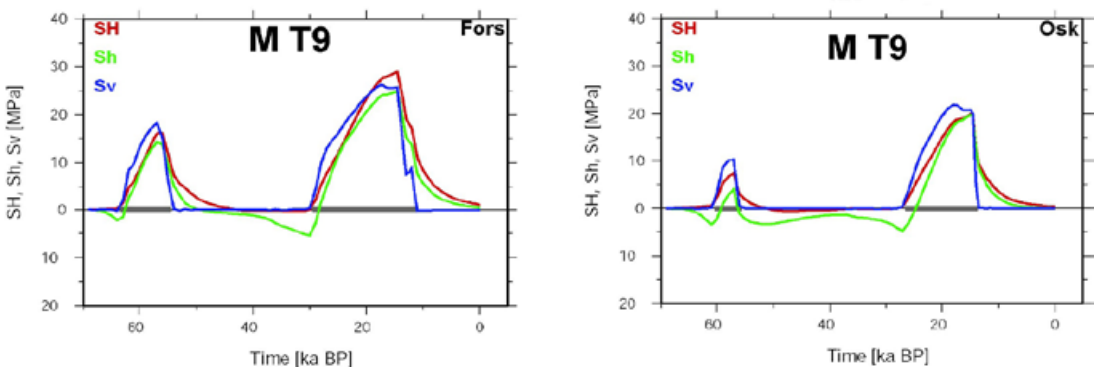

Figure 3-2. *Example of the temporal evolution of vertical and horizontal stress components at 500 m depth at Forsmark (left) and Laxemar (right) during the Weichselian glaciation, from /Lund et al. 2009/.*

The changes in the vertical stress with time reflect the changes in ice sheet thickness /Lund et al. 2009/. Because of the bending of the crust and the associated development of compressive flexural stresses in the upper crust, the horizontal stresses develop in a much more complex manner than the vertical stress in response to the slow loading and unloading during a glacial cycle. The glacially induced horizontal stresses depend not only on the elastic properties of the rock beneath the ice but also on how the properties vary with depth and on the behaviour of the viscous mantle under the elastic crust. When the ice load and the associated vertical stress disappear at the end of the glaciation, the flexural stresses, which make out a substantial fraction of the glacially induced horizontal stresses, will remain for long times.

At the Forsmark site, the present-day horizontal *in situ* stresses /Glamheden et al. 2007a/ are significantly higher than the *in situ* vertical stress and sufficiently high to balance the stress reduction associated with the forebulge, meaning that vertical stress is the least principal stress at all times. However, at the Laxemar site, the present-day minor horizontal *in situ* stress and the vertical *in situ* stress have similar magnitudes /Hakami et al. 2008/, which implies that the orientation of the minor principal stress during the glacial phase will vary with time. Given that, at least at the Forsmark site, the horizontal stresses are larger than or equal to the vertical stress and that (during the retreat phase) the excess horizontal stresses exist also outside the ice front, it appears that jacking, if it happens, will be a concern primarily for sub-horizontal fractures. Therefore, in the present report, only the initiation of hydraulic jacking of perfectly horizontal fractures is considered, see Section 4.2.

3.3 Ice sheet profiles

The ice sheet profile, used in the present study, is given by a generic representation of a steady-state ice along its flow line following /Paterson 1994/, cf. Eq. 3-1 and Figure 3-3 (black curve).

$$h_{ice}(x) = MaxHeight\left(1-\left(\frac{SlopeWidth-x}{SlopeWidth}\right)^{4/3}\right)^{3/8} \qquad 3\text{-}1$$

Here, the ice reaches its maximum height (*MaxHeight*) of 3,000 m at a distance (*SlopeWidth*) of 400 km from the ice front (Figure 3-3, black ice sheet profile). For comparison, numerical reconstructions of the Weichselian ice sheet are shown along with the theoretical profile. When comparing the steady-state profile, in this study used for both advancing, stationary and retreat phases, one can note that it is much steeper than the reconstructed retreating profiles. The reconstructed profile from the Weichselian retreat phase (at 14.3 kyrs BP) is on theoretical ground expected to be less steep than the generic steady-state profile, since ice sheet profiles during retreats generally are less steep than during steady-state conditions and advances. Furthermore, it is of the same steepness as a reconstructed *advancing* profile of the Weichselian ice sheet at a stage when the ice front just has reached the Forsmark area (at approximately 30 kyrs ago). There may be many factors contributing

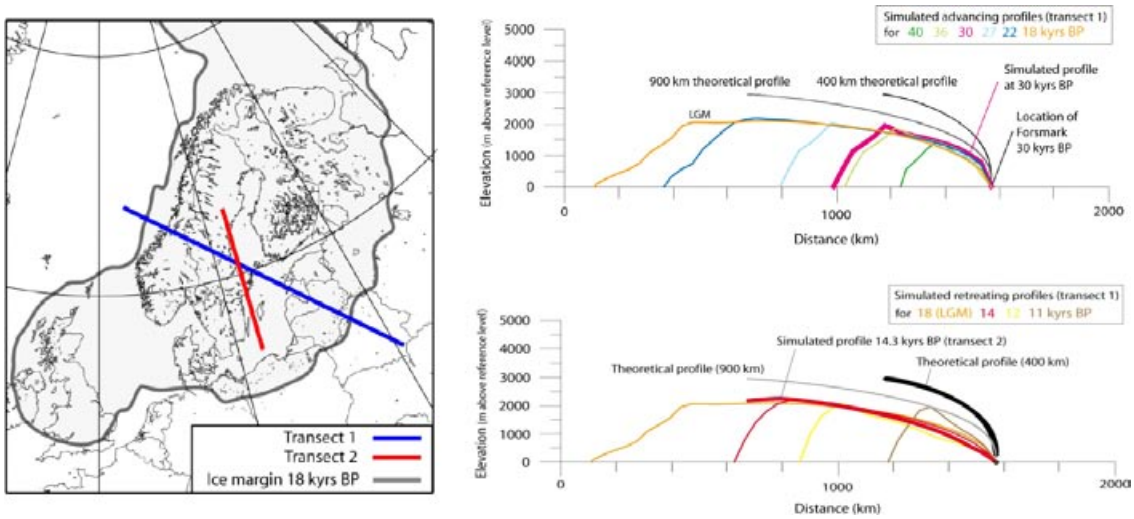

Figure 3-3. *Ice sheet profiles corresponding to a theoretical steady-state ice sheet (black curve, cf. Eq. 3-1) and numerical simulations of the advancing Weichselian ice sheet (top right figure) and the retreating Weichselian ice sheet (lower right figure) along the transects shown in the left figure, from /SKB 2010/. Please note that there is a strong exaggeration of the scale on the vertical axis.*

to the fact that the advancing profile of the reconstructed Weichselian ice sheet is not, as expected, steeper than the theoretical steady state profile, such as prevailing basal thermal and hydrological conditions, topography, and ice sheet-climate interactions, see also /SKB 2010/. In conclusion, the steady state ice profile used in the study is of an adequate steepness for describing advancing phases of the Weichselian ice sheet, and on the conservative side when describing phases of a stationary or retreating ice sheet.

It is often assumed that the hydrostatic pressure at the boundary between the ice and the rock is about 90% of the thickness of the ice /*e.g.* Grasby and Chen 2005, Moeller et al. 2007, Bense and Person 2008/ or about 98% of the mechanical load induced by the ice sheet. In the present study, the ratio between hydrostatic pressure at ice/bed interface and mechanical load is assumed to be uniform along the flow line (set to 98% in the reference calculations) and the effects of subglacial tunnels are not taken into account. The implications of assuming other ratios between hydrostatic water pressure and ice load are addressed in Figure 6-6, Figure 7-1 and subsection on seasonal variations in Chapter 8.

As previously mentioned, the ice sheet profile during retreat is likely to be less steep than during the advance. However, for the purpose of this study, the same steep ice slope (Eq. 3-1) is used in the analyses to model an advancing ice front as well as a retreating ice front. Two different transient boundary conditions are considered, cf. Figure 3-4:

- BC1. The ice changes linearly in height keeping the height to slope width ratio constant at all times (left figure).
- BC2. The ice remains constant in height at all times (right figure).

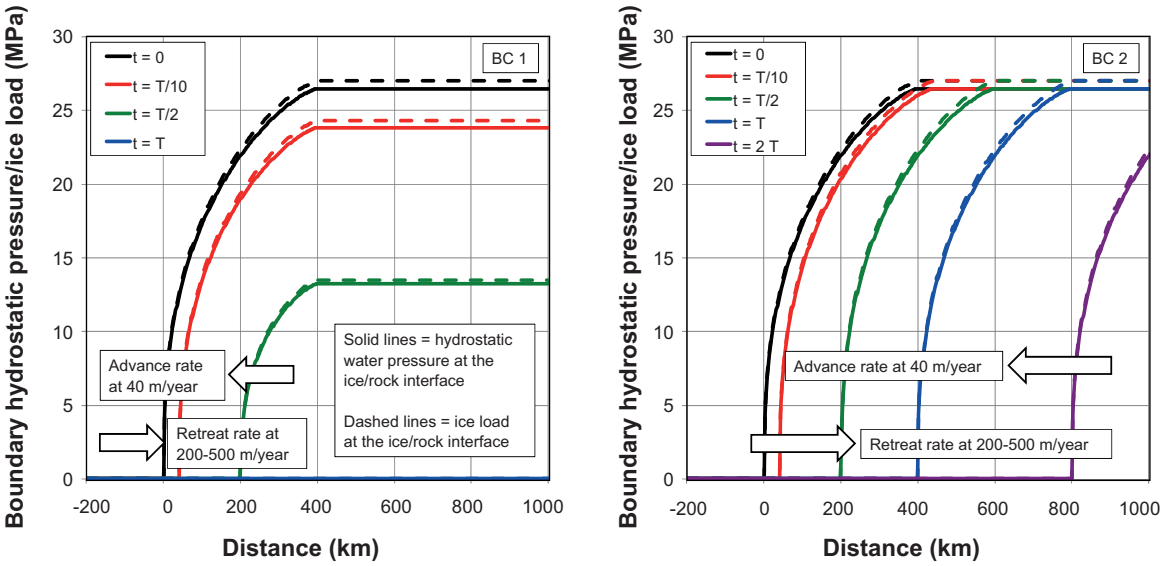

Figure 3-4. *Transient water pressure boundary conditions (solid lines) and ice load at the ground surface (dashed lines). The water pressure is set to 90% of the ice sheet thickness, i.e. 98% of the ice load assuming the density of ice to be 917 kg/m³. Left: BC1, linear change in height keeping height to slope width ratio constant. Right: BC2, constant height during both advancement and retreat. The parameter T (years) is related to the speed v (m/year) of the ice front by T = 400,000·v.*

4 Means to address hydraulic jacking

4.1 Ground water flow equation

4.1.1 General

In general, horizontal pressure gradients are much smaller than the vertical gradient (cf. *e.g.* Figure 6-2), which often leads to the assumption that the resulting deformations are purely vertical /Neuzil 2003/. For a temporally changing, but areally homogeneous load, an expression for groundwater flow, where variations in salinity and temperature are not considered /Neuzil 2003/ (also known as constant-density flow), is given by Eq. 4-1,

$$\nabla \cdot (k \nabla P) = S_S \frac{\partial P}{\partial t} - S_S \varsigma \frac{\partial \sigma_{zz}}{\partial t} \qquad 4\text{-}1$$

where

P is groundwater pressure (Pa).

k is the hydraulic conductivity of the rock (m/s).

S_S is the one-dimensional specific storage coefficient of the rock (m^{-1}).

ζ is the one-dimensional loading efficiency (-), which represents the change in fluid pressure to change in vertical load under conditions of lateral confinement /Neuzil 2003/. This quantity can take on values between zero and one. For mean value properties of the rock mass at Forsmark it evaluates at approximately 0.4 (see Appendix A).

σ_{zz} is the vertical stress due to the overburden (Pa).

4.1.2 Linear diffusion equation

If the hydraulic conductivity can be assumed to be a constant and the overburden stress does not change significantly with time, or no part of the mechanical load is transferred to the fluid pressure, the groundwater flow equation (Eq. 4-1) reduces to a linear diffusion equation for the pore pressures. However, during a glacial period, the overburden stress must be assumed to vary with time, see *e.g.* Figure 3-2. Therefore, the approach, whereby the effects due to the overburden stress are ignored, will obviously introduce some errors. These errors are, as indicated by results from 1-D analyses, reasonably small, cf. Appendix A. This means that the pore pressure distribution can be captured fairly well by a linear diffusion equation.

The transient behaviour of the pore pressures due to a temporally and spatially varying boundary pressure can now be found by examining solutions to the linear diffusion equation. The linear diffusion equation is given by Eq. 4-2, where κ (m^2/s) is the hydraulic diffusivity of the rock. A verification example is presented in Appendix B.

$$\nabla^2 P - \frac{1}{\kappa}\frac{\partial P}{\partial t} = 0 \text{ , with } -\infty < x < \infty \text{ and } y \geq 0 \qquad 4\text{-}2$$

The hydraulic diffusivity is expressed as the ratio between hydraulic conductivity and the specific storage coefficient, cf. Eq. 4-3. In the present modelling work, the specific storage coefficient in a linear elastic medium is represented by a one-dimensional specific storage coefficient /Itasca 2005a/ in which it is assumed that the solid grains (*i.e.* intact rock) are incompressible /Neuzil 2003/, cf. Eq. 4-4. Estimates of the hydraulic diffusivity can be made by use of the hydro-mechanical data provided in Sections 5.1 and 5.2. The diffusivity is used as input for transient modelling of the glacially induced pore pressure in Chapters 6 and 8.

$$\kappa = \frac{k}{S_S} \qquad 4\text{-}3$$

$$S_S = \rho g \left(\frac{n}{K_w} + \frac{1}{K + (4/3)G} \right) \qquad 4\text{-}4$$

Here,

ρ water density (1,000 kg/m^3), which is assumed to be pressure-independent;

g the acceleration due to gravity (9.81 m/s^2);

n effective porosity (-);

K_w the water bulk modulus ($2.2 \cdot 10^9$ Pa);

$K = E/(3(1–2\nu))$ the rock bulk modulus (Pa).

$G = E/(2(1+\nu))$ the rock shear modulus (Pa).

E and ν are Young's modulus and Poisson's ratio of the rock mass, respectively.

4.2 Criterion for hydraulic jacking

Hydraulic jacking of horizontal fractures is initiated when the pore pressure (P) in a fracture exceeds both the vertical stress (σ_v) acting on it and the fracture's tensile strength (T), cf. Eq. 4-5.

$$P \geq \sigma_v + T \qquad 4\text{-}5$$

Here, the pore pressure is the sum of the glacially induced pore pressure (in the following denoted excess pore pressure) and the hydrostatic pressure at a given depth below the ground surface. The glacially induced pore pressure is calculated using the analytical and numerical methods described in Sections 4.3 and 4.4. The vertical stress at a given depth below the ground surface is the sum of the glacially induced vertical stress and the vertical *in situ* stress.

The following assumptions will be made in all modelling work:

- It is assumed that the fractures have no tensile strength, *i.e.* $T = 0$.
- The hydrostatic pressure at the ice/bed interface corresponds to 90% of the height of the ice (or approximately 98% of the mechanical load), cf. Figure 3-4 (solid lines). For an exception of this see Figure 6-6, Figure 7-1 and text on seasonal variations in subsection 8.3.2.
- The glacially induced vertical stress is assumed to be equal to the weight of the ice at all times and at all depths, cf. Figure 3-4 (dashed lines) and Appendix C. The density of ice is set to 917 kg/m^3.
- The *in situ* vertical stress is assumed to be equal to the weight of the overlying rock at all depths. The density of the rock mass is set to 2,700 kg/m^3.

4.3 Analytical solutions

As both propagation of pore pressures and conduction of heat are problems obeying the diffusion equation, the solutions and solution techniques presented in /Carslaw and Jaeger 1959/ can be used to derive the analytical expressions presented in the following subsections.

4.3.1 Stationary ice sheet

The steady state pore pressure distribution in a semi-infinite rectangular solid is a solution of a special case of the diffusion equation, Eq. 4-2. Here, x is the horizontal coordinate and y is the vertical coordinate ($y = 0$ represents the ground surface). As time tends to infinity, the time-dependency vanishes and the equation reduces to Laplace's equation, Eq. 4-6.

$$\frac{\partial^2 P_{SS}}{\partial x^2} + \frac{\partial^2 P_{SS}}{\partial y^2} = 0 \text{ , with } -\infty < x < \infty \text{ and } y \geq 0 \qquad \text{4-6}$$

The steady state solution, $P_{SS}(x, y)$, where the plane at $y = 0$ is kept at a pressure given by the function $f_0(x)$, is presented in /Carslaw and Jaeger 1959/ (with some rearrangement of the integration variable), Eq. 4-7. The hydrostatic pressure at ice/bed interface, $f_0(x)$, used in the steady state modelling is shown in Figure 6-1 (left, plot symbols).

$$P_{SS}(x,y) = \frac{1}{\pi}\int_{-\infty}^{\infty} \frac{f_0(y \cdot x' + x)}{1 + x'^2} dx' \qquad \text{4-7}$$

4.3.2 Non-stationary ice sheet

The solution to the 2D diffusion equation (Eq. 4-2) in a semi-infinite rectangular solid with a time-varying boundary hydrostatic pressure $f(x, t)$ at the ground surface ($y = 0$) and zero initial pore pressure is given by Eq. 4-8. The hydrostatic pressure at ice/bed interface used in the modelling is shown in Figure 3-4 (solid lines). A verification example is presented in Appendix B.

$$P(x,y,t) = \frac{2}{\pi}\int_{y/2\sqrt{\kappa t}}^{\infty}\left(\int_{-\infty}^{\infty} f\left(x + y\frac{\eta}{\mu}, t - \frac{y^2}{4\kappa\mu^2}\right)\exp\left(-\mu^2\right)\exp\left(-\eta^2\right)d\eta\right)d\mu \qquad \text{4-8}$$

If the pore pressures are initially given by a steady state distribution, $P_{SS}(x, y)$, (Eq. 4-7) and subsequently decrease at the ground surface ($y = 0$) with $f(x, t)$, the solution is given by Eq. 4-9:

$$\begin{aligned} P(x,y,t) = P_{SS}(x,y) &- \frac{2}{\pi}\int_{y/2\sqrt{\kappa t}}^{\infty}\left(\int_{-\infty}^{\infty} f_0\left(x + y\frac{\eta}{\mu}\right)\exp\left(-\mu^2\right)\exp\left(-\eta^2\right)d\eta\right)d\mu \\ &+ \frac{2}{\pi}\int_{y/2\sqrt{\kappa t}}^{\infty}\left(\int_{-\infty}^{\infty} f\left(x + y\frac{\eta}{\mu}, t - \frac{y^2}{4\kappa\mu^2}\right)\exp\left(-\mu^2\right)\exp\left(-\eta^2\right)d\eta\right)d\mu \end{aligned} \qquad \text{4-9}$$

4.3.3 Calculation of maximum jacking depth

Jacking of horizontal fractures occurs when the pore pressure exceeds the normal (here vertical) stress acting on the fracture. It can be shown that the maximum jacking depth occurs directly beneath the ice margin, where the glacially induced vertical stress is assumed to be zero. An algorithm for finding the maximum jacking depth for a given diffusivity was programmed into the mathematical spreadsheet program MathCad. A schematic view of the steps needed is presented in Figure 4-1.

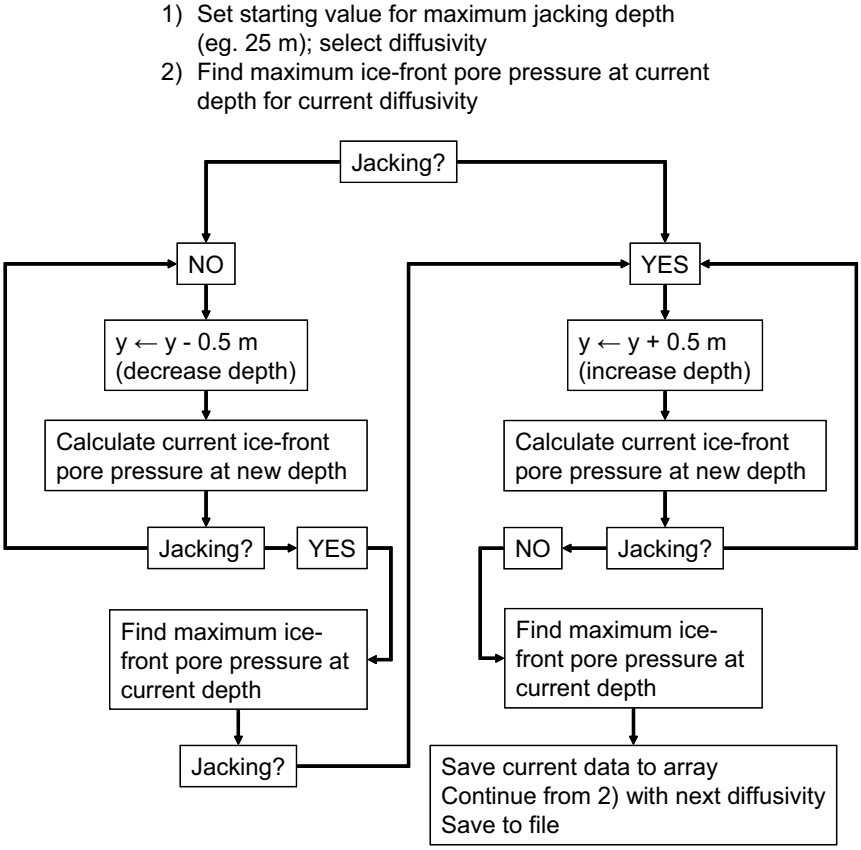

Figure 4-1. *Schematic view of an algorithm to find the maximum jacking depth for a given value of the hydraulic diffusivity.*

4.4 Numerical methods

In media with non-uniform distributions of hydro-mechanical properties or fractured media, the analytical solutions (described above) cannot be used; instead numerical methods have to be relied on.

4.4.1 Homogeneous rock

In both codes (*FLAC* and Code_Bright) used for the modelling of pore pressure diffusion in homogeneously fractured rock, the thermal logic is used. Input to the codes is given by thermal conductivity, specific heat and density. These quantities represent here hydraulic conductivity and specific storage coefficient (equivalent with heat capacity) and the density of water.

FLAC

FLAC (Fast Lagrangian Analysis of Continua) is a two-dimensional code based on the explicit finite difference method /Itasca 2005a/.

The code's main advantage is that non-uniform distributions of properties can easily be applied. Using the built-in programming language *FISH* /Itasca 2005a/, transient boundary conditions can be applied or changes in material properties while time-stepping can be made. However, the code's main disadvantage is that the time-step is inversely proportional to diffusivity, which means that an increase in diffusivity by one order of magnitude will result in a significantly increased running time.

In the present report, *FLAC* is used for the following modelling tasks:

- As an independent way to verify the analytical solutions (cf. Appendix B).
- Investigation of the effects of variations in hydraulic diffusivity with depth (cf. Appendix D).
- Investigation of the effects of open taliks in combination with permafrost (cf. Section 8.4).

Code_Bright

Code_Bright /CIMNE 2004/ is a finite element program specifically developed to analyse coupled THM processes in saturated and unsaturated porous media.

The code's main advantage is that it is fast for all values of the diffusivity. However, it is difficult to specify spatially and temporally varying boundary conditions or make continuous changes to material properties with time.

In the present report, Code_Bright is used to investigate the potential for hydraulic jacking for continuous permafrost conditions without taliks, cf. Section 8.3.

4.4.2 Rock with few conductive fractures (UDEC)

UDEC (Universal Distinct Element Code) is a two-dimensional code based on the distinct element method /Itasca 2005b/. It is used to model the response of discontinuous media, such as fractured rock, due to either static or dynamic loading. The discontinuous medium is represented by a number of discrete blocks. In the case of deformable materials, each block is divided into a mesh of finite-difference elements, each of which responds to a prescribed stress-strain law. The steady state pore pressures are calculated by a built-in algorithm that is based on scaling of the fluid bulk modulus and the domain volumes, which makes them unimportant and the fluid and mechanical time steps can arbitrarily be set to the same value. The fluid flow takes place in the fractures between impermeable blocks.

The upper limit of the apertures, at zero or tensile normal stress, is governed by a global parameter, CAPRATIO. This limits all apertures in the model to CAPRATIO times the largest user-specified residual aperture. In the current modelling work, CAPRATIO is set to 1, *i.e.* the initially largest apertures remain fixed during the calculations.

In the present report, *UDEC* is used to investigate the potential for hydraulic jacking in rock with a few long and highly transmissive fractures in otherwise low permeability rock, cf. Chapter 7.

5 Data

5.1 Forsmark

The rock mass in the candidate area at Forsmark is subdivided into fracture domains with similar fracture frequency characteristics (denoted FFMxx) as shown in Figure 5-1. The nuclear waste repository is planned to be located in fracture domains FFM01 and FFM06.

5.1.1 Mechanical properties of the rock mass and fractures

The elastic properties of the rock mass and the *in situ* stresses for the numerical modelling work in Chapter 7 are based on data from the preliminary site descriptive models v. 1.2 and 2.1 for Forsmark /SKB 2005, 2006c/, cf. Table 5-1 and Figure 5-2. For the transient modelling in Chapters 6 and 8 the elastic properties of the rock mass are based on data for fracture domain FFM01 (see Figure 5-1) from the latest site description of Forsmark (SDM-Site) /SKB 2008/, cf. Table 5-1. The elastic properties are only used to eestimate the value of the specific storage coefficient, cf. subsection 5.1.3. The mechanical properties of the fractures (cf. Table 5-2) are generic without link to observed site conditions and have very high shear strength to avoid shearing. Note that when evaluating the resulting effective stresses and potential for jacking, the vertical stress is calculated from the weight of the overburden (rock and ice) and added in a post-processing step as described in Section 4.2.

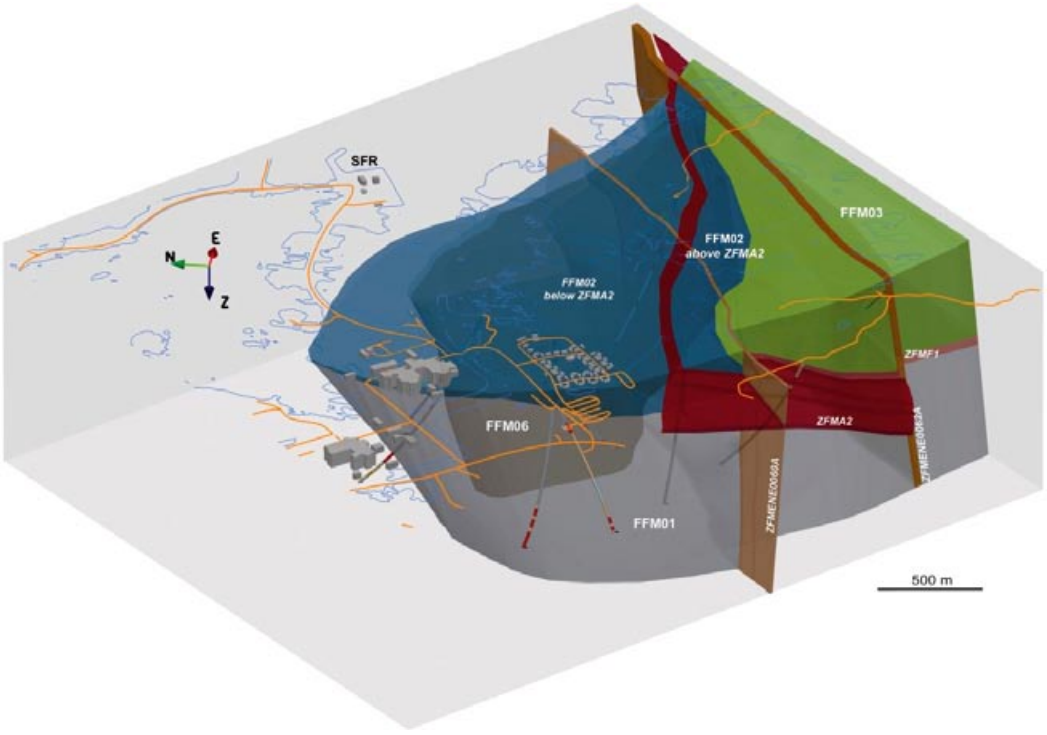

Figure 5-1. *3D view (from south west) of Fracture domains FFM01, FFM02, FFM03 and FFM06 in and surrounding the candidate area at Forsmark (from /Olofsson et al. 2007/). Note that fracture domains FFM04 and FFM05 border the candidate area and are not shown in the figure.*

Table 5-1. Mechanical properties of the rock mass based on preliminary site description v. 2.1 /SKB 2006c/ and SDM-Site /SKB 2008/.

Rock mass property	Unit	Value (prel. SDM)	Value (SDM-Site)
Density rock	kg/m^3	2,700	2,700
Young's modulus	GPa	67	70
Poisson's ratio	–	0.23	0.24

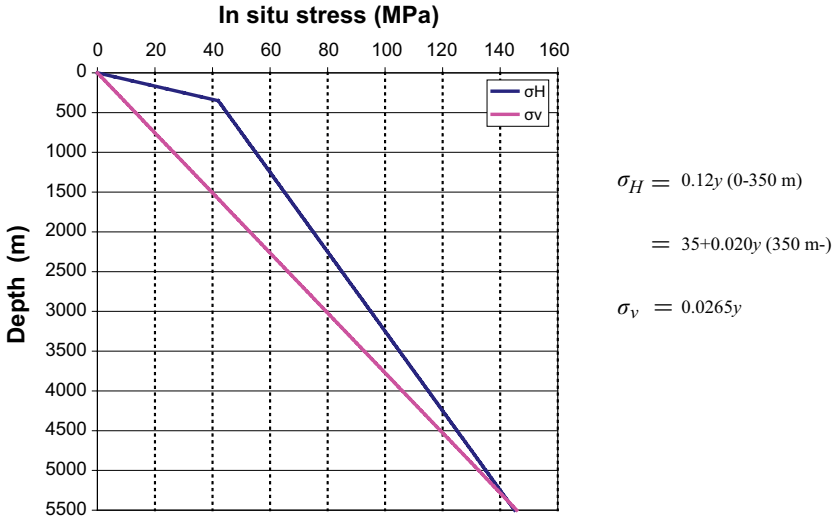

Figure 5-2. *Major horizontal and vertical in situ stresses as functions of depth based on preliminary site description v. 1.2 for Forsmark /SKB 2005/. In the 2D modelling, the intermediate principal stress component is ignored.*

Table 5-2. Mechanical and strength properties of the fractures.

Fracture property	Unit	Value
Joint normal stiffness		
Mesh	GPa/m	200
Explicitly modelled fractures	GPa/m	200
Joint shear stiffness		
Mesh	GPa/m	200
Explicitly modelled fractures	GPa/m	200
Friction angle	°	63
Cohesion	MPa	1,000

5.1.2 Rock mass hydraulic conductivity

The bulk hydraulic conductivity of the rock mass in Fracture domains FFM01, FFM02, FFM03, FFM04 and FFM05 at Forsmark site (see Figure 5-1 for locations) varies between $1{\cdot}10^{-9}$ and $1{\cdot}10^{-8}$ m/s /Follin et al. 2007, p. 149/. In the absence of data for the Hydrogeological DFN modelling stage 2.2 it was proposed that FFM06, which is located close to FFM01 (cf. Figure 5-1), would have similar properties to FFM01. More recently acquired data do not contradict this hypothesis /SKB 2008/. Estimates of the hydraulic conductivity in the different fracture domains at Forsmark and in different depth intervals are presented in Figure 5-3.

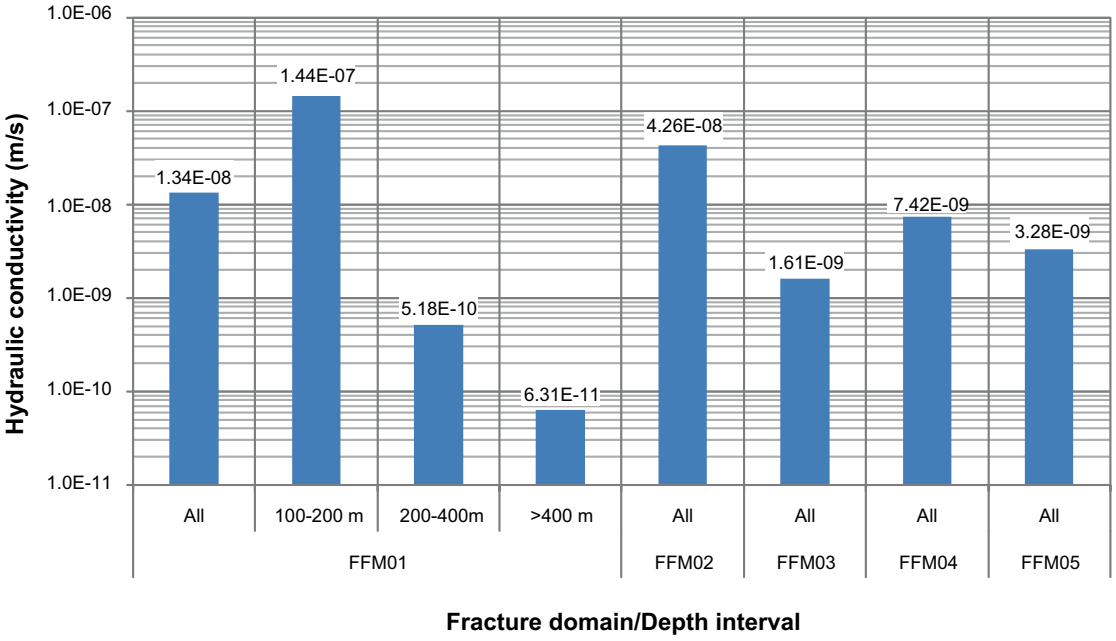

Figure 5-3. *Estimates of the bulk hydraulic conductivity in different fracture domains (FFMx) at Forsmark and in different depth intervals, compiled from Tables 10-15 to 10-20 and 10-22 to 10-24 in /Follin et al. 2007/.*

5.1.3 Specific storage coefficient

The mean values of the rock mass elastic properties in fracture domain FFM01 at are about 70 GPa (Young's modulus) and 0.24 (Poisson's ratio), respectively /SKB 2008/, cf. Table 5-1. The porosity of the dominating rock type (101057) in rock domain RFM029 is around 0.2% /SKB 2008/. Figure 5-4 shows the hydraulic diffusivity as a function of hydraulic conductivity for variations of ±15 GPa in Young's modulus with porosity values assumed to be in the range 0.1–1%. The resulting values of the specific storage coefficient (Eq. 4-3) are in the range $1.0 \cdot 10^{-7}$–$1.6 \cdot 10^{-7}$ m^{-1} ($1.3 \cdot 10^{-7}$ m^{-1} for mean value properties).

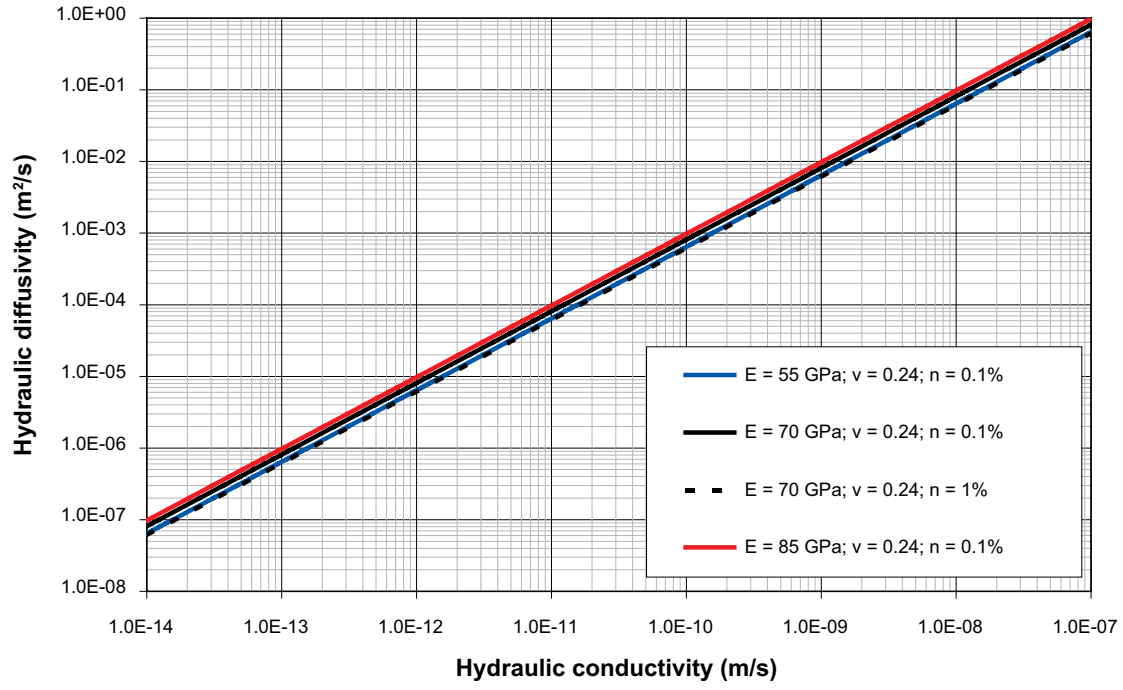

Figure 5-4. *Hydraulic diffusivity as a function of hydraulic conductivity for typical values (including uncertainty spans) of the rock's deformation properties at Forsmark.*

5.1.4 Fracture transmissivity

The mean value fracture transmissivities are in the range $3 \cdot 10^{-9}$ to $1.5 \cdot 10^{-8}$ m^2/s in fracture domains FFM01 and FFM02 regardless of depth as shown in Figure 5-5.

5.2 Laxemar

The rock mass in the focused area at Laxemar is subdivided into fracture domains with similar fracture frequency characteristics (denoted FSM_x) as shown in Figure 5-6. The rock mass is also subdivided into so-called hydraulic rock domains (denoted HRD_x) /Rhén et al. 2003/ with similar hydrogeological properties. Here, HRD_EW007 corresponds to FSM_EW007, HRD_N corresponds to FSM_N, HRD_W corresponds to FSM_W and HRD_C corresponds the fracture domains FSM_C, FSM_NE005 and FSM_C grouped together /Rhén et al. 2008/.

5.2.1 Rock mass hydraulic conductivity

Estimates of the variations in hydraulic conductivity with depth in the four hydraulic rock domains (HRD_EW007, HRD_N, HRD_W and HRD_C, cf. Figure 5-6) are presented in Figure 5-7. A rough estimate of the hydraulic conductivity taken over all four hydraulic rock domains is around $1 \cdot 10^{-7}$ m/s based on data in Table 9-1 in /Rhén et al. 2008/. The conductivities at Laxemar appear to be higher at all depths than the corresponding estimates for Forsmark, cf. Figure 5-3.

5.2.2 Specific storage coefficient

The mean values of the elastic properties of the rock mass in the focused area at Laxemar are in the range 50–59 GPa (Young's modulus) and 0.3 (Poisson's ratio), respectively /Hakami et al. 2008/. The porosity of the dominating rock types in rock domains RSMA01, RSMD01, RSMM01 and RFMBA03 is in the range 0.16–0.35% /SKB 2009/. Assuming the porosity to be 0.1–1% and Young's modulus to be 40–70 GPa, the resulting values of the specific storage coefficient (Eq. 4-4) are in the range $1.1 \cdot 10^{-7}$–$1.9 \cdot 10^{-7}$ m^{-1}.

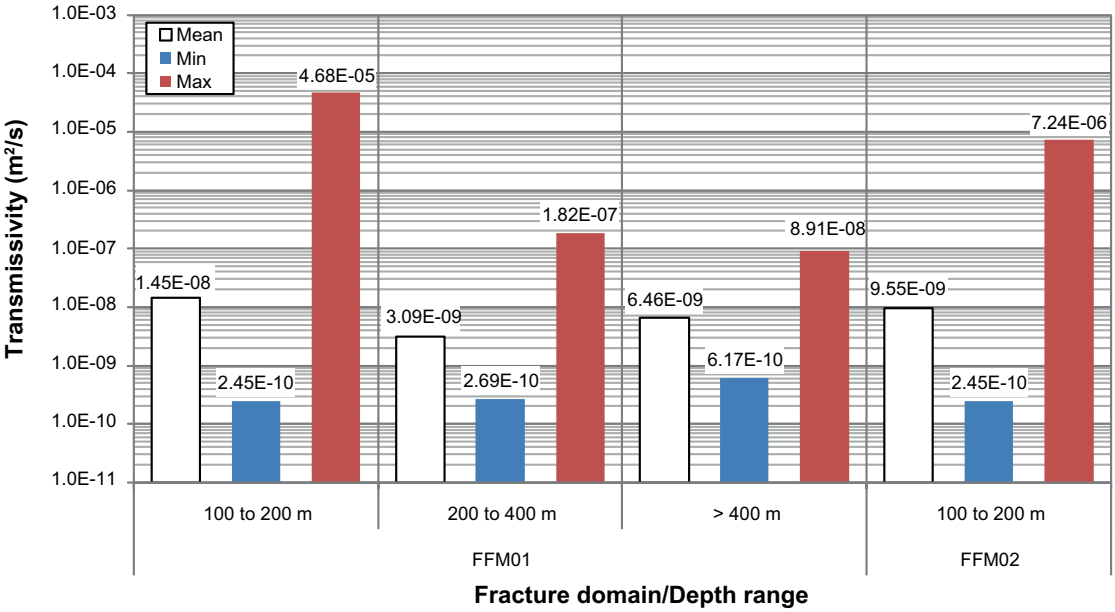

Figure 5-5. Fracture transmissivities in different depth intervals in fracture domains FFM01 and FFM02 at Forsmark, compiled from Table 10-25 in /Follin et al. 2007/.

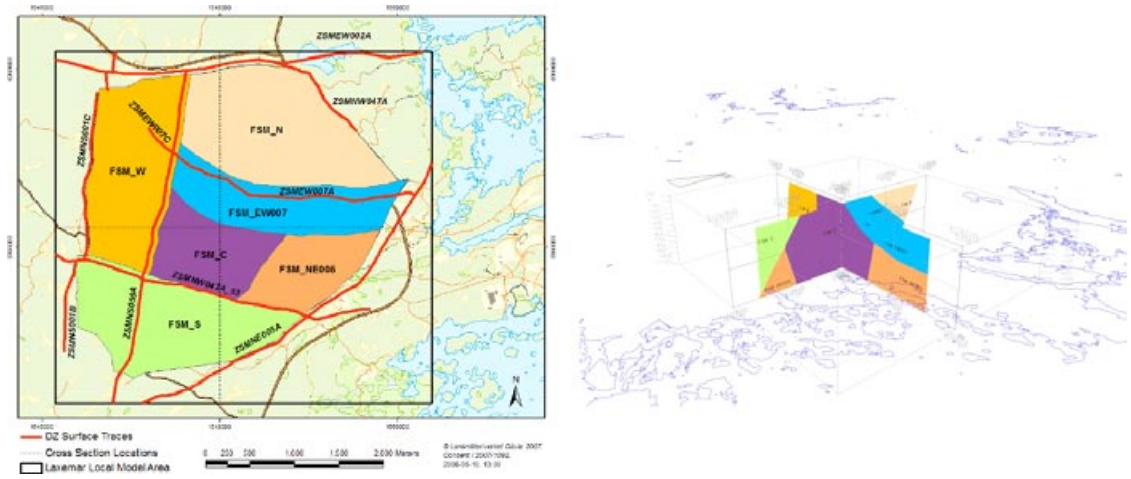

Figure 5-6. *Left: Surface view of fracture domains in the focused area at Laxemar, from /Hakami et al. 2008. Right: 3D view to the north west of the fracture domains in the Local model volume, from /Wahlgren et al. 2008/.*

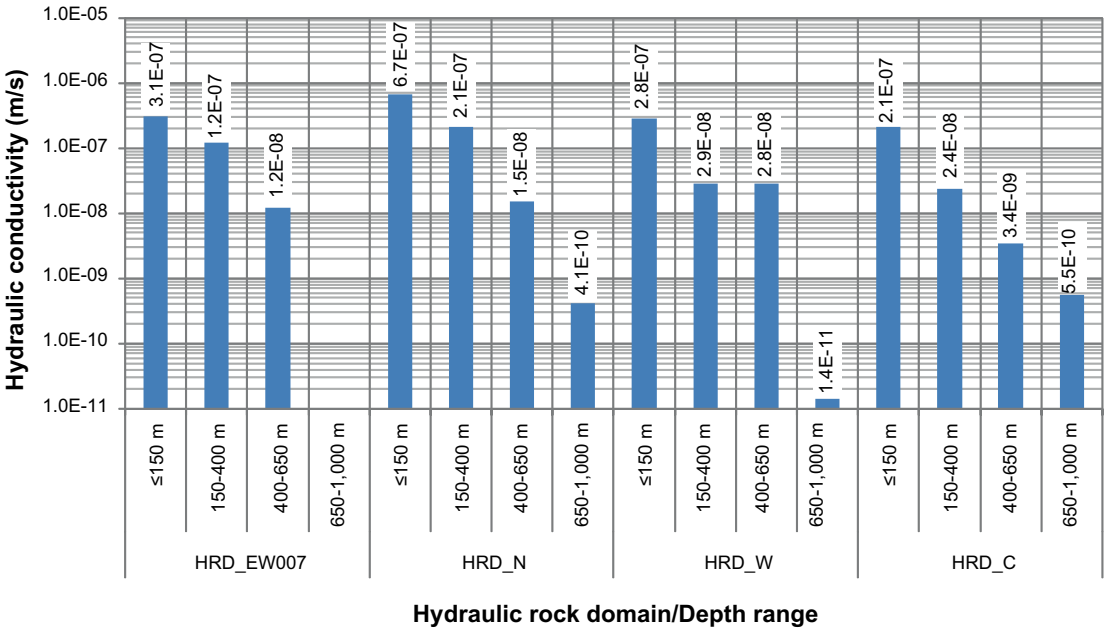

Figure 5-7. *Estimates of the bulk hydraulic conductivity in different hydraulic rock domains (HRD_x) at Laxemar and in different depth intervals, compiled from Table 9-12 in /Rhén et al. 2008/.*

5.2.3 Fracture transmissivity

The minimum, mean and maximum value fracture transmissivities in hydraulic rock domains HRD_EW007, HRD_N, HRD_W and HRD_C are presented in Figure 5-8. The mean transmissivities are in the range $4 \cdot 10^{-9}$–$1.3 \cdot 10^{-7}$ m^2/s. At comparable depths, the transmissivities at Laxemar appear to be approximately one order of magnitude greater than at Forsmark.

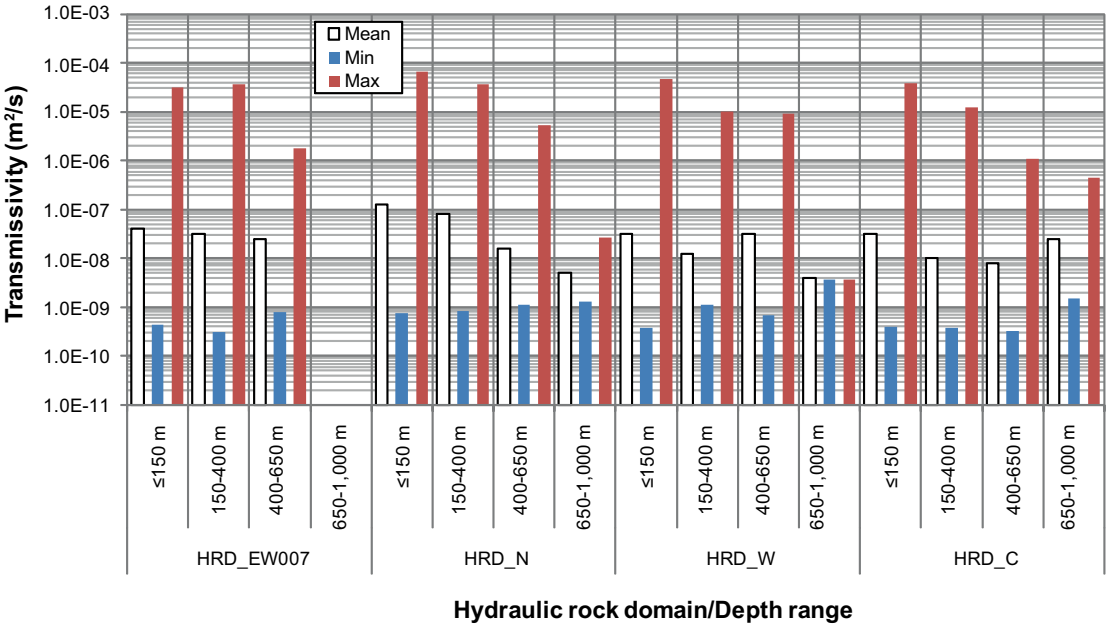

Figure 5-8. *Fracture transmissivities in different depth intervals in different hydraulic rock domains (HRD_x) at Laxemar, compiled from Table 9-12 in /Rhén et al. 2008/.*

6 Homogenous rock model

6.1 General

The present chapter is related to the potential for hydraulic jacking in homogeneously fractured rock. Homogeneous rock is here defined as rock in which the contrasts between the transmissivity of the fractures and the surrounding rock are sufficiently small that it can be treated as a continuum and the hydraulic properties can be approximated with a globally valid bulk hydraulic diffusivity.

The analytical expressions (Eqs. 4-7, 4-8 and 4-9) introduced in Chapter 4 will be used to investigate the pore pressure distribution and evolution due to spatially and temporally varying hydrostatic water pressures at the ice/bed interface (Figure 3-4). The objective is to estimate the maximum depth to which hydraulic jacking of horizontal fractures can occur for a given value of the bulk hydraulic diffusivity. The following is addressed:

- Hydraulic jacking as the ice front is advancing or during stationary conditions, cf. Sections 6.2 and 6.3.1.
- Hydraulic jacking during the retreat of the ice front – importance of retreat speed, cf. Section 6.3.2:
  - Retreat from steady state conditions.
  - Influence of advance rate (40 m/year) followed by periods of quasi-stationary conditions (0–10,000 years) before retreat.

6.2 Stationary ice front

A steady state pressure distribution can be considered an upper bound estimate of the pore pressures due to an advancing ice sheet, where the hydrostatic pressure at the ice/bed interface corresponds to the ice at its maximum height and extent. The ice has been present for an infinitely long time and the highest possible pore pressures have been allowed to develop everywhere in the modelled rock mass. In the steady state solution the time-dependency vanishes and the solution is independent of the hydraulic diffusivity, cf. Eq. 4-7.

Figure 6-1 (left) shows the hydrostatic pressure at the ice/bed interface together with the analytically calculated steady state excess pore pressure distribution 100 m, 500 m and 1,000 m below the ground surface compared with the corresponding effective vertical stress (dashed lines). The hydrostatic pressure at the ice/bed interface, is calculated from the equation for the height of the ice (Eq. 3-1), assuming that the pressure corresponds to 90% of the height of the ice. Figure 6-1 (right) shows the pore pressure and effective stress as functions of depths beneath the ice margin. Here, hydraulic jacking may be initiated to depths of around 30 m.

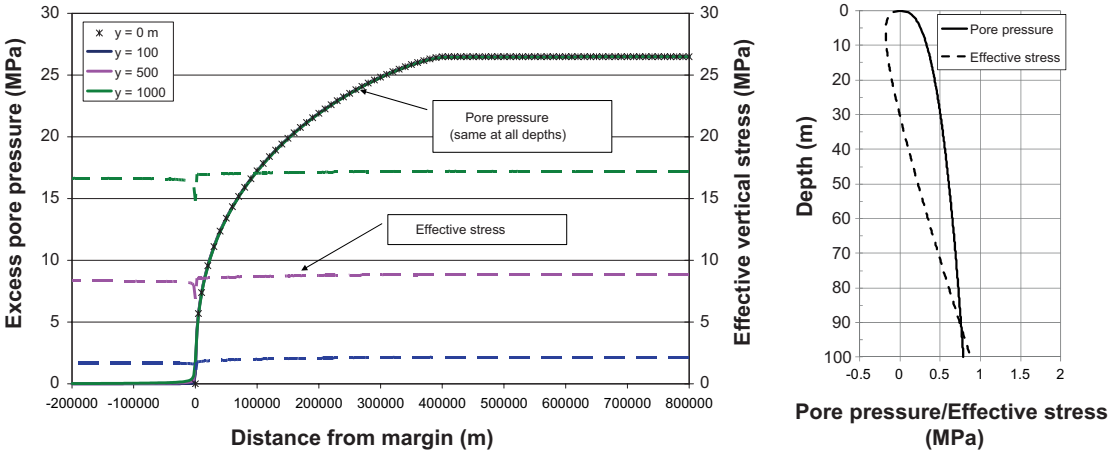

Figure 6-1. Left: Analytically calculated steady state excess pore pressure distribution (solid lines) and corresponding effective vertical stress (dashed lines) at 100 m, 500 m and 1,000 m depth compared with the boundary pressure function, f(x) at y = 0 m. Right: Corresponding pore pressure and effective stress as functions of depth beneath the ice margin. Here, hydraulic jacking is initiated to depths of about 30 m.

6.3 Non-stationary ice front

6.3.1 Approaching ice front

As stated in the previous section, steady state models give an upper bound estimate of the pore pressure distribution from an approaching ice front. However, in reality the ice front will not be stationary for an infinitely long time. In the following example, it is assumed that the ice front approaches at a speed of 40 m/year as shown in Figure 3-4. Figure 6-2 shows the steady state pore pressure distribution and the pore pressure distribution after 10,000 years for two values of the rock mass hydraulic diffusivity (cf. Figure 5-3 and subsection 5.1.3): $1 \cdot 10^{-1}$ m^2/s (upper figure, corresponds approximately to hydraulic conditions in the upper 400 m of rock) and $1 \cdot 10^{-4}$ m^2/s (lower figure, corresponds to hydraulic conditions at large depths).

For high values of the hydraulic diffusivity, the pore pressure distribution is approximately equal to the steady state pressure distribution regardless of which one of the two boundary conditions (BC1 or BC2) is used. For low values of the hydraulic diffusivity, the pore pressure distribution does not approach steady state conditions in 10,000 years. However, an ice sheet that advances at a much slower speed will gradually approach the steady state pore pressure distribution. Furthermore, the choice of boundary conditions (BC1 or BC2) has an influence on the results.

In conclusion, assuming that the pore pressures have reached steady state during the advance of the ice front appear to be an adequate approximation when the hydraulic diffusivity is high, but will overestimate the pore pressures for low diffusivities and at large depths. This is demonstrated in more detail in the following sections.

6.3.2 Retreating ice front

During the latest deglaciation, the margin of the Weichselian ice sheet retreated with speeds between 200 m/year and 300 m/year at present day Oskarshamn site and Forsmark site /SKB 2006b/, respectively. These retreat speeds are used for reference in the following. However, according to /Talbot 1999/, the ice front of the Weichselian ice retreated about 1,000 km in 2,000 years, corresponding to a speed of 500 m/year. This case is analysed for completeness as an upper bound option.

In the following it is assumed that the ice front moves with a constant speed during the entire retreat phase.

Importance of the ice front retreat speed

Steady state models (described in Section 6.2) give an upper bound estimate of the pore pressure distribution from an advancing ice sheet. As seen in Figure 6-2, the initial pore pressure, for low diffusivities, is greatly over-predicted and consequently hydraulic jacking is only expected at much shallower depths.

Figure 6-3 shows the resulting maximum jacking depths, assuming that the ice front retreats with a constant speed from a steady state pressure distribution (Figure 6-1). As seen in the figure, the different boundary conditions and retreat rates appear to influence the maximum jacking depth only when the hydraulic diffusivity is lower than about $5 \cdot 10^{-3}$ m^2/s. Depending on whether the ice is decreasing in height (BC1) or remains constant in height (BC2) during the retreat, the maximum jacking depths for a hydraulic diffusivity of $1 \cdot 10^{-3}$ m^2/s are in the following intervals: 110–180 m (for a speed of 200 m/year), 170–280 m (300 m/year) and 275–450 m (500 m/year). However, the bulk hydraulic diffusivity at Forsmark is around 10^{-2}–10^{-1} m^2/s (cf. subsections 5.1.2 and 5.1.3). In this diffusivity range, the maximum jacking depth is between 50 and 75 m for both boundary conditions provided that the ice front retreats with at most 500 m/year.

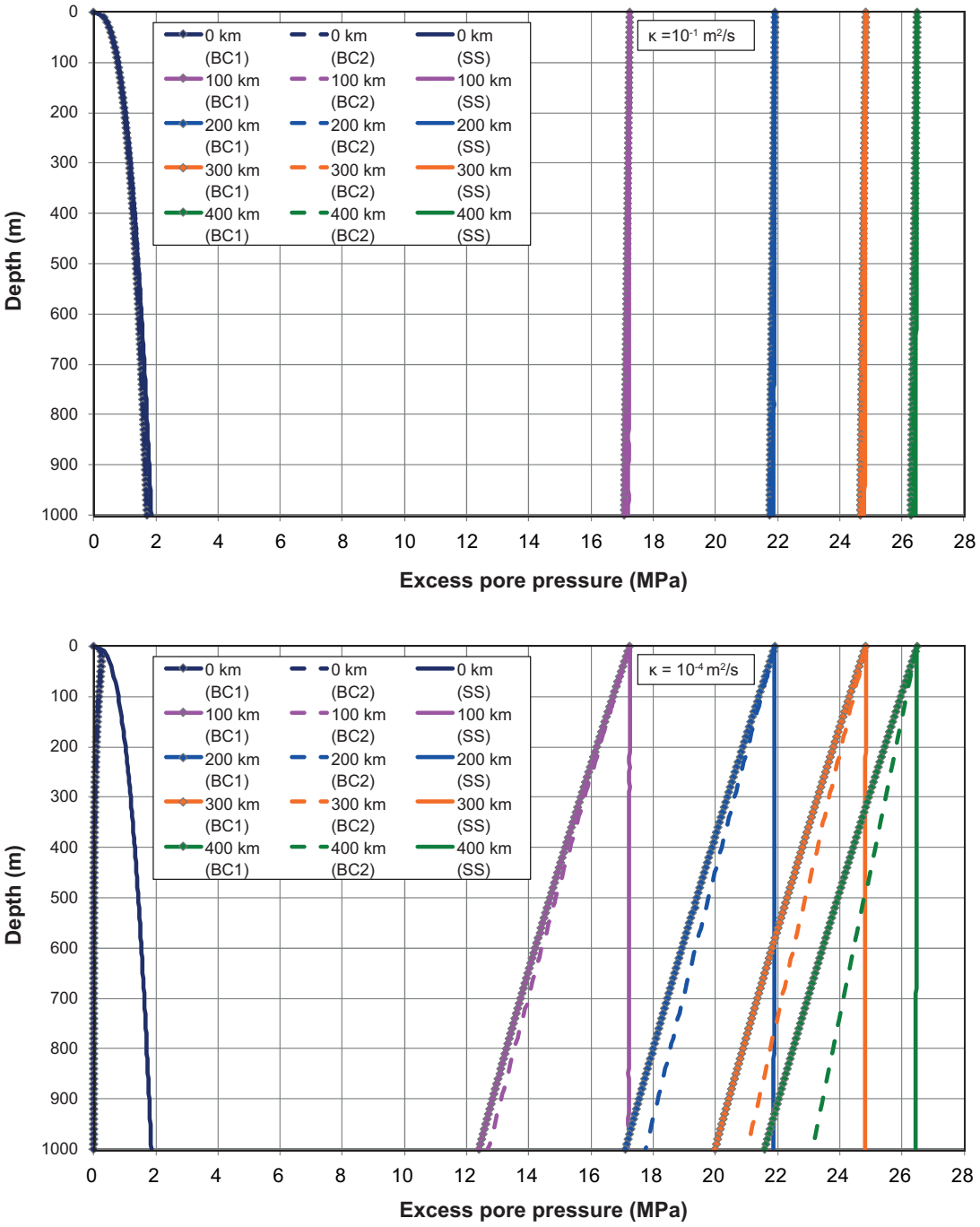

Figure 6-2. *Pore pressure distribution as functions of depth at the ice front, 100 km, 200 km, 300 km and 400 km in under the ice after 10,000 years (the ice front has been approaching at a speed of 40 m/year) for the two boundary conditions BC1 and BC2 (Figure 3-4) compared with the corresponding steady state case (SS). The given values of the hydraulic diffusivity $1 \cdot 10^{-1}$ m²/s (top) and $1 \cdot 10^{-4}$ m²/s (bottom) correspond to hydraulic conductivities of about $1.0 \cdot 10^{-8}$ m/s and $1.0 \cdot 10^{-11}$ m/s, respectively.*

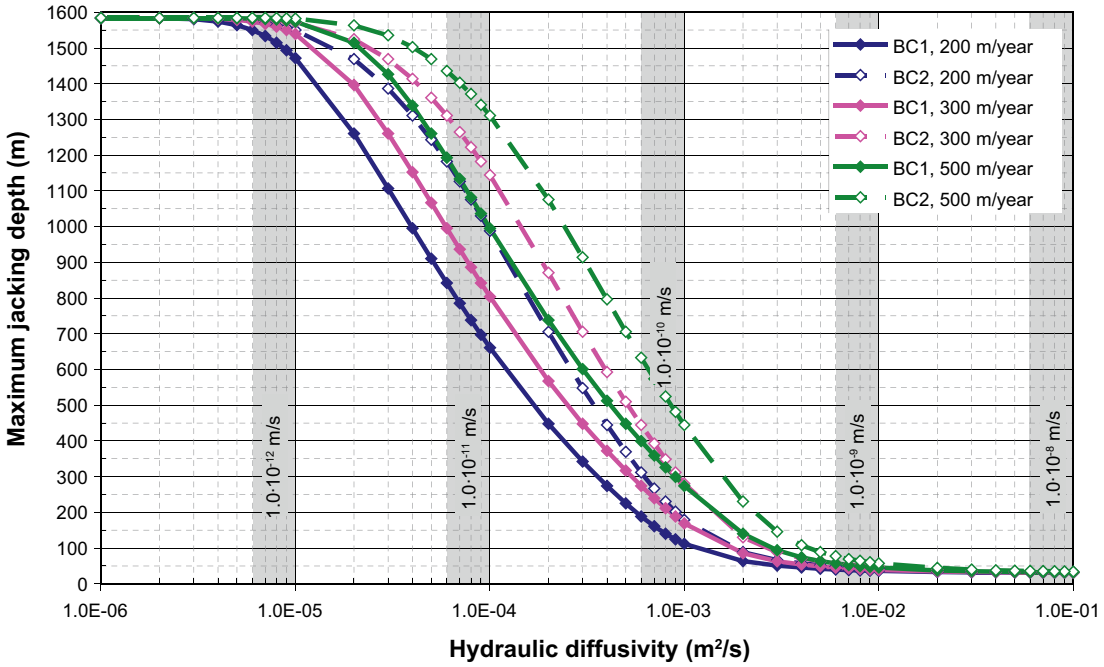

Figure 6-3. *Maximum jacking depth at the ice front as a function of hydraulic diffusivity for given values of the frontal retreat rate. Retreat from steady state pressure distribution. Grey-shaded areas indicate diffusivity ranges associated with different values of the bulk hydraulic conductivity (cf. Figure 5-4).*

Figure 6-4 shows the maximum jacking depths due to an ice that is advancing from zero pore pressure (ignoring the *in situ* hydrostatic pressure) at constant speed until its full height is reached and then retreats back to zero height with a (different) constant speed, see Figure 3-4. Comparing the results from Figure 6-3 and Figure 6-4 it is clearly seen that the maximum jacking depths for rock with low diffusivity are greatly over-predicted if the pressures are initially given by a steady state distribution. However, for the diffusivity range relevant for Forsmark (10^{-2}–10^{-1} m^2/s), the maximum jacking depths appear to be practically independent of the initial conditions.

Importance of duration of ice sheet cover

The maximum jacking depth for a given value of the hydraulic diffusivity depends not only on the retreat speed, but also on the advance speed and the amount of time the ice is covering the site before it begins to retreat. During the deglaciation, it is possible that the ice sheet makes a temporary halt in the recession, and stays quasi-stationary for ~1,000 years or more, *e.g.* during Younger Dryas /SKB 2006a/. Here, the worst case scenario is looked at; after having reached its maximum height the ice front is stationary with constant height for a given number of years before retreating.

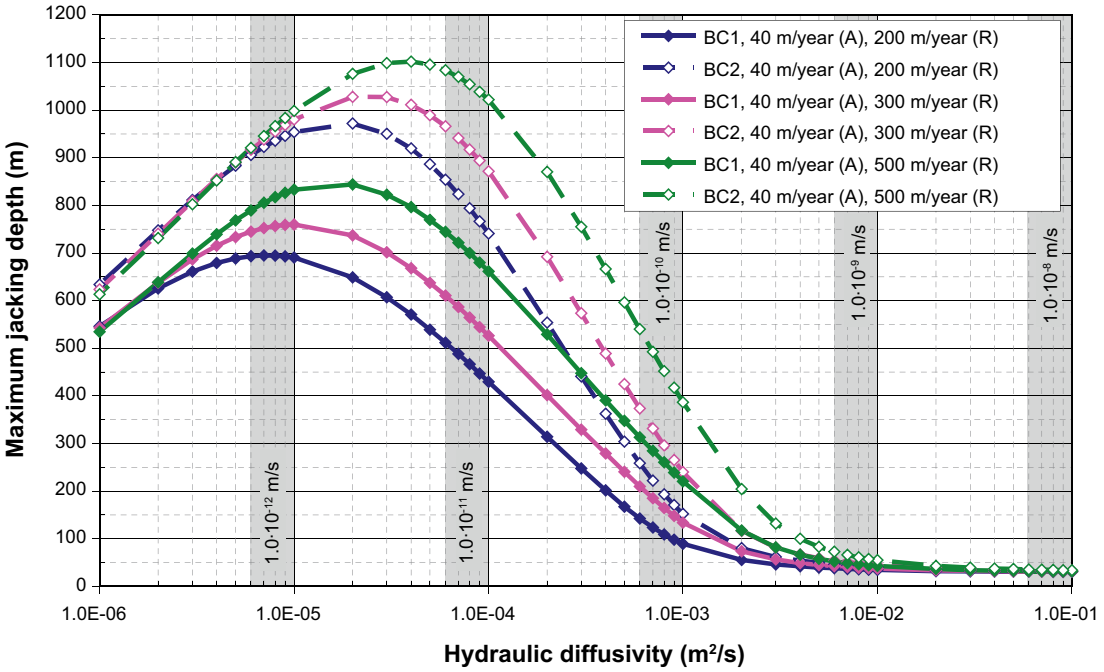

Figure 6-4. *Maximum jacking depth at the ice front as a function of hydraulic diffusivity. The ice front (A)dvances from initially zero pressure at 40 m/year for 10,000 years and (R)etreats from maximum hydrostatic pressure at the ice/bed interface at 200–500 m/year. Grey-shaded areas indicate diffusivity ranges associated with different values of the bulk hydraulic conductivity (cf. Figure 5-4).*

Figure 6-5 shows the maximum jacking depth for an ice sheet that is advancing at a speed of 40 m/year and retreating at a speed of 300 m/year. The results are compared with a case where the ice front retreats at a speed of 300 m/year from a steady state pressure distribution (cf. previous section). As seen in the figure, the maximum jacking depths for rock with low diffusivity are greatly over-predicted if the ice front retreats from a stationary ice pressure distribution. For the value of the hydraulic diffusivity of $1 \cdot 10^{-3}$ m^2/s, the difference in maximum jacking depth between an ice sheet that is retreating as soon as it has reached its maximum height and an ice front that is retreating from a steady state pressure distribution is only about 50 m. This difference decreases with increasing hydraulic diffusivity. For the diffusivity range relevant for Forsmark (10^{-2}–10^{-1} m^2/s), the maximum jacking depth is around 50 m and appears to be practically independent of the duration of stationary conditions.

Importance of pressure potential under the ice sheet

In the previous section the water pressure potential under the ice sheet is assumed to be 90% of the height of the ice. Given the ice profile of Eq. 3-1, if the hydrostatic pressure at the ice/bed interface exceeds the mechanical load, jacking will occur under the ice sheet for a steady state pressure distribution. Figure 6-6 shows pore pressure distribution and corresponding effective stresses at 100 m and 500 m depth for values of the pressure potential between 82.5–100% of the height of the ice. Here, the ice front retreats with 300 m/year from a steady state pressure distribution. As the pressure potential increases, the largest drops in effective stress are not necessarily found at the ice front.

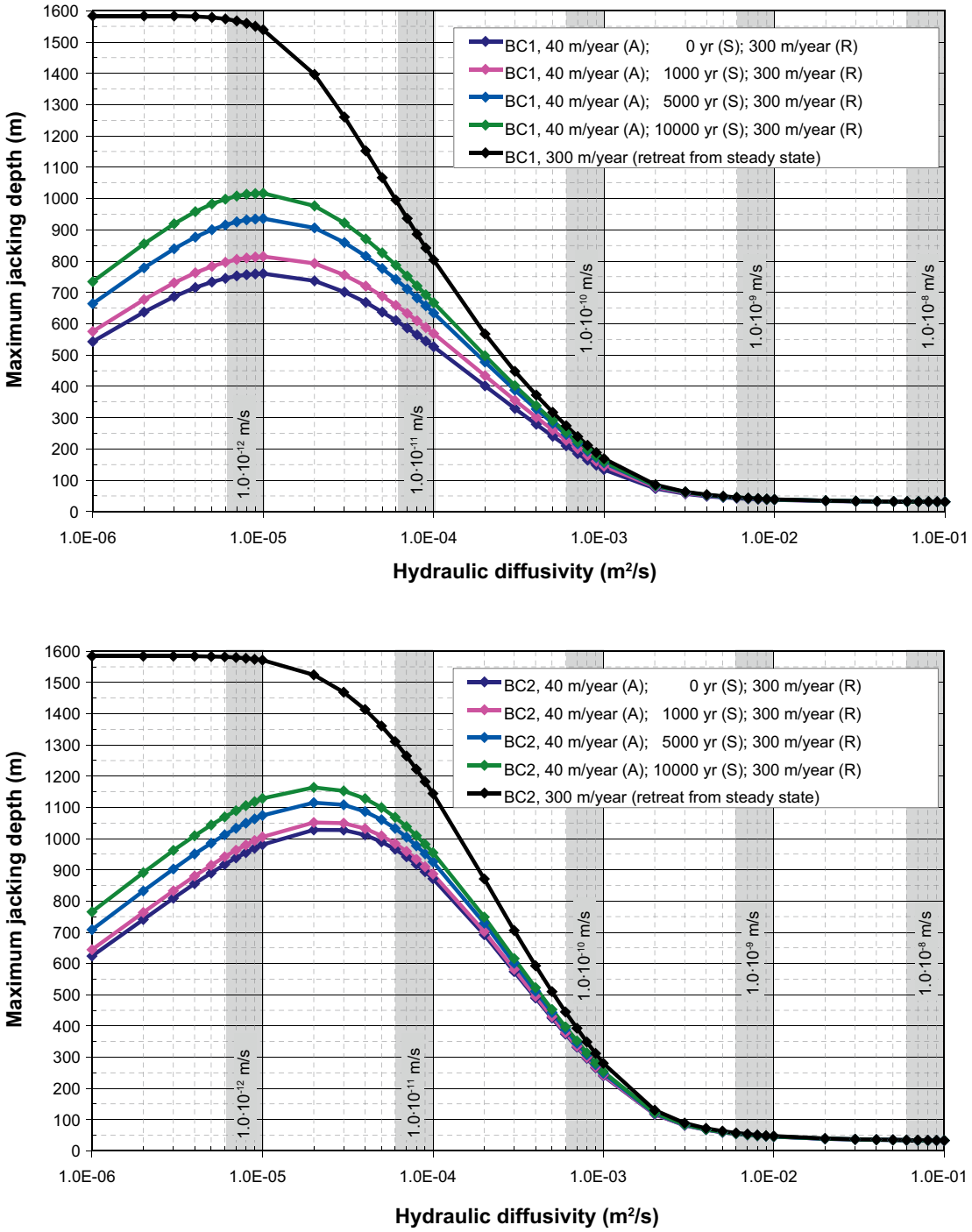

Figure 6-5. *Maximum jacking depth at the ice front as a function of hydraulic diffusivity. The ice front (A)dvances from initially zero pressure at 40 m/year for 10,000 years, is (S)tationary for a given number of years at maximum height and (R)etreats from maximum hydrostatic pressure at the ice/bed interface at 300 m/year. BC1 (change in height), top. BC2 (constant height), bottom. Grey-shaded areas indicate diffusivity ranges associated with different values of the bulk hydraulic conductivity (cf. Figure 5-4).*

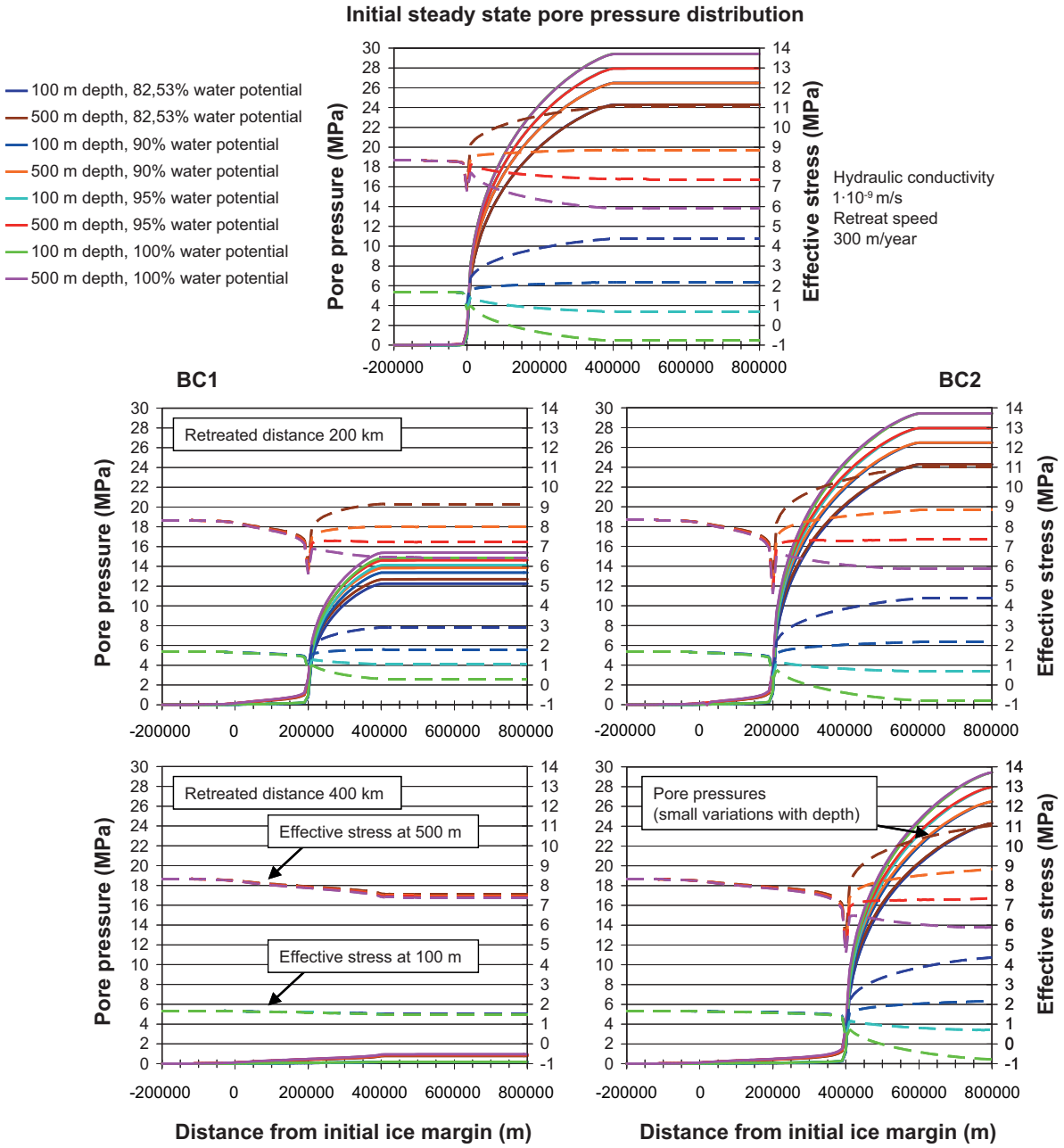

Figure 6-6. *Pore pressure distribution (solid lines, left y-axes) and corresponding effective stresses (dashed lines, right y-axes) at 100 m and 500 m depth. Top: Initial steady state conditions. Left column: Ice front retreats according to BC1 (change in height). Right column: Ice front retreats according to BC2 (constant height).*

6.4 Summary

The analytical expressions, used to assess the maximum jacking depths in the present chapter, cannot account for spatial variations of the hydraulic diffusivity. Analyses conducted in Appendix D show that the variations of the hydraulic conductivity with depth (high near the ground surface and decreasing with depth) at Forsmark and Laxemar (cf. Chapter 5) will prevent an upwards transfer of pore pressures from regions with low permeability when the ice retreats, thus allowing for faster pressure reduction in the upper parts of the rock. This will result in reduced maximum jacking depths compared with the estimates given here.

Two assumptions are made regarding the transient evolution of the ice sheet profile during the advance and subsequent retreat of the ice front denoted BC1 and BC2 (cf. Figure 3-4). In the analyses the hydrostatic pressure is set to 90% of the ice sheet thickness at all times. For this assumption regarding the hydrostatic pressure, the largest reduction of the effective vertical stress at any depth (and maximum jacking depth if hydraulic jacking occurs) is always found at positions located directly beneath the ice margin. If the hydrostatic pressure is set to a higher ratio of the ice sheet thickness (see Figure 6-6) the maximum jacking depth increases and the largest reduction in effective vertical stress may be found at positions beneath the ice sheet. However, this possibility is not considered in the assessment of the maximum jacking depths made here. The following can be concluded from the analyses regarding the jacking depths during the advancement, periods of stationary conditions and subsequent retreat of the ice front:

- If the hydraulic diffusivity is high, the pore pressure distribution during the advancement of an ice sheet is independent of the choice of boundary condition (BC1 or BC2) and may be approximated by a steady state pore pressure distribution, cf. Figure 6-2 (top). The resulting maximum jacking depth beneath the ice margin is about 30 m, cf. Figure 6-1 (right). However, for low hydraulic diffusivities and at large depths this approximation will overestimate the pore pressures, cf. Figure 6-2 (bottom). Furthermore, the results are influence by the choice of boundary condition.
- Typical bulk diffusivity values at the Forsmark and Laxemar sites are in the range $5 \cdot 10^{-3}$–1 m^2/s (corresponds to hydraulic conductivities in the range $1 \cdot 10^{-9}$–$1 \cdot 10^{-7}$ m/s and a specific storage coefficient in the range $1 \cdot 10^{-7}$–$1.9 \cdot 10^{-7}$ m^{-1}, cf. Chapter 5). In this diffusivity range, the jacking depths are of the order of 50 m and seem to be practically independent of the retreat speed (200–300 m/year), duration of the preceding period of stationary ice front conditions and choice of boundary condition (BC1 or BC2), cf. Figure 6-3 to Figure 6-5. Even for the fastest suggested retreat speed (500 m/year), the maximum jacking depth is unlikely to be more than 100 m. For lower values of the hydraulic diffusivity, the retreat speed, duration of the preceding period of stationary ice front conditions and choice of boundary condition have a significant impact on the maximum jacking depth.

7 Modelling of rock with few conductive fractures

7.1 General

Steady state models give an upper bound estimate of the magnitudes of the pore pressures during the advance of an ice sheet. In homogeneously fractured rock, the steady state pressure, where the hydrostatic pressure at the ice/bed interface corresponds to at most 90% of the height of the ice, is not sufficient to initiate hydraulic jacking at depths greater than about 30 m, cf. Figure 6-1 (right). However, long highly transmissive horizontal fractures in otherwise low permeability rock might transfer high pore pressures from areas under the ice out to the ice front, where the lack of vertical stress additions due to the ice load to counterbalance the pore pressures could potentially initiate hydraulic jacking at large depths. /Lindblom 1997/ argued that the entire pressure from the ice load could potentially be transferred to the ice margin. In the present chapter, investigations regarding conditions, under which horizontal fractures can increase the pressure to such an extent that hydraulic jacking occurs at positions near the ice front.

Based on /Lindblom's 1997/ theory, Figure 7-1 (top) shows the estimated fracture length needed in impermeable rock (indicated in the lower right part of figure) to initiate jacking at given depths beneath the ice margin given the ice sheet profile in Eq. 3-1. As seen in the figure, fracture lengths of several kilometres are needed for sufficiently high pore pressures to propagate undisturbed to the ice front and thereby initiate hydraulic jacking. For example, the minimum fracture length needed in order to initiate jacking at 200 m depth is 1.2 km (marked with a red circle) provided that the hydrostatic pressure at the ice/bed interface is 90% of the height of the ice and that the rock is perfectly impermeable everywhere. When the draining of fractures due to the rock's non-zero permeability is taken into account, the required lengths would be even greater. This observation points to the very specific conditions regarding fractures and background permeability required to initiate jacking at large depths.

In the following sections, the steady-state pore pressure distribution, and possibility of hydraulic jacking, due to a stationary ice front in low permeability rock with a few long and highly transmissive fractures is investigated numerically for a number of assumptions regarding fracture configurations and their connectivity, fracture transmissivities, and rock mass hydraulic conductivity. The steady state pore pressure distribution is studied by use of the 2D numerical code *UDEC* /Itasca 2005b/.

7.2 Subhorizontal fractures

Figure 7-2 shows deformation zones intersecting an approximately 7 km long NW-SE profile along the candidate volume at Forsmark. The majority of the gently dipping deformation zones shown in the figure intersect the right part of the profile and appear to be outside the local model volume (outlined by a box in the right part of the figure), *i.e.* the proposed location of the repository. None of the gently dipping deformation zones shown in Figure 7-2 have the required lengths to initiate hydraulic jacking at the depths shown in Figure 7-1 (lower left). Furthermore, as the major horizontal *in situ* stress at Forsmark is oriented 145° with respect to North /SKB 2008/, *i.e.* almost parallel to the NW-SE profile, the normal *in situ* stress acting on the fractures shown in the figure will be significantly greater than the vertical stress.

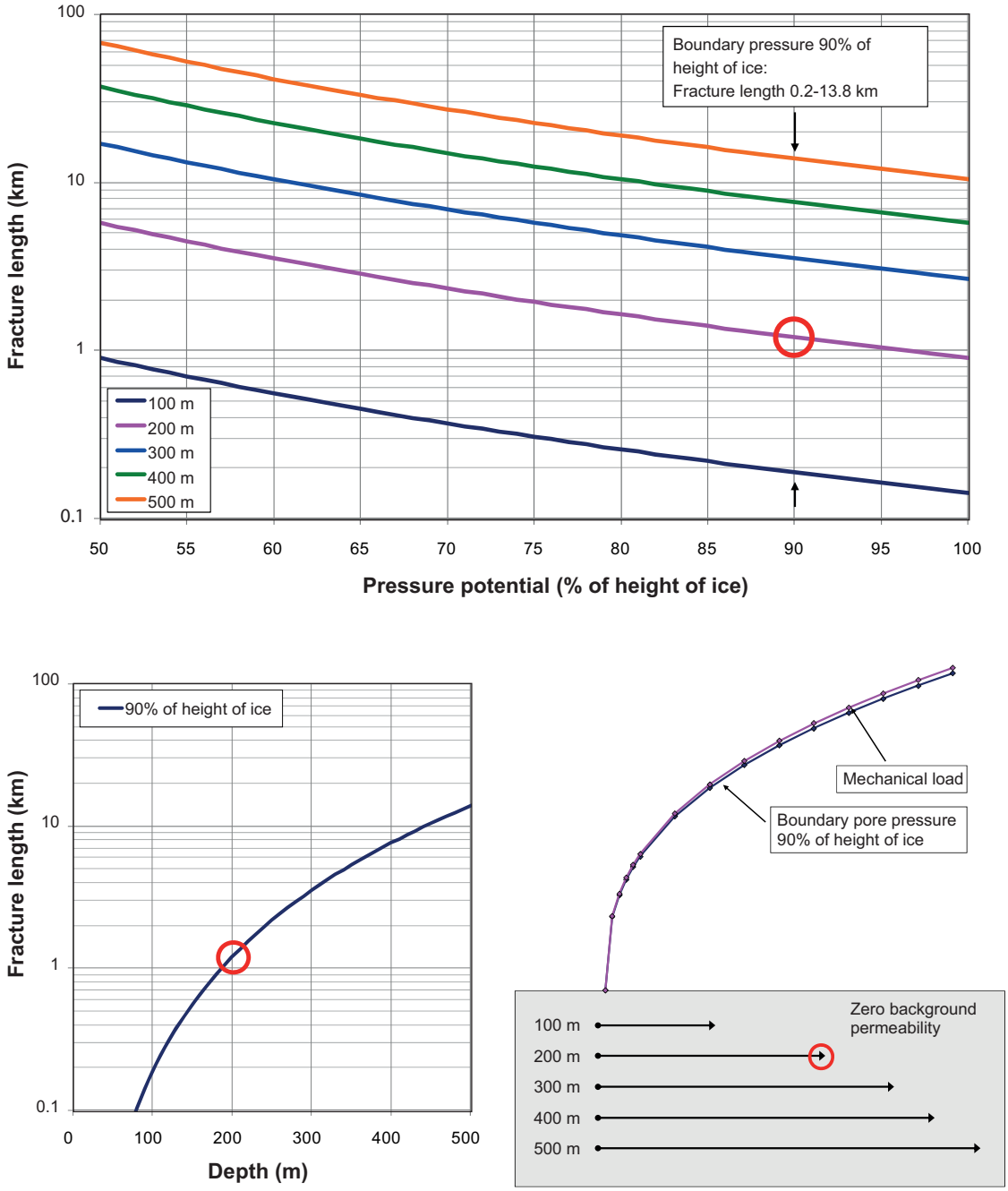

Figure 7-1. *Top: Fracture length needed in impermeable rock to initiate jacking at different depth as functions of the hydrostatic pressure potential at the ice/bed interface given the ice sheet profile of Eq. 3-1. Bottom: Fracture length as a function of depth for the base case where the hydrostatic pressure at the ice/bed interface corresponds to 90% of the height of the ice. The red circle shows fracture length at 200 m depth for a hydrostatic pressure at the ice/bed interface corresponding to 90% of the height of the ice.*

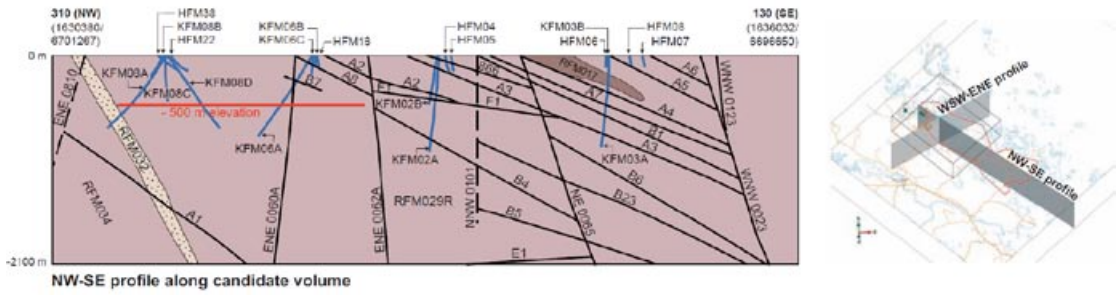

Figure 7-2. *Deformation zones in a NW-SE profile along the candidate volume at Forsmark, from /SKB 2008/.*

7.3 Description of UDEC models

7.3.1 Geometry

The *UDEC* models have dimensions 50,000 m x 5,500 m (horizontally x vertically). To simulate the rock's *in situ* permeability, a number of parallel joints separated by 150 m at an angle ±45° with respect to the *x*-axis are included in the models (see Figure 7-3, left). As the blocks in *UDEC* are impermeable, the required *in situ* rock permeability is achieved by adjusting the initial apertures in the background mesh accordingly.

In addition to the background mesh, there are five horizontal fractures at 50 m, 100 m, 300 m, 500 m and 700 m below the ground surface. Here all conducting discrete features are denoted fractures and are represented as perfectly planar entities, irrespective of their actual lengths, widths or properties, *i.e.* there are no distinctions between "fractures" and "fracture zones". The horizontal fractures extend either 2,000 m or 10,000 m beyond the ice margin with their right end a horizontal distance of 5,000 or 15,000 m under the ice. The fractures are either connected to each other and the ground surface by the background mesh, or in addition to the mesh connected by a fracture dipping 45° whose top end is located 5,000 or 15,000 m from the ice margin.

The initial value for the hydraulic apertures is specified such that no reduction of apertures is allowed under high normal stress and the initially largest apertures remain fixed during the calculations.

A schematic view of the *UDEC* model and the various fracture systems are shown in Figure 7-3 left and right, respectively. The ice front is located at the centre of the model at $x = 0$.

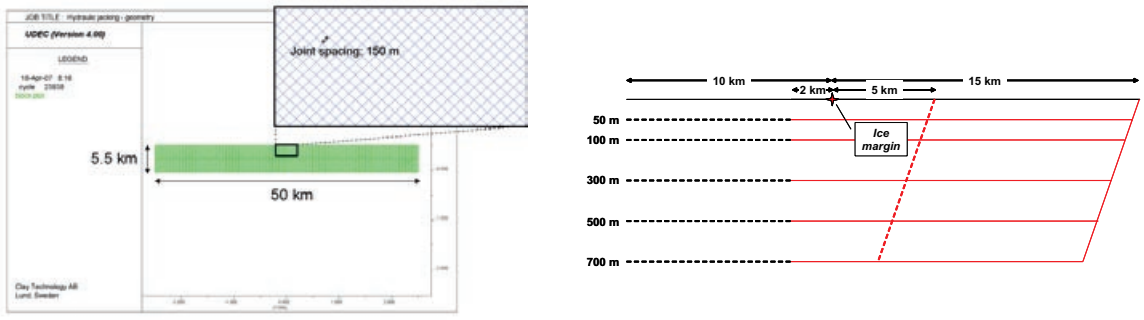

Figure 7-3. *Outline of UDEC model geometry (left). The inset shows the background mesh representing the hydraulic conductivity of the rock mass. Schematic view of the modelled fracture systems (right), not to scale.*

7.3.2 Input data

Mechanical input data (elastic properties of the rock mass and *in situ* stresses) to the numerical models are taken from the preliminary site descriptions v. 1.2 and 2.1 for Forsmark /SKB 2005, 2006c/, cf. Table 5-1. The mechanical and strength properties of the fractures are given in Table 5-2. The major and minor principal stresses are aligned with the model axes, whereas the intermediate principal stress component is ignored. The stress magnitudes are presented in Figure 5-2 as functions of depth. Note that when evaluating the resulting effective stresses and potential for jacking, the vertical stress is calculated from the weight of the overburden (rock and ice) and added in a post-processing step as described in Section 4.2.

Estimates of the hydraulic conductivity of the rock mass and fracture transmissivities are based on data from /Follin et al. 2007/, cf. Figure 5-3 and Figure 5-5. Descriptions of each of the numerical models are provided in Section 7.4 with hydraulic data given in Table 7-1.

7.3.3 Boundary conditions

Roller boundaries are applied on the bottom and vertical boundaries, *i.e.* no flexural stresses are taken into account. The left half of the top boundary is free to move in the vertical direction, whereas the right half has a vertical stress boundary representing the ice load, *i.e.* the weight of the ice in Eq. 3-1, see Figure 7-4 (left).

The initial pressure distribution is given by the hydrostatic pressure, which is also used as boundary condition on the left vertical boundary. The bottom boundary is assumed to be impermeable. The additional hydrostatic pressure on the top boundary due to the ice load is 90% of the height of the ice (*i.e.* approximately 98% of the mechanical load), cf. Figure 7-4 (left). The ice sheet is assumed to stretch out much further than the model's right boundary and reaches its maximum of 3,000 m at 400 km from the ice margin. Thus, the pore pressure on the right vertical boundary is given by the hydrostatic pressure added to the analytical steady state solution at the point 25,000 m from the ice margin (Eq. 4-7), cf. Figure 7-4 (right).

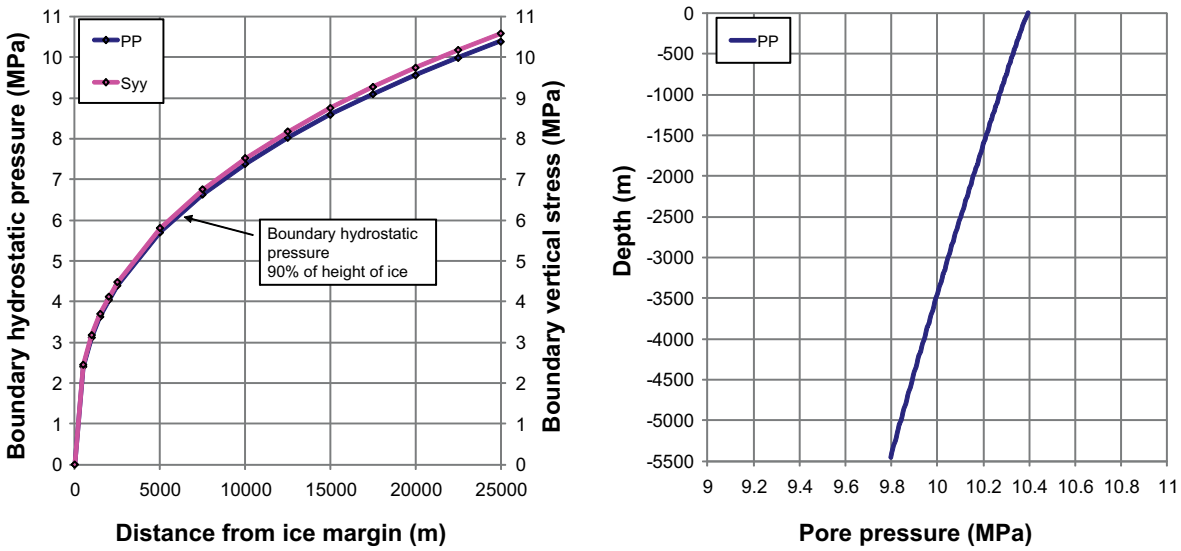

Figure 7-4. *Glacially induced vertical stress (Syy) and pressure distribution (PP) applied on the top boundary representing the ground surface (left). The excess pore pressure on the right vertical boundary is given by analytically obtained steady state pore pressures at 25 km from the ice margin as a function of depth (right).*

7.4 Model descriptions

The current work comprises the results from eight numerical models, see Table 7-1 for hydraulic properties. The following properties' effects on the maximum jacking depth are studied in particular:

- Fracture configurations
  - Number of fractures in fracture system
  - Fracture length outside ice margin
  - Fracture length beneath ice sheet
  - Fracture connection to ground surface
- Hydraulic properties
  - Homogeneous properties at all depths
  - Depth-dependent hydraulic properties

Model 1a – System of five horizontal fractures at 50, 100, 300, 500 and 700 m depth. The fractures begin 15,000 m beneath ice sheet and terminate 2,000 m beyond ice front. Connection to ground surface at 15,000 m. Constant hydraulic properties at all depths.

Model 1b – System of five horizontal fractures at 50, 100, 300, 500 and 700 m depth. The fractures begin 15,000 m beneath ice sheet and terminate 10,000 m beyond ice front. Connection to ground surface at 15,000 m. Constant hydraulic properties at all depths.

Model 1c – System of five horizontal fractures at 50, 100, 300, 500 and 700 m depth. The fractures begin 5,000 m beneath ice sheet and terminate 2,000 m beyond ice front. Connection to ground surface at 5,000 m. Constant hydraulic properties at all depths.

Model 2a – System of five horizontal fractures at 50, 100, 300, 500 and 700 m depth. The fractures begin 15,000 m beneath ice sheet and terminate 2,000 m beyond ice front. Connection to ground surface via background mesh. Constant hydraulic properties at all depths.

Model 2b – System of five horizontal fractures at 50, 100, 300, 500 and 700 m depth. The fractures begin 15,000 m beneath ice sheet and terminate 10,000 m beyond ice front. Connection to ground surface via background mesh. Constant hydraulic properties at all depths.

Model 3a – System of five horizontal fractures at 50, 100, 300, 500 and 700 m depth. The fractures begin 15,000 m beneath ice sheet and terminate 2,000 m beyond ice front. Connection to ground surface at 15,000 m. Increased background hydraulic conductivity above 400 m.

Model 6a – System of five horizontal fractures at 50, 100, 300, 500 and 700 m depth. The fractures begin 15,000 m beneath ice sheet and terminate 2,000 m beyond ice front. Connection to ground surface at 15,000 m. Increased background hydraulic conductivity above 400 m. Depth-dependent fracture transmissivity.

Model 7a – One horizontal fracture at 500 m depth. The fracture begins 15,000 m beneath ice sheet and terminates 2,000 m beyond ice front. Connection to ground surface at 15,000 m. Constant hydraulic properties at all depths.

Table 7-1. Model map and fracture hydraulic properties.

Model name	Mesh hydraulic conductivity (m/s)	Transmissivity (m^2/s) (horizontal fractures)	Transmissivity (m^2/s) (connection fracture)	Capratio[1]
Model 1a (base case)	$1 \cdot 10^{-11}$ (all depths)	$5 \cdot 10^{-8}$ (all depths)	$5 \cdot 10^{-8}$ (all depths)	1
Model 1b	$1 \cdot 10^{-11}$ (all depths)	$5 \cdot 10^{-8}$ (all depths)	–	1
Model 1c	$1 \cdot 10^{-11}$ (all depths)	$5 \cdot 10^{-8}$ (all depths)	$5 \cdot 10^{-8}$ (all depths)	1
Model 2a	$1 \cdot 10^{-11}$ (all depths)	$5 \cdot 10^{-8}$ (all depths)	$5 \cdot 10^{-8}$ (all depths)	1
Model 2b	$1 \cdot 10^{-11}$ (all depths)	$5 \cdot 10^{-8}$ (all depths)	–	1
Model 3a	$1 \cdot 10^{-9}$ (0–400 m) $1 \cdot 10^{-11}$ (400 m–)	$5 \cdot 10^{-8}$ (all depths)	$5 \cdot 10^{-8}$ (all depths)	1
Model 6a	$1 \cdot 10^{-9}$ (0–400 m) $1 \cdot 10^{-11}$ (400 m–)	$5 \cdot 10^{-5}$ (0–100 m) $5 \cdot 10^{-9}$ (300 m) $5 \cdot 10^{-7}$ (500 m) $5 \cdot 10^{-8}$ (700 m)	$4.93 \cdot 10^{-4}$ (0–100 m) $1.20 \cdot 10^{-4}$ (100–200 m) $2.91 \cdot 10^{-5}$ (200–300 m) $7.07 \cdot 10^{-6}$ (300–400 m) $1.72 \cdot 10^{-6}$ (400–500 m) $4.17 \cdot 10^{-7}$ (500–600 m) $1.01 \cdot 10^{-7}$ (600–700 m)	1
Model 7a	$1 \cdot 10^{-11}$ (all depths)	$5 \cdot 10^{-8}$ (500 m)	$5 \cdot 10^{-8}$ (all depths)	1

1. The maximum contact hydraulic aperture is given by the value of Capratio multiplied by the maximum residual aperture in the model.

7.5 Results

7.5.1 Fracture configurations

The number of fractures in the fracture system, their lengths both under the ice and beyond ice front as well as a direct connection (and its location) to the ground surface at high pressure will have an impact on the maximum jacking depth. In the current section, the rock mass has a hydraulic conductivity of 10^{-11} m/s at all depths and the fractures have a transmissivity of $5 \cdot 10^{-8}$ m^2/s.

Number of fractures in fracture system

Figure 7-5 shows the effective stress as a function of depth for two assumptions regarding the number of fractures in the fracture system:

- Model 1a – System of five fractures at 50, 100, 300, 500 and 700 m depth.
- Model 7a – One fracture at 500 m depth.

In both cases the fractures start a horizontal distance of 15,000 m in under the ice, where there is direct connection to the ground surface, and terminate 2,000 m from the ice margin.

As seen in the figure, the system of several fractures tends to increase the excess pore pressure near the ice margin compared with the case with a single fracture and thus cause jacking.

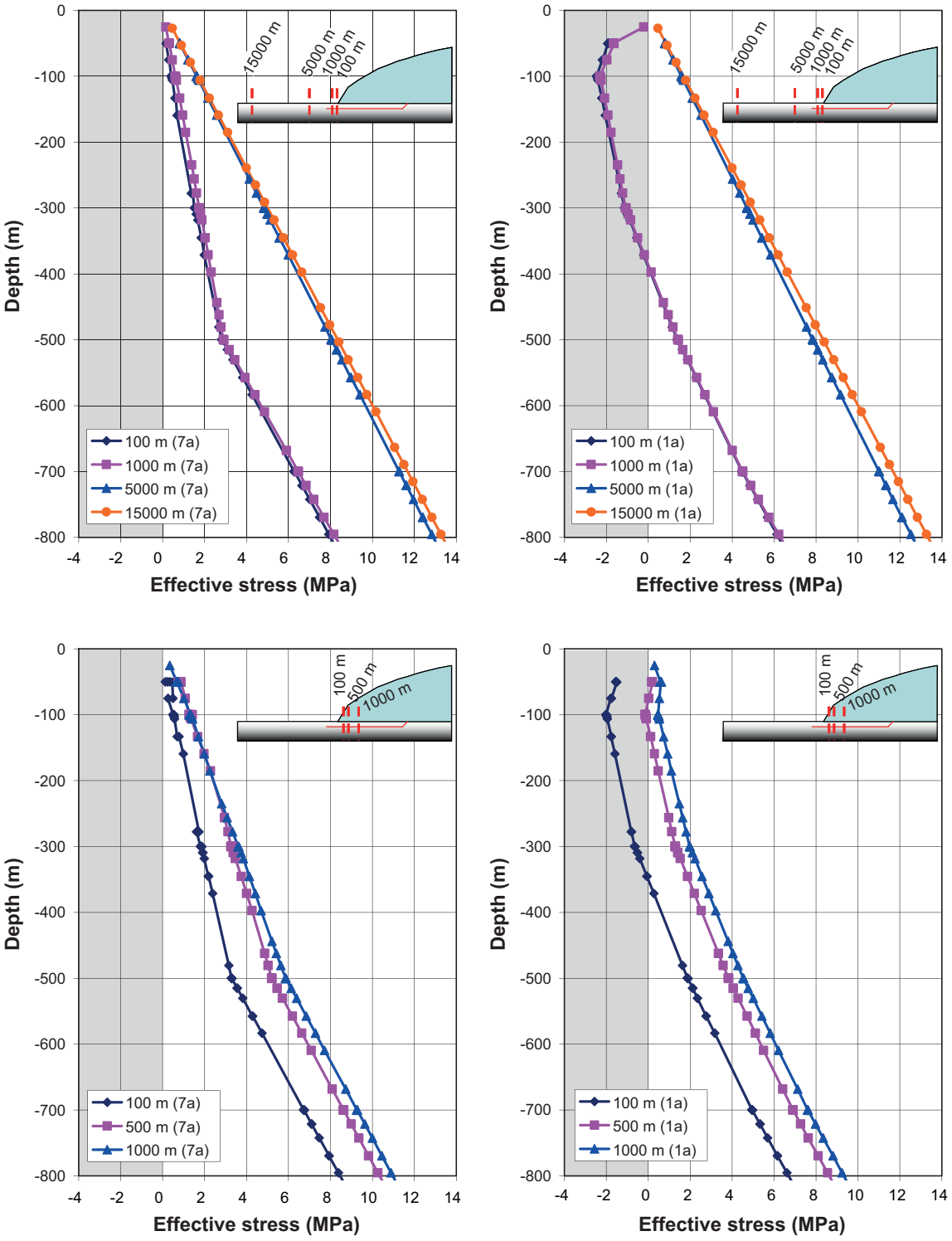

Figure 7-5. *Effective vertical stress at given positions from the ice front. Grey areas represent depths to which jacking can occur. Left column: One single fracture at 500 m depth connected to the ground surface at high pressure. Right column: System of fractures at 50, 100, 300, 500 and 700 m depth connected to the ground surface at high pressure.*

Fracture lengths and connectivity

The fractures' lengths have a significant effect on the maximum jacking depth, both in terms of the length under the ice and the distance it can transfer the pore pressures beyond the ice front. In the current section, comparisons are made between fracture systems of different lengths as well as the effects of a direct link to the ground surface at high pressure.

Figure 7-6 (beyond the ice margin) and Figure 7-7 (beneath the ice sheet) show the effective stress as functions of depth for three different assumptions regarding fracture length:

- Model 1c – Fractures start 5,000 m from the ice front and terminate 2,000 m beyond the ice front (left).
- Model 1a – Fractures start 15,000 m from the ice front and terminate 2,000 m beyond the ice front (middle).
- Model 1b – Fractures start 15,000 m from the ice front and terminate 10,000 m beyond the ice front (right).

As seen in the figures, fractures that start at far under the ice and terminate a short distance beyond the ice front result in the largest jacking depths. A large extension of the fractures beyond ice front will decrease the jacking depth further as will fractures with their starting point nearer to the ice margin.

At positions near the ice margin, the maximum jacking depths are 275–300 m (Model 1c), 350–400 m (Model 1a) and 225–280 m (Model 1b). Even though Model 1b has the smallest jacking depth of the three models, the risk of jacking extends to a much further horizontal distance away from the ice margin than in the other two models.

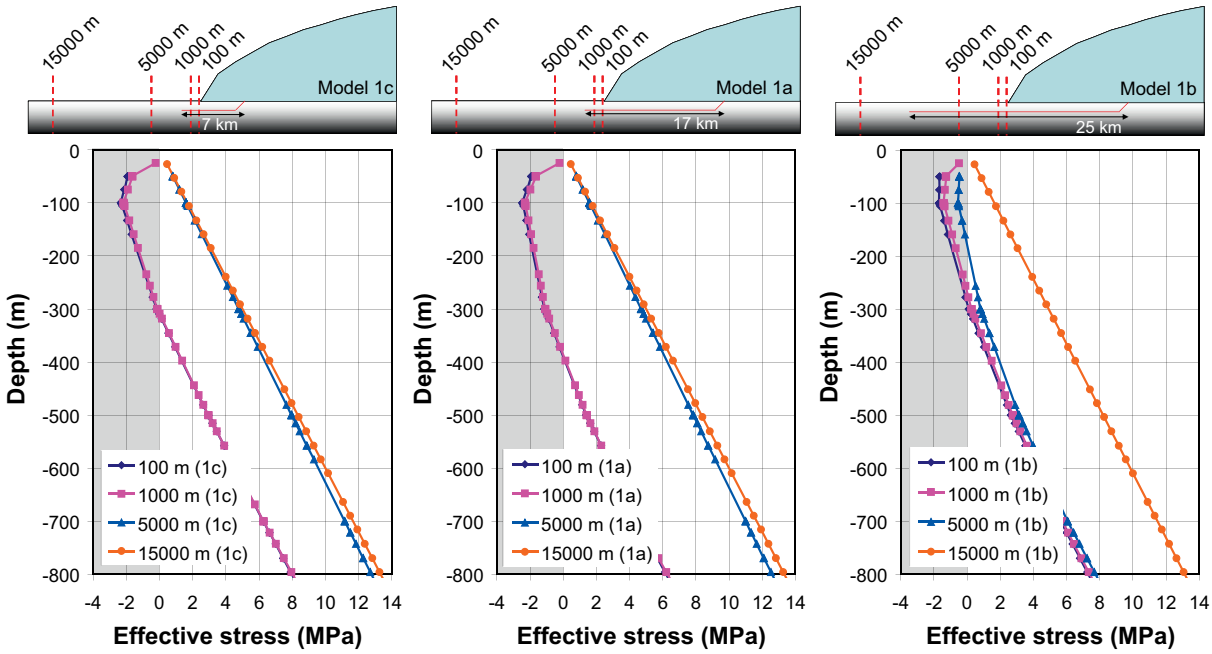

Figure 7-6. *Effects due to length of fractures. Left: Short fractures, start and terminate near the ice front. Middle: Long fractures, start at positions far under the ice and terminate near the ice front. Right: Long fractures, start and terminate far from the ice front.*

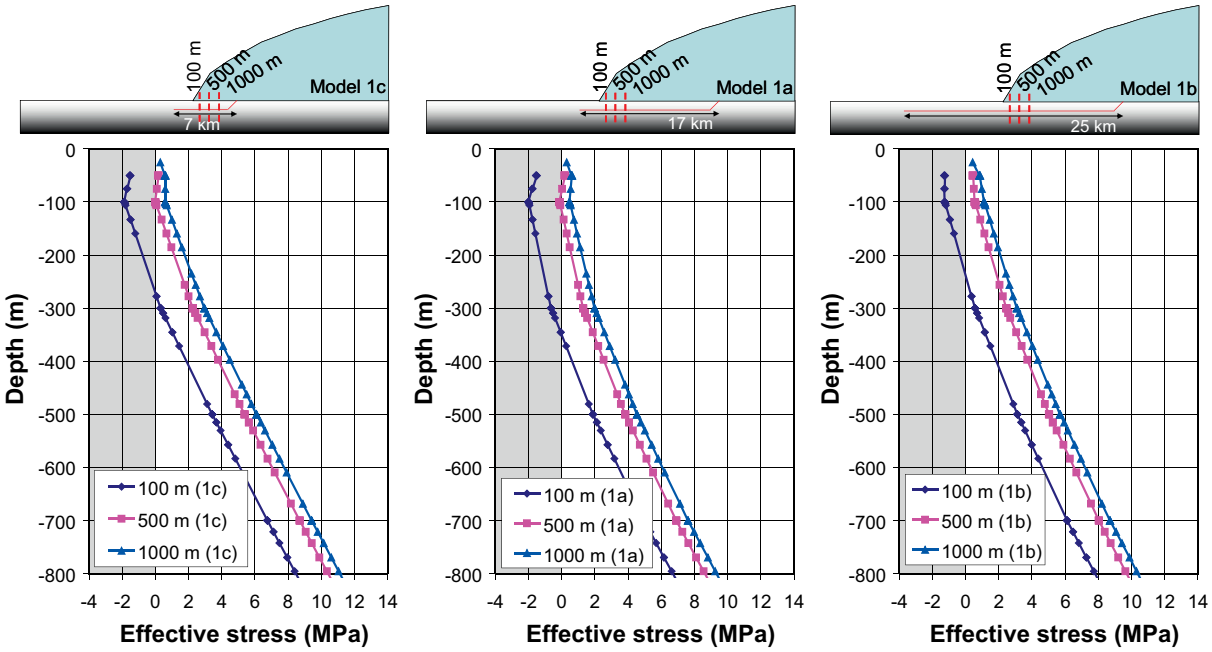

Figure 7-7. *Effects due to length of fractures. Left: Short fractures, start and terminate near the ice front. Middle: Long fractures, start at positions far under the ice and terminate near the ice front. Right: Long fractures, start and terminate far from the ice front.*

A direct connection to the ground surface at high pressure will also increase the jacking depth, but to a much smaller degree. Figure 7-8 (beyond ice margin) and Figure 7-9 (beneath the ice sheet) show the effective stress as functions of depth for four different assumptions regarding fracture connectivity:

- Model 1a – Fractures terminate 2,000 m from the ice margin. Direct connection the ground surface at high pressure (top left).
- Model 1b – Fractures terminate 10,000 m from the ice margin. Direct connection the ground surface at high pressure (top right).
- Model 2a – Fractures terminate 2,000 m from the ice margin. Connection to the ground surface via background mesh (bottom left).
- Model 2b – Fractures terminate 10,000 m from the ice margin. Connection to the ground surface via background mesh (bottom right).

At shallow depths, the pore pressure in the fractures is mainly governed by the hydrostatic pressure at the ice/bed interface. At greater depths the pressures are governed by the pressure in the connecting fracture (Models 1a and b). In Models 2a and b where the horizontal fractures are only connected to each other by the background mesh, the pressures are averaged over the length of the fractures.

Jacking is possible to a depth of 300–400 m in the models where the fractures terminate 2 km from the ice margin (Models 1a and 2a). The corresponding jacking depths for the models where the fractures terminate 10 km from the ice margin (Models 1b and 2b) are around 200–300 m. The first 100 m under the ice sheet, jacking is possible to depths of between 250–350 m in the models with the shorter fractures and 150–250 m in the models with longer fractures. 500 m and further in under the ice sheet, the glacially induced vertical stress counter-balances the pore pressures and consequently jacking will not occur. Consequently, in these four models, the presence of a direct connection to the ground surface at high pressure adds 50–100 m to the jacking depth.

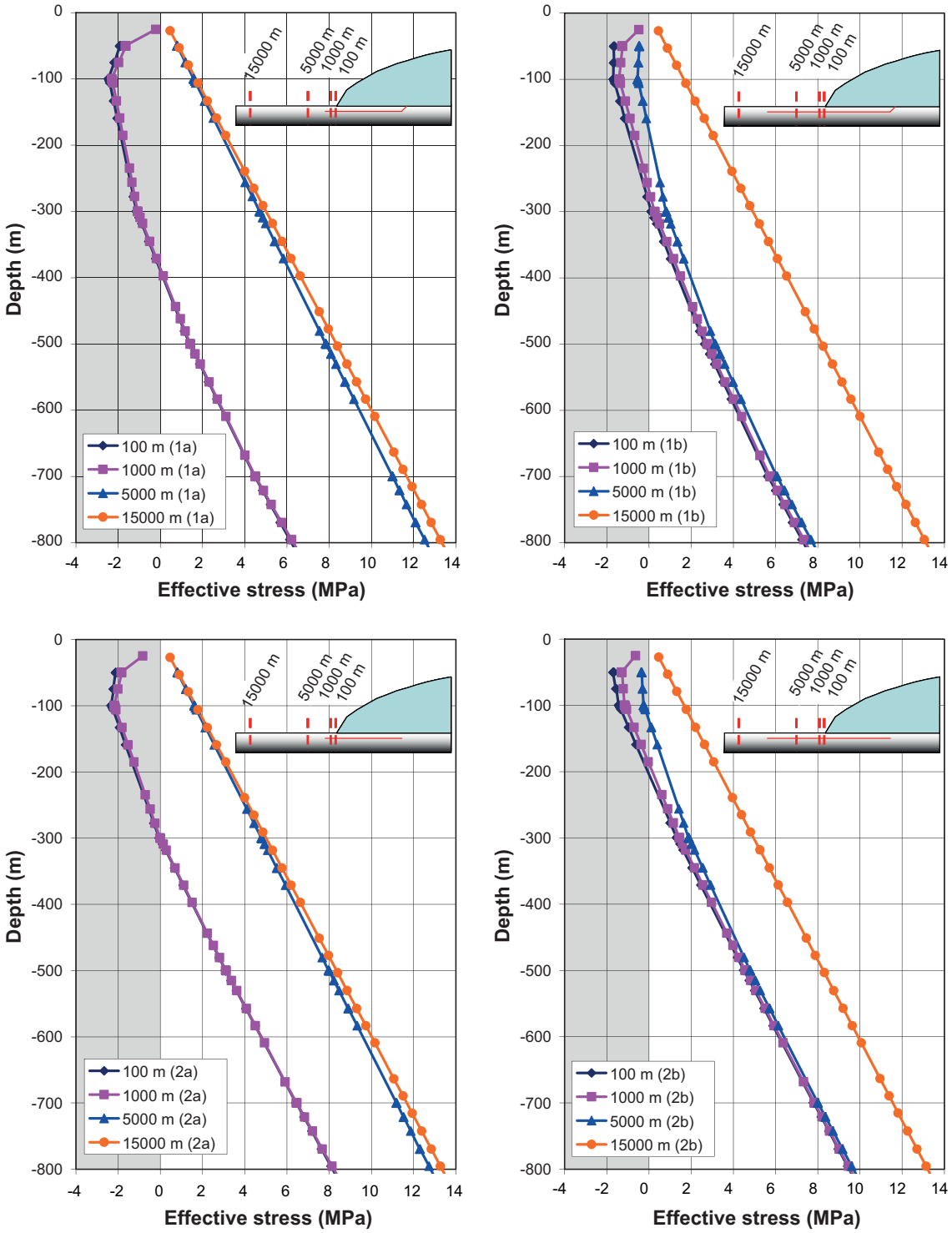

Figure 7-8. *Effective vertical stress at given positions from the ice front. Grey areas represent depths to which jacking can occur. The maximum jacking depth, 400 m, is found in the upper left with horizontal fractures extending 15 km into the high pressure region under the ice, but only 2 km into the low pressure region outside the ice, and with direct connection to the high-pressure boundary at the ice-ground interface. The other fracture constellations give smaller jacking depths.*

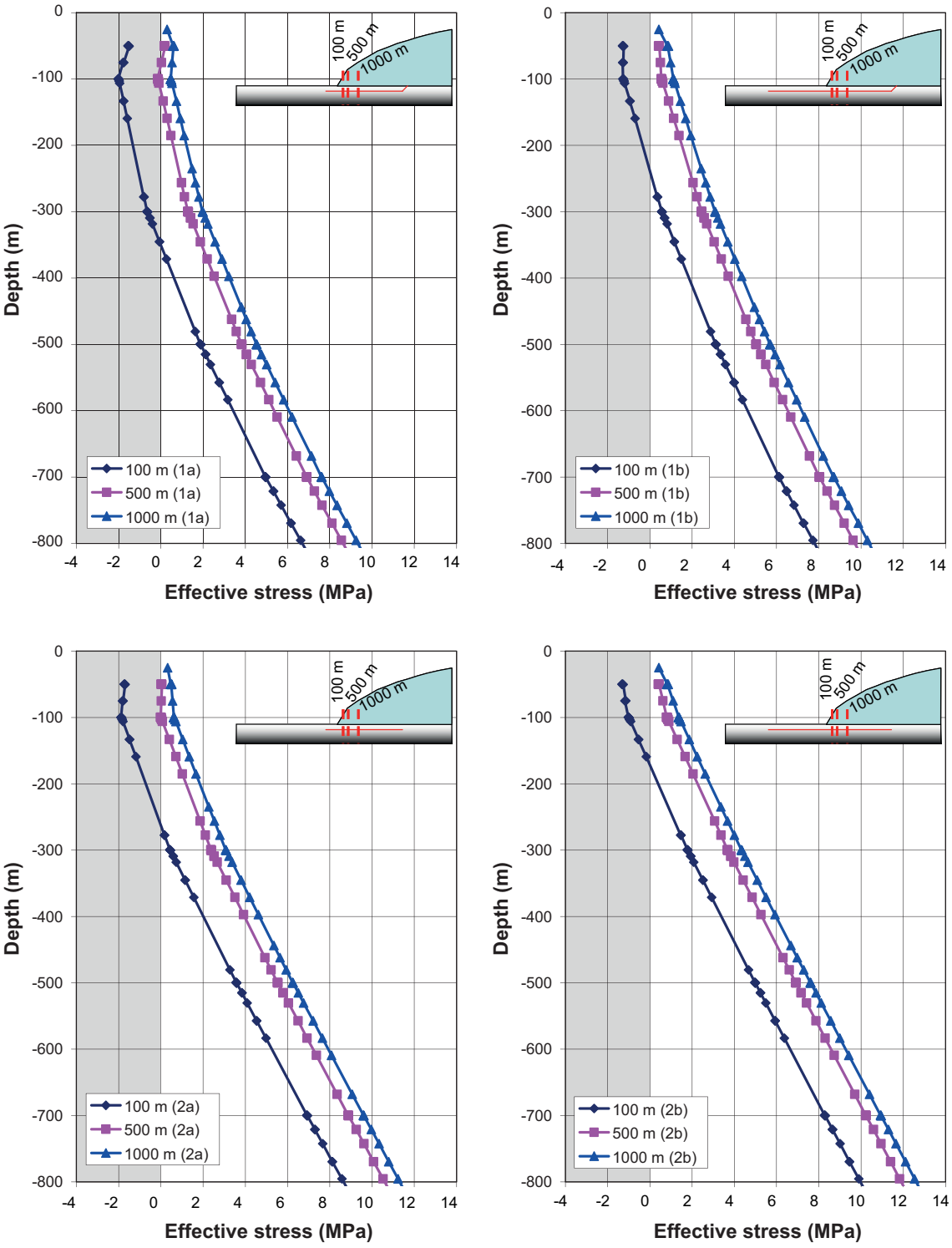

Figure 7-9. *Effective vertical stress at given positions beneath the ice sheet. Grey areas represent depths to which jacking can occur. The maximum jacking depth, 350 m, is found in the upper left with horizontal fractures extending 15 km into the high pressure region under the ice, but only 2 km into the low pressure region outside the ice, and with direct connection to the high-pressure boundary at the ice-ground interface. The other fracture constellations give smaller jacking depths.*

7.5.2 Depth-dependent hydraulic properties

As seen in the previous section, the largest jacking depths are found in Model 1a, where the horizontal fractures extend 15 km into the high pressure region under the ice, but only 2 km into the low pressure region outside the ice, and with direct connection to the high-pressure boundary at the ice-ground interface. In the following, the fracture configuration in Model 1a, is used and the hydraulic properties of the rock and fractures are varied.

Figure 7-10 and Figure 7-11 show the resulting effective stresses positions beyond the ice front and under the ice sheet, respectively, as a function of depth for three different assumptions regarding fracture transmissivity and background permeability:

- Model 1a (top left) – constant fracture transmissivity and low background conductivity (same as in the previous section).
- Model 3a (top right) – same as Model 1a, but increased background hydraulic conductivity above 400 m.
- Model 6a (bottom left) – same as Model 3a and depth-dependent transmissivity in all fractures.

In Model 1a, the maximum jacking depth is about 400 m. Increasing the background hydraulic conductivity in the upper parts of the rock to $1.0 \cdot 10^{-9}$ m/s (Model 3a), will remove the risk of jacking completely. When the contrasts between the background permeability and fracture transmissivity are yet again increased (Model 6a), the maximum jacking depth is 450 m.

Jacking of horizontal fractures is not exclusively a problem beyond the ice front. It is also possible that highly permeable fractures can increase the pressure to such an extent that jacking occurs under the ice sheet.

In Model 1a (top left), jacking is possible to a depth of about 350 m for the first 100 m under the ice sheet. At horizontal distances of 500 m and more in under the ice sheet, the glacially induced vertical stress counterbalances the pore pressures and consequently jacking will not occur. In the model with higher background conductivity in the upper parts of the rock (Model 3a), jacking will not occur anywhere under ice sheet. In Model 6a, the maximum jacking depth is 400 m a horizontal distance 100 m under the ice sheet and decreases to about 225 m a horizontal distance of 1,000 m under the ice sheet.

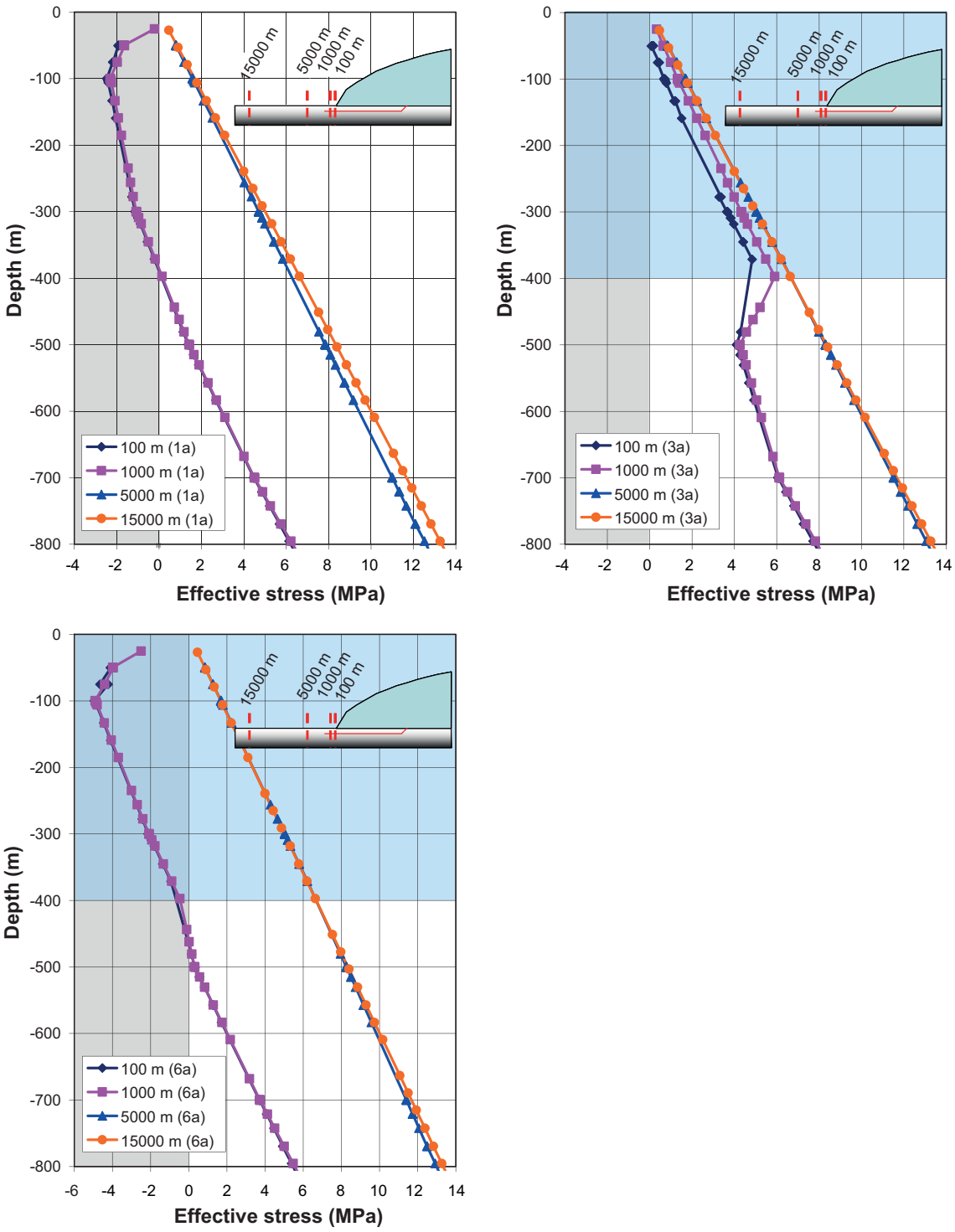

Figure 7-10. *Effective vertical stress at given positions away from the ice front. Jacking can occur when effective stress is negative. Top left: Uniform low background conductivity, and constant fracture transmissivity. Top right: Increased background conductivity above 400 m (marked in blue). Bottom left: Increased background conductivity above 400 m (marked in blue) and depth-dependent transmissivity in all fractures.*

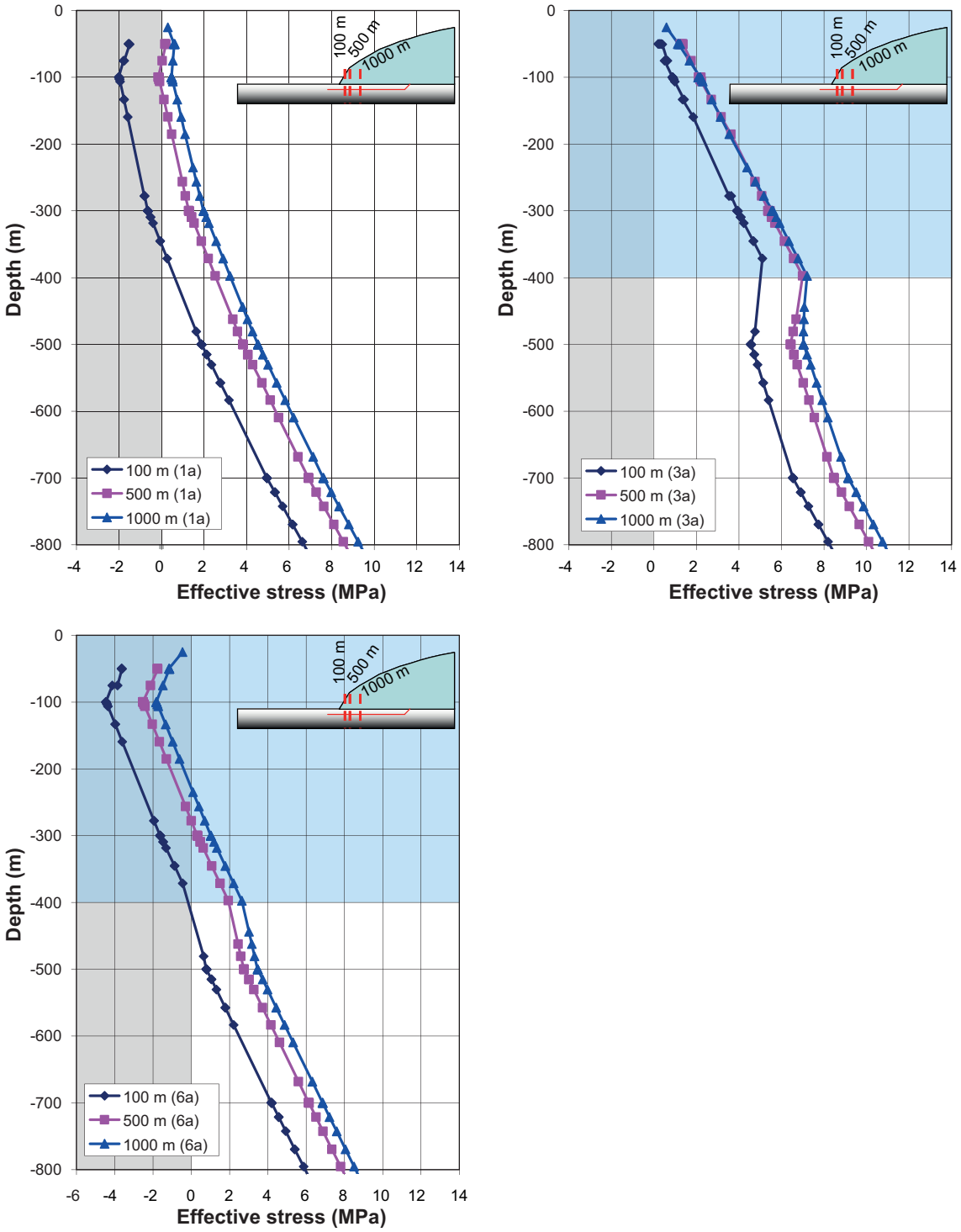

Figure 7-11. *Effective vertical stress at given positions beneath the ice sheet. Jacking can occur when effective stress is negative. Top left: Uniform low background conductivity, and constant fracture transmissivity. Top right: Increased background conductivity above 400 m (marked in blue). Bottom left: Increased background conductivity above 400 m (marked in blue) and depth-dependent transmissivity in all fractures.*

7.6 Summary

In order for hydraulic jacking to be initiated at large depths, there need to be very long, highly transmissive, horizontal or gently dipping fractures with one end at a position with high excess pore pressure and the other at a short distance beyond the ice margin. Analytical estimates suggest that fracture lengths of around 10 km or more are needed in impermeable rock to initiate jacking at repository depth (Figure 7-1, lower left). In accordance with the conditions favouring hydraulic jacking a great depths by /Hökmark et al. 2006/ (cf. Chapter 1), the following can be concluded from the 2D numerical models (a summary of the maximum jacking obtained from each numerical model is provided in Table 7-2):

- A direct connection to the ground surface at the high pressure end will increase the jacking depth (Figure 7-8 and Figure 7-9).
- Reducing the lengths under the ice sheet or extending the fractures' lengths outside the ice margin will result in smaller jacking depths (Figure 7-6 and Figure 7-7). Although the fracture length beneath the ice sheet is reduced to a third in Figure 7-6 (left), there is a comparatively small reduction in jacking depth. As the ice sheet profile is steepest near the ice margin, further reductions in fracture length under the ice will result in more substantial reductions in jacking depth.
- A system of long horizontal fractures will increase the pore pressure at the ice margin compared with a single fracture, cf. Figure 7-5.
- The depth-dependency of the hydraulic conductivity at Forsmark is likely to reduce the jacking depth, cf. Figure 7-10 (top right), Figure 7-11 (top right) and Appendix D.
- Although hydraulic jacking can be observed to a depth of 450 m in Model 6a (Figure 7-10, lower left), it should be noted that the fractures in this model extend 15 km in under the ice sheet. Such fractures have not been observed at Forsmark, cf. Figure 7-2. Furthermore, the contrasts between the hydraulic conductivity in the upper 400 m of the rock and the transmissivity of the fractures may have been exaggerated, cf. Figure 5-3 and Figure 5-5.

Table 7-2. Summary of model results.

Model code	Maximum jacking depth (m)
Model 1a	400 m
Model 1b	280 m
Model 1c	300 m
Model 2a	300 m
Model 2b	200 m
Model 3a	No jacking
Model 6a	450 m
Model 7a	No jacking

8 Permafrost impact

8.1 General

The time period leading up to a glaciation is characterized by cold climate during which permafrost in many cases may develop in front of an advancing ice sheet. Permafrost is defined as ground that remains at or below 0°C for at least two consecutive years /Gascoyne 2000/ and can be considered to be a more or less impermeable layer /e.g. Vidstrand 2003/, which considerably reduces or prevents vertical and lateral flow of groundwater. However, at large depths below the permafrost, the groundwater flow is relatively unaffected /McEwen and de Marsily 1991/.

In the reference glaciation cycle of the SR-Can safety assessment /SKB 2006b/, the Forsmark and Laxemar sites experience two major glacial advances and subsequent retreats, see Figure 3-1. Preceding each glacial advance, both sites are located above sea-level with permafrost conditions as the ice front advances towards and over them /SKB 2006b/. During the most severe permafrost period in the reference glacial cycle the permafrost reaches a maximum depth of 250 m at Forsmark and 160 m at Laxemar /SKB 2006b/, cf. Figure 8-1. Furthermore, sensitivity analyses show that it is possible for permafrost to reach repository level (approximately 400 m) at Forsmark, whereas this is unlikely at Laxemar even for surface conditions very favourable for permafrost growth /SKB 2006b/. The difference in maximum permafrost depth at the two sites is mainly due to differences in the thermal properties of the bedrock and differences in geographical location, which in turn affect climate, ice sheet evolution and permafrost development /SKB 2006b/.

In the model results of SR-Can /SKB 2006b/ it was seen that when the ice sheet comes to cover the Forsmark and Laxemar sites, the permafrost under the ice sheet generally stopped growing at the sites and started to degrade. This general picture is used in the design of the more generic permafrost cases in the present study.

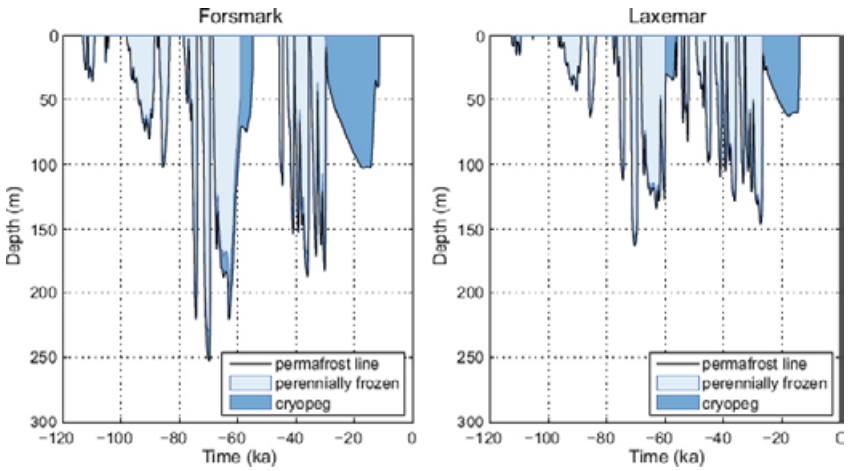

Figure 8-1. *Calculated maximum depths of permafrost, perennially frozen ground and cryopeg (part of ground where water remains unfrozen at sub-zero temperatures) for the reference glacial cycle at Forsmark and Laxemar, from /SKB 2006a/.*

The present study concerns the potential for hydraulic jacking during combined glacial and permafrost conditions. Two main scenarios are considered. The first scenario relates to the situation with continuous permafrost in front of the advancing ice sheet, cf. Section 8.3. Continuous permafrost is defined as areas with more than 90% permafrost coverage although in the present modelling work it represents a situation without taliks (unfrozen parts in the permafrost body). The second scenario considers the possible occurrence of open taliks in the near vicinity of the repository region, cf. Section 8.4. A number of issues have been identified, which could have an impact on the potential for hydraulic jacking and the associated maximum jacking depth (cf. Figure 8-2):

- Permeability of the rock below the permafrost.
- Permafrost depth.
- Melting rate of the permafrost (determines the distance between the permafrost melt zone and the ice margin).
- Distance from the repository site to the ice margin at the time when the permafrost layer has first melted at some position behind the advancing ice front. In the present modelling work, it is assumed that combined glacial and permafrost conditions may prevail for up to 10,000 years, cf. Figure 3-1 (last glacial advance and retreat) and Figure 8-1. As a typical figure of the speed by which the ice front is advancing is 40 m/year /SKB 2006a/, the furthest distance the repository can be located at, in order to be located directly beneath the ice margin at some point during the advancement of the ice front, is 400 km.
- Seasonal boundary pressure variations at the permafrost melt zone.

8.2 Permafrost thickness and melting rates

Based on the results of SR-Can (Figure 8-1), the initial thickness of the permafrost is set to 200 m (approximately the mean value of the maximum permafrost thickness at Forsmark and Laxemar in the reference glacial cycle). The permafrost is assumed to start melting from below in the areas the ice sheet covers as it advances over the site. In front of the ice sheet, the permafrost thickness remains constant. The melting rate of the permafrost depends mainly on how long the ice sheet is cold based or warm based. For the purpose of this study, three different scenarios regarding permafrost melting rate /SKB 2006a/ are investigated (cf. Figure 8-3):

- **Case A:** This case is based on the main scenario in SR-Can /SKB 2006a/. The permafrost melts linearly, from below, by 0.03 m/a during the first 4,300 years (*i.e.* 125 m) and thereafter the remaining 75 m in 30 years (2.5 m/a).
- **Case B:** The permafrost melts linearly, from below, by 1 m/a for 200 years.
- **Case C:** The 200 m of permafrost melt linearly, from below, in 7,900 years (0.025 m/a).

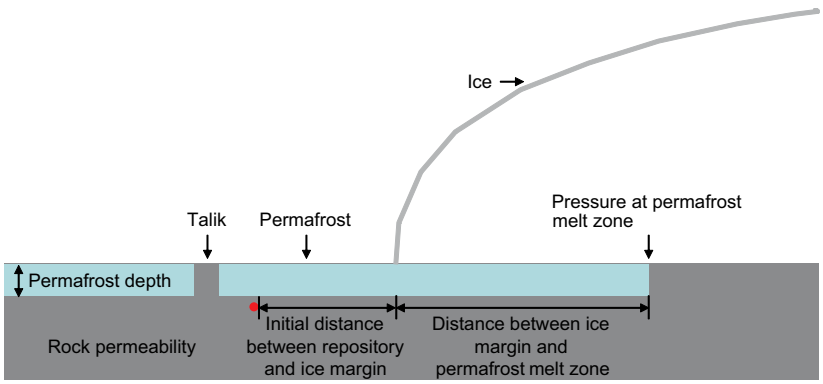

Figure 8-2. *Schematic view of issues that have the potential to influence the maximum jacking depth during permafrost conditions.*

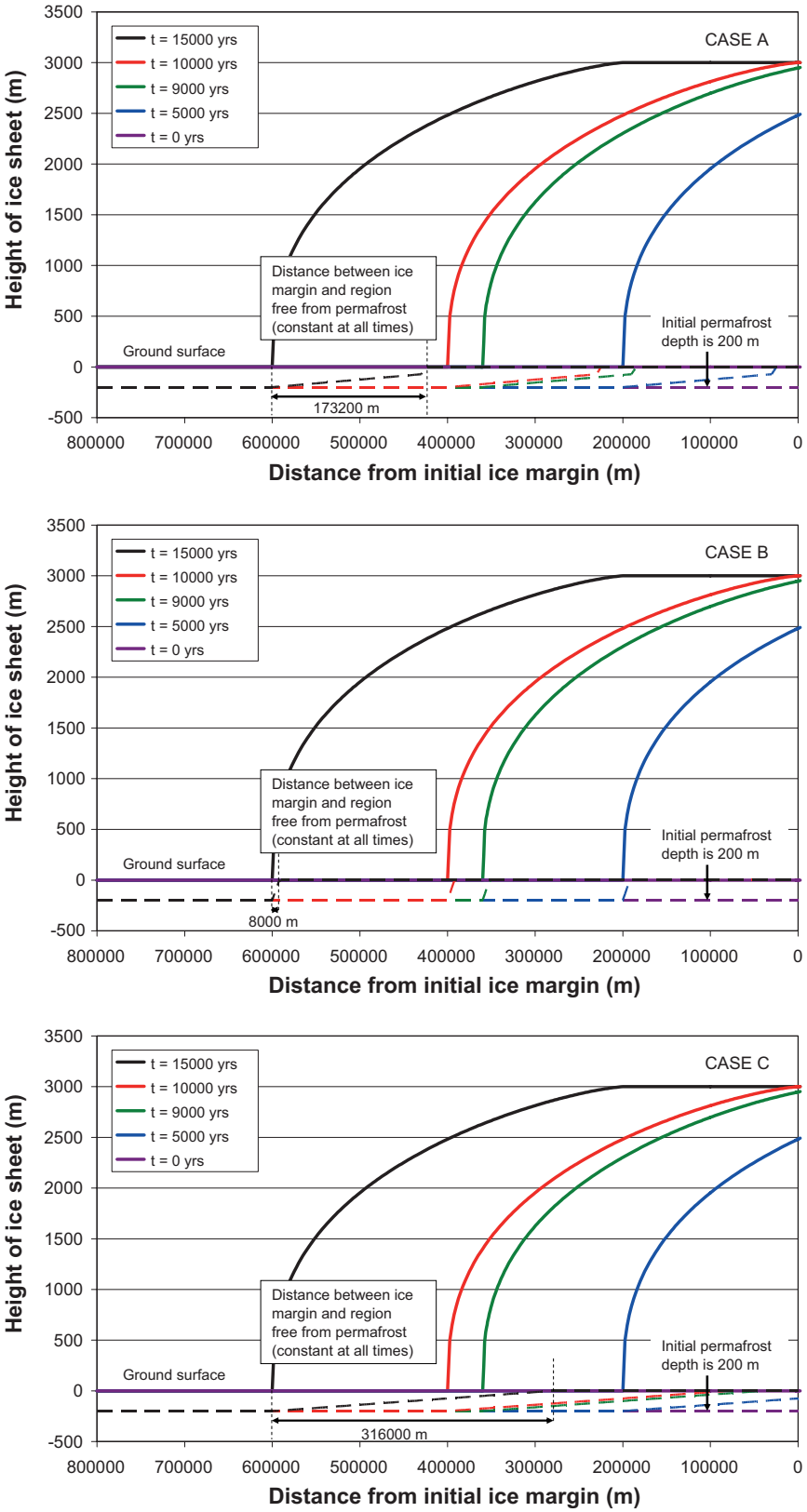

Figure 8-3. *Visualisation of the three permafrost melting rates Cases A, B and C (see main text). Solid lines represent the position of the advancing ice front at given times. At time t = 0 years the permafrost layer has first melted at some position behind the advancing ice front. Dashed lines represent the corresponding permafrost depth at given times (same colour scheme as for the solid lines applies).*

8.3 Continuous permafrost without taliks

8.3.1 Description of numerical models

The evolution of the excess pore pressure beneath continuous permafrost without taliks is investigated in 2D by use of the thermal logic in the numerical code Code_Bright /CIMNE 2004/ (cf. subsection 4.4.1). Here, the rock mass is represented by a rectangular block – 500.5 km (width) by 40 km (depth), cf. Figure 8-4. As, for a given permafrost melting rate, the distance between the permafrost melt zone and the ice margin remains constant during the advancement of the ice front (cf. Figure 8-2 and Figure 8-3), one major simplification to the problem is made. Instead of letting the ice front advance across the landscape, it remains stationary during the entire modelled period at maximum height (cf. Figure 3-3, black curve) and the point of interest, *i.e.* that representing the repository, moves towards the ice margin. The hydrostatic pressure, on parts of the ice/bed interface not covered by permafrost, is as in previous sections kept at 90% of the height of the ice (approximately 98% of the mechanical load) during the entire modelled period, without account of any seasonal variations (unless explicitly stated otherwise) and the initial excess pore pressure is assumed to be zero. The other boundaries are impermeable. The model is subdivided into three layers with the mesh graded in such a way that it is finest near the ice margin and increases with distance from that point:

- 0–200 m (permafrost layer). In the numerical models, all areas covered by permafrost are impermeable ($\kappa = 1.0 \cdot 10^{-14}$ m^2/s). The linear reduction in permafrost depth shown in Figure 8-3 is judged to be of little importance; therefore the permafrost is represented by a rectangular region of uniform thickness.
- 200–400 m (layer of rock with high diffusivity). Based on site data, cf. Section 5.1, the diffusivity in this layer is set to either $1.0 \cdot 10^{-1}$ m^2/s (denoted 'high') or $1.0 \cdot 10^{-2}$ m^2/s (denoted 'low'). The diffusivity in regions behind the permafrost melt zone, which are above 200 m but not covered by permafrost, is set to the same value.
- Below 400 m (layer of rock with low diffusivity). The diffusivity in all regions below 400 m is set to $1.0 \cdot 10^{-4}$ m^2/s.

8.3.2 Results

Importance of distance between permafrost melt zone and ice margin

If the permeability in the near-surface parts of the rock is considerably higher than below, the propagation of pore pressures in this layer can be approximated by a 1D expression. Although the 1D approach will overestimate the excess pore pressures (and corresponding maximum jacking depths) as in reality the flow will not be purely horizontal, it will give a good idea of the importance of the input parameters (*i.e.* diffusivity and permafrost melting rates). It also allows for the possibility to quickly rule out certain combinations of parameters without having to rely on extensive and time consuming numerical work. Results from the 1D analyses (presented in Appendix E) show that for the 'low' diffusivity (here $1.0 \cdot 10^{-2}$ m^2/s), hydraulic jacking will not be initiated beneath the permafrost for the melting rates Cases A and C (see Section 8.2). For the melting rate Case B, the maximum jacking depth is around 400 m. However, for the 'high' diffusivity (here $1.0 \cdot 10^{-1}$ m^2/s), the 1D results show that excess pore pressure is sufficiently high to initiate hydraulic jacking at depths of several hundred metres for all three melting rates.

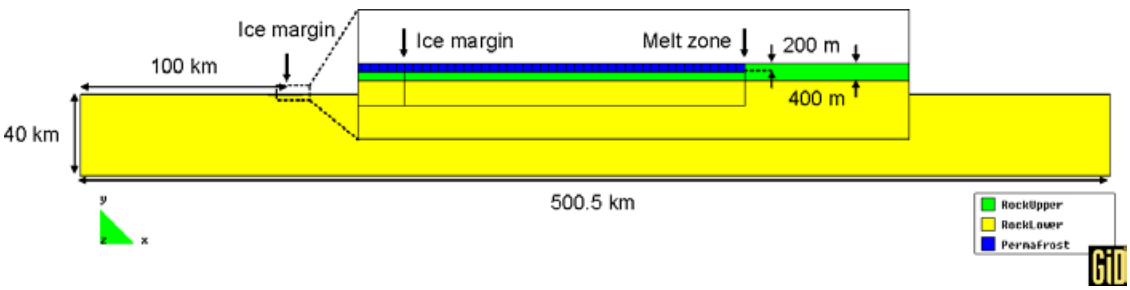

Figure 8-4. *Schematic view of Code_Bright model.*

Similarly to the modelling work where the influence of permafrost is not considered, the maximum jacking depth is found at positions directly beneath the ice margin. Figure 8-5 (top) shows numerical estimates of the maximum excess pore pressure beneath the permafrost at the ice margin as functions of distance between the permafrost melt zone and the ice margin. There are negligible variations in excess pore pressure with depth in the high-diffusivity upper part of the rock. Therefore, the excess pore pressures can be translated into maximum jacking depths (*i.e.* depth where the effective vertical stress is zero). These are shown in the lower part of the figure.

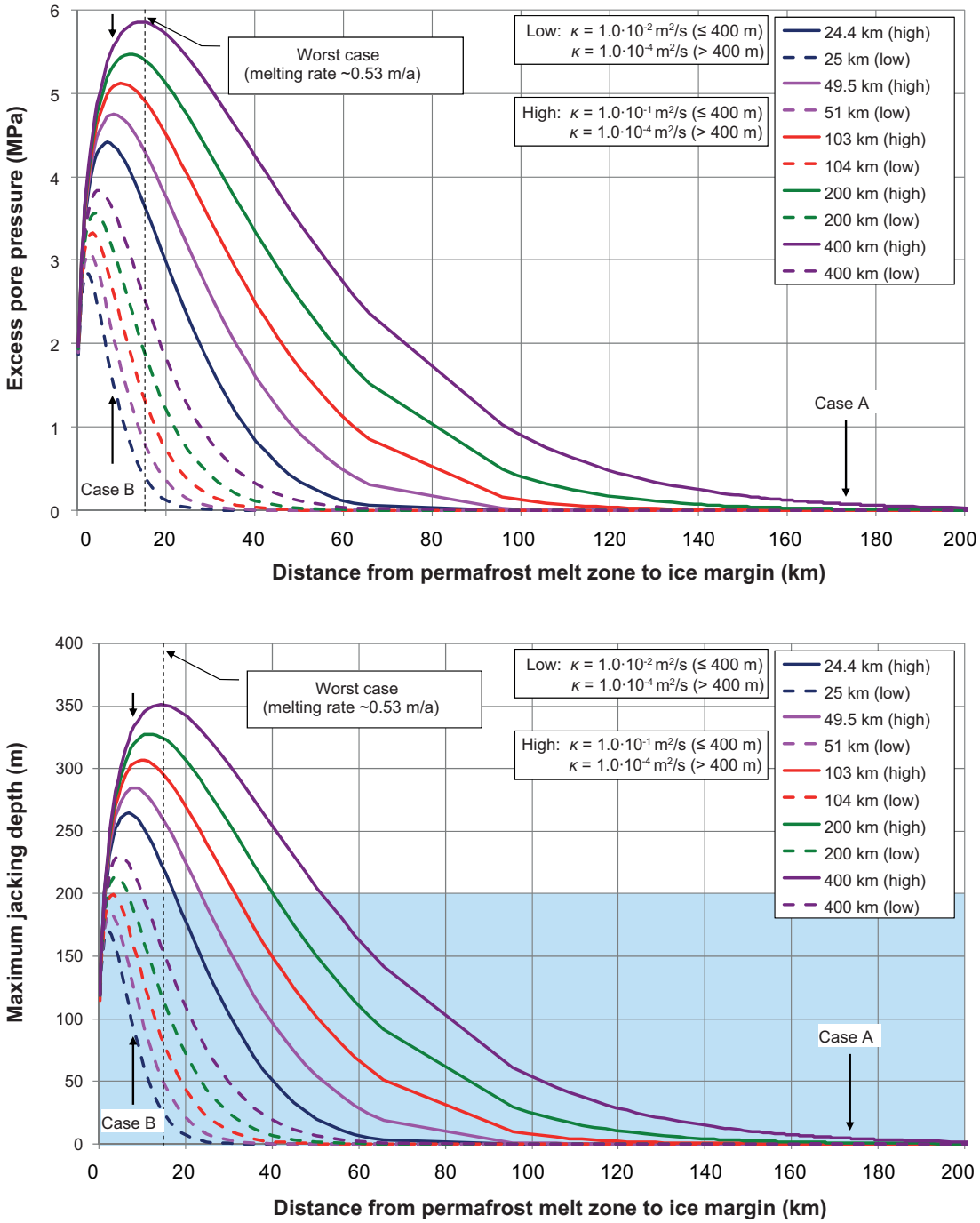

Figure 8-5. *Top: Excess pore pressure beneath the ice margin as a function of the distance from the permafrost melt zone to the ice margin. Bottom: The corresponding maximum jacking depths are calculated from the excess pore pressures as these do not vary with depth in the high diffusivity upper part of the rock. Blue area represents depths covered by permafrost. Note that jacking can only occur beneath the permafrost region (>200 m).*

By inspection of Figure 8-5, it can be concluded that in Cases A and C the excess pore pressure at the ice margin is only sufficient to cause hydraulic jacking to a depth of a few metres below the ground surface and therefore need no further investigation.

In order to avoid jacking at depths below 200 m, a distance of at least 50 km between the permafrost melt zone and the ice margin is required (this corresponds to a melting rate of 0.16 m/a or slower). It is also possible to identify a 'worst case'; a distance of 15 km from the permafrost melt zone to the ice margin (corresponding to a melting rate of about 0.53 m/a) gives the maximum possible jacking depth of 350 m. However, this case is only marginally worse than Case B. Therefore, Case B will be focused on in the following sections.

Importance of permafrost depth

In the SR-Can safety assessment sensitivity analysed showed that under extreme circumstances, permafrost can reach 400 m depth at Forsmark /SKB 2006a/.

The distance between the permafrost melt zone and the ice margin depends on the speed by which the ice front is advancing, the permafrost melting rate and the initial depth of the permafrost (Eq. 8-1), *i.e.* for the same assumptions regarding melting rate, the distance between the ice margin and permafrost melt zone increases with increased permafrost depth. The maximum jacking depth would therefore be a balance between increased hydrostatic pressure at the ice/bed interface and increased propagation distance, cf. Figure 8-6. However, for the same distance between the ice margin and the permafrost melt zone and the same assumptions regarding hydraulic diffusivity, the excess pore pressure beneath the ice margin will be the same regardless of the depth of the permafrost.

$$distance = icefront\_speed * \left(\frac{permafrost\_depth}{melting\_rate} \right) \qquad 8\text{-}1$$

As seen in Figure 8-5, the most important parameter to consider is the diffusivity of the rock beneath the permafrost. The hydraulic conductivity decreases with depth (cf. Figure 5-3), it will therefore be reasonable to assume that the effective diffusivity beneath the permafrost will also be lower when deeper permafrost is considered, cf. Figure 8-6.

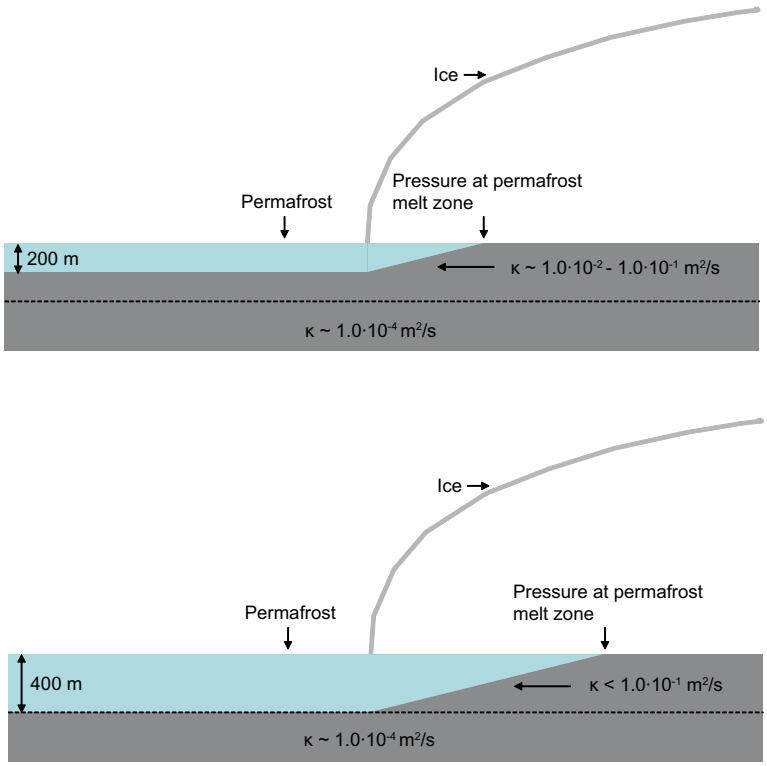

Figure 8-6. *Permafrost depth and diffusivity assumptions beneath the permafrost.*

Of the three suggested melting rates of the permafrost (cf. Section 8.2), Cases A and C can be ruled out in a similar fashion to the previous section if the permafrost depth reaches 400 m; in Case A (with 400 m permafrost) the distance between the ice margin and the permafrost melt zone is almost 450 km in Case C even longer.

In Case B (with 400 m permafrost), the distance between the ice margin and the permafrost melt zone is 16 km. The corresponding distance when 200 m permafrost is considered is 8 km. Assuming the higher option of diffusivity ($\kappa = 10^{-1}$ m^2/s above 400 m, 10^{-4} m^2/s below 400 m), the resulting difference in maximum jacking depth is only marginal, cf. Figure 8-5. However, if the effective diffusivity can be assumed to be one order of magnitude lower (*i.e.* $\kappa = 10^{-2}$ m^2/s above 400 m, 10^{-4} m^2/s below 400 m) in the case of 400 m permafrost, the maximum jacking depth is more than halved.

Evolution of excess pore pressure beneath the permafrost (Case B)

As shown in the previous section, for the higher option of diffusivity in the upper 400 m of the rock (10^{-1} m^2/s) the melting rate associated with Case B gives approximately the largest possible jacking depth and is studied in more detail in the current section.

Figure 8-7 (top) shows the temporal development of the excess pore pressure beneath the permafrost and corresponding maximum jacking depth (lower figure) for points that are initially at horizontal positions 100, 75, 50, 25 and 0 km, respectively, from the ice margin. The maximum jacking depth occurs for a point that is initially 400 km from the ice margin (329 m for high diffusivity and 216 m for low diffusivity), cf. Figure 8-5.

The excess pore pressure increases significantly as the points move towards the ice margin and in under the ice; the coloured strips show the transit time from ice margin to permafrost melt zone for each initial distance from the ice margin. The temporal evolution of the corresponding jacking depth follows the same pattern with one major difference. The maximum jacking depth occurs directly below the ice margin, as the point moves in under the ice there is a significant drop in jacking depth.

Although hydraulic jacking can potentially occur to a depth of about 350 m, there are circumstances under which the maximum jacking depth could be significantly reduced. The most significant factor that would reduce the jacking depth is seasonal variations in the hydrostatic pressure at the ice/bed interface, cf. next section. Other possibilities are the presence of open taliks in the near vicinity of the repository (see Section 8.4).

Seasonal variations

In the previous sections, the hydrostatic pressure at the ice/bed interface has been represented by an annual mean value corresponding to 90% of the height of the ice without account of seasonal variations.

As on many present glaciers, it can be assumed that the water pressure at the ice/bed interface is low during the winter season, here set to zero. The previously assumed annual average (*i.e.* 90% of height of the ice) is here applied for the summer season. During the spring season, the production of surface melt water in combination with a reduced capacity of the basal hydrological system after the winter is likely to temporarily raise the water pressure at the ice/bed interface to pressures higher than 90% of the height of the ice. An example of such pressure variations is presented in Figure 8-8, where the pressure is represented by a sinusoidal function, with an additional peak between winter and summer representing spring conditions with a water pressure of 100% of the height of the ice. Potential situations with basal hydraulic pressures higher than ice overburden pressure are neglected since such situations are believed to be rare on ice sheets.

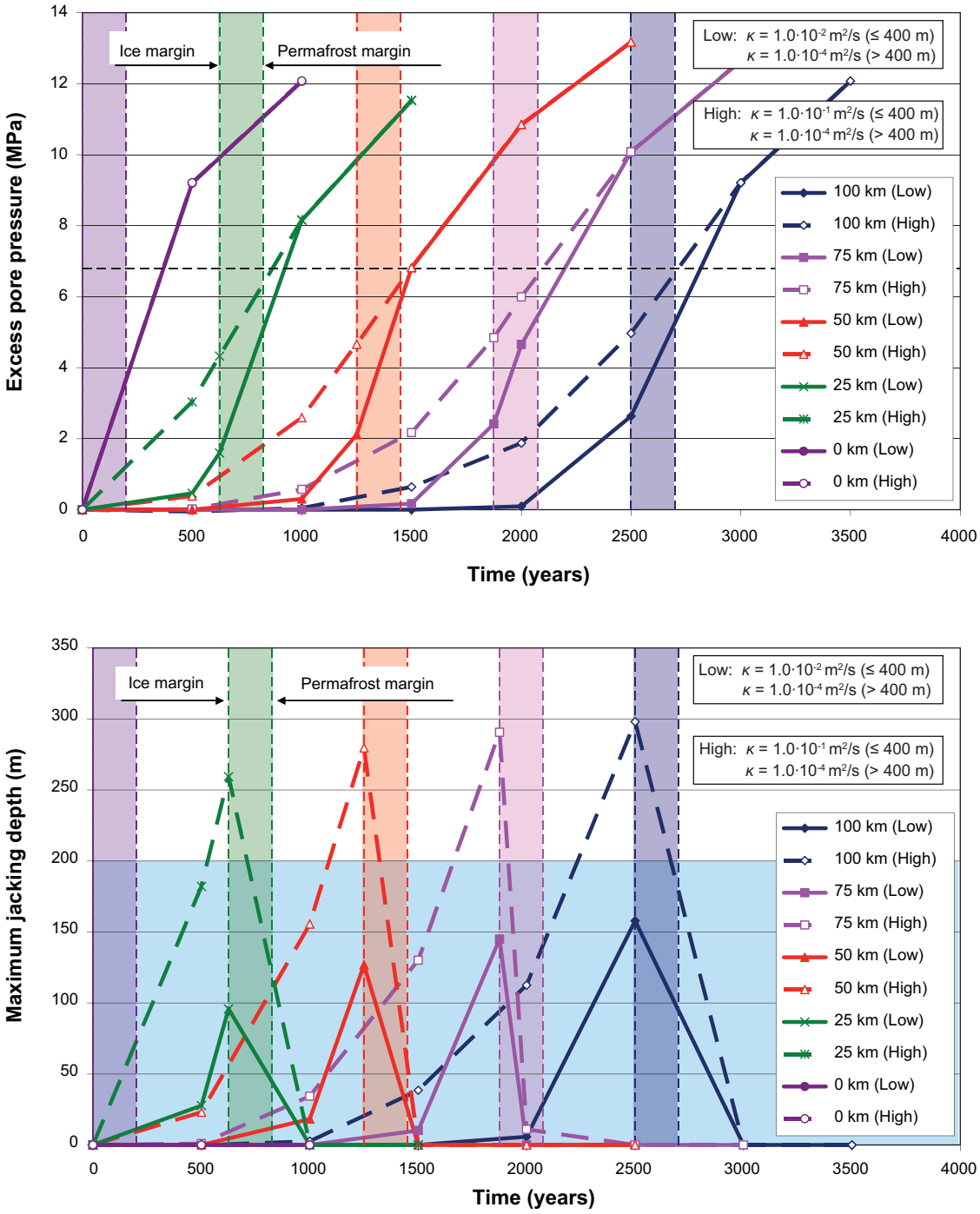

Figure 8-7. *Case B. Top: Temporal evolution of the excess pore pressure at 400 m depth for points that are initially 100 km, 75 km, 50 km, 25 km or 0 km from the ice margin. Boundary pressure at the permafrost melt zone is marked with a dashed line. Bottom: The corresponding maximum jacking depths are calculated from the excess pore pressures as these do not vary with depth in the high diffusivity upper part of the rock. Blue area represents depths covered by permafrost. Note that jacking can only occur beneath the permafrost region (>200 m). Coloured strips represent the transit time from the ice margin to the permafrost melt zone.*

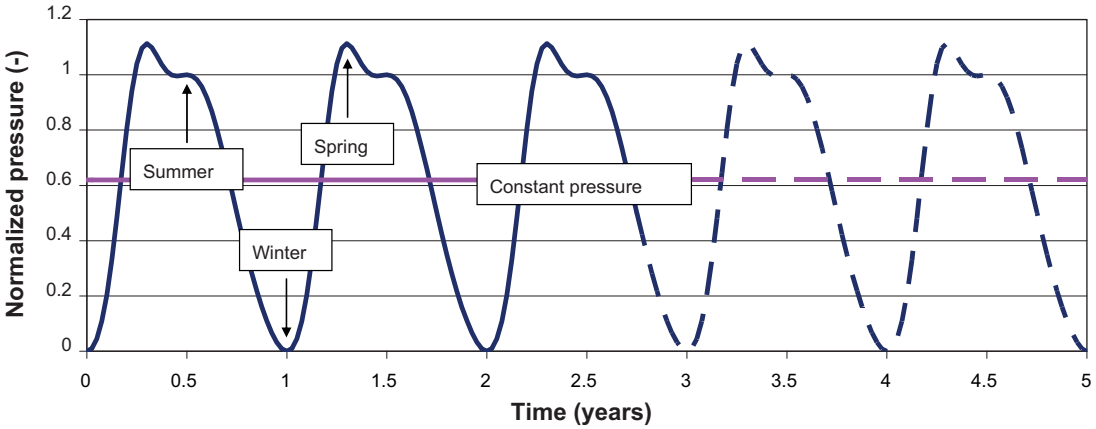

Figure 8-8. *Example of seasonal variations in hydrostatic pressure at the ice/bed interface as a function of time. Here, normalised pressures of 0 represents winter conditions, 1.11 represents spring conditions and 1 represents summer conditions.*

As shown in Appendix E, analytical 1D-expressions may be used to find an upper bound estimate of the pore pressures beneath the permafrost region. A similar 1D-expression with a time-varying boundary pressure, $\phi(t)$, /Carslaw and Jaeger 1959/ can be used to study the influence of seasonal variations, cf. Eq. 8-2. The boundary pressure, $\phi(t)$, is presented in Figure 8-8.

$$P(x,t) = \int_{x/2\sqrt{\kappa t}}^{\infty} \phi\left(t - \frac{x^2}{4\kappa\mu^2} \right) \exp(-\mu^2) d\mu \qquad 8\text{-}2$$

Figure 8-9 (middle and lower) shows the normalised excess pore pressure as functions of distance from the permafrost melt zone after 100 years and 10,000 years, respectively, evaluated at times corresponding to winter, spring and summer and compared with models with constant boundary pressure (see Appendix E). In this example, the diffusivity is set to $1.0 \cdot 10^{-1}$ m^2/s. As seen in the figure, at positions further away than 2 km from the pressure boundary, seasonal variations are not noticed and the curves coincide with corresponding results where the boundary pressure is kept at a constant value of 0.62. Note that this distance depends on the diffusivity assumed for the rock mass; if the diffusivity is higher, the distance seasonal variations are noticeable will be longer.

In the example presented below, the effective boundary pressure corresponds to about 62% of the annual mean (90% of the height of the ice) used in previous calculations. This would correspond to a reduction by 38% in the jacking depth estimates (for Case B) presented in the previous sections, *i.e.* the maximum jacking depth would be reduced from about 329 m to 204 m (high diffusivity) and 216 m to 134 m (low diffusivity). However, the impact of the spring peak will depend on the time frame of the pressure peak. A much shorter peak than the one assumed here is unlikely to have a significant influence on the effective boundary pressure, *i.e.* the effective boundary pressure will be 50% of the annual mean boundary pressure. In this case the jacking depth estimates would be halved.

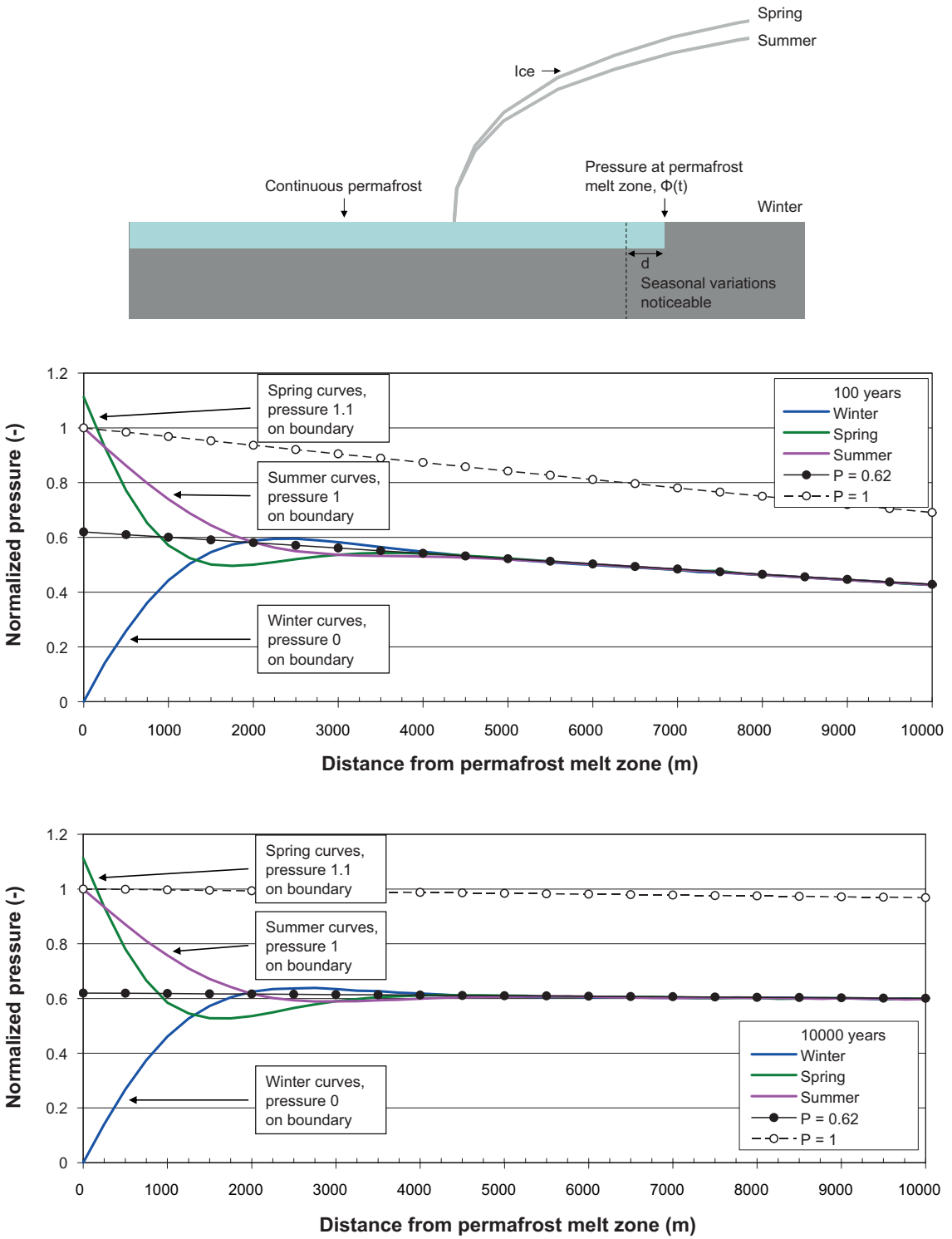

Figure 8-9. *Top: Conceptual view of problem. Middle and lower: Normalized excess pore pressure for a value of the hydraulic diffusivity of $1 \cdot 10^{-1}$ m^2/s after 100 and 10,000 years, respectively. Coloured lines represent model with included seasonal variations, whereas black lines with plot symbols represent models with constant boundary pressure.*

8.4 Influence of taliks

Taliks are defined as parts of the ground that stay perennially unfrozen in a landscape dominated by permafrost /*e.g.* Vidstrand 2003/. Preliminary results of 2D modelling for the SR-Site safety assessment of the permafrost conditions at Forsmark /Hartikainen et al. 2010/ indicate that, under certain circumstances, there will be two open taliks located approximately 4 and 9 km downstream (cf. Figure 8-10), respectively, the repository site. In the permafrost simulations by /Hartikainen et al. 2010/, the taliks are formed under two future lakes that will develop along the investigated profile at Forsmark due to isostatic uplift.

It is here assumed that the ice sheet advances parallel to the line along which the repository and the two taliks are located, cf. Figure 8-11. Given the geographical orientation (SW-NE) of the profile in Figure 8-10, this angle of ice sheet advance would in reality hardly be the case at Forsmark, from where the talik-repository configuration is obtained. However, this is of minor importance for the present purpose of making more generic studies of the effect of taliks. Note that proper site-specific analyses would require that all taliks, *i.e.* not only from one profile as shown in Figure 8-10, were incorporated in the models.

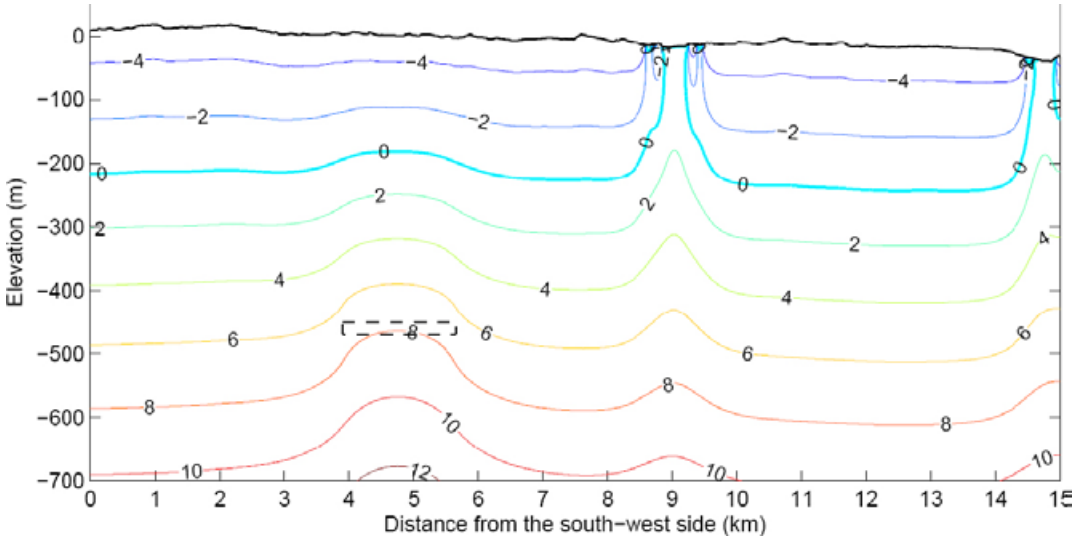

Figure 8-10. *Preliminary results from 2D modelling, of a profile located in a SW-NE direction, of the permafrost situation at Forsmark during cold and dry climate before the ice sheet has reached the site, cf. /Hartikainen et al. 2010/. The depth of the permafrost is given by the zero isotherm. Two taliks are present at approximately 9 km and 15 km in the profile. Repository location marked with a dashed line.*

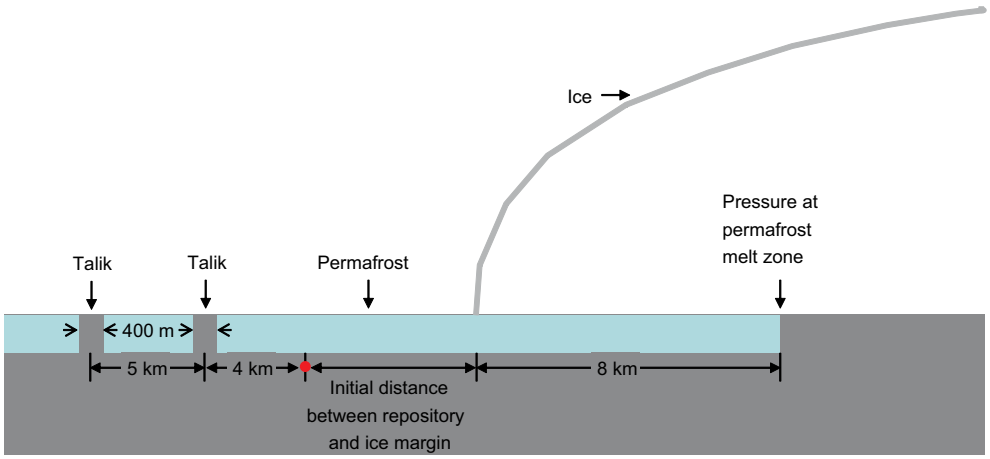

Figure 8-11. *Initial talik and permafrost configuration. Note that it is assumed that the ice sheet advances parallel to the line along which the repository and the two taliks are located. At the Forsmark site, from where this talik-repository configuration is obtained, this angle of ice sheet advance is unlikely.*

8.4.1 Description of numerical models

The influence of open taliks within the permafrost body is investigated by use of the thermal logic in the 2D numerical code *FLAC* (see subsection 4.4.1). Here, the rock mass is represented by a rectangular block – 800 km (width) by 40 km (depth). The model is meshed with square elements of side length 200 m in the upper 800 m; in the remaining parts of the model, rectangular element of side length 200 m (horizontally) and 400 m (vertically). As in the section on continuous permafrost (Section 8.3), the ice front remains stationary during the entire modelled period and the point representing the repository moves (together with the taliks) towards the ice margin. The movement of the taliks towards the ice margin is achieved by an algorithm in the built-in programming language *FISH*, whereby, as time progresses, the algorithm closes the taliks at the old position (*i.e.* replaces permeable material with null-material) and opens the taliks at the new position (replaces null-material with permeable material with the same diffusivity as the layer beneath the permafrost). Each talik has a width of 400 m. The hydrostatic pressure, on parts of the ice/bed interface not covered by permafrost, is as in previous sections kept at 90% of the height of the ice (approximately 98% of the mechanical load) during the entire modelled period, without account of any seasonal variations and the initial excess pore pressure is assumed to be zero. The other boundaries are impermeable. The model is subdivided into three layers:

- 0–200 m (permafrost layer). The permafrost is represented by a rectangular region of uniform thickness, which is made perfectly impermeable by use of a so-called null-material /Itasca 2005a/. Each talik, which is represented by two zones in the models, has the same diffusivity as rock directly beneath it. The boundary pressure at the talik locations is given by the hydrostatic pressure due to the ice, *i.e.* zero outside the ice and according to Figure 3-4 (right) under the ice.
- 200–400 m (layer of rock with high diffusivity). The diffusivity in this layer is set to either $1.0 \cdot 10^{-1}$ m^2/s (denoted ‘high’) or $1.0 \cdot 10^{-2}$ m^2/s (denoted ‘low’). The diffusivity in regions above 200 m not covered by permafrost is set to the same value.
- Below 400 m (layer of rock with low diffusivity). The diffusivity in all regions below 400 m is set to $1.0 \cdot 10^{-4}$ m^2/s.

8.4.2 Results

Three assumptions are made with regard to the repository’s initial distance from the ice margin; similarly to previous sections, the maximum jacking depths are found directly beneath the ice margin:

- 25 km (repository is located beneath the ice margin after 625 years).
- 100 km (repository is located beneath the ice margin after 2,500 years).
- 400 km (repository is located beneath the ice margin after 10,000 years).

Figure 8-12 (top) shows the excess pore pressure at the ice margin beneath the permafrost as functions of the initial distance to the ice margin for two assumptions regarding diffusivity. The lower figure shows the corresponding maximum jacking depth.

Similarly to the results presented in Section 8.3 the excess pore pressures are translated into maximum jacking depths (*i.e.* depth where the effective vertical stress is zero), which may result in jacking depths less than 200 m, *i.e.* within the permafrost body; hydraulic jacking can only occur beneath the permafrost region (>200 m). Maximum jacking depths, which occur within the permafrost body, presented in Figure 8-12 are marked in blue.

As in Section 8.3, the maximum jacking is around 330 m (high diffusivity) and around 220 m (low diffusivity) when the influence of taliks is not considered. When taliks are included in the models, the maximum jacking depth is reduced to about 145 m (high diffusivity) and 190 m (low diffusivity). In the model with high diffusivity and taliks, there are only marginal variations in maximum jacking depth when the initial distance between repository and ice margin is varied. Generally, it seems that the taliks are more influential if the diffusivity is high.

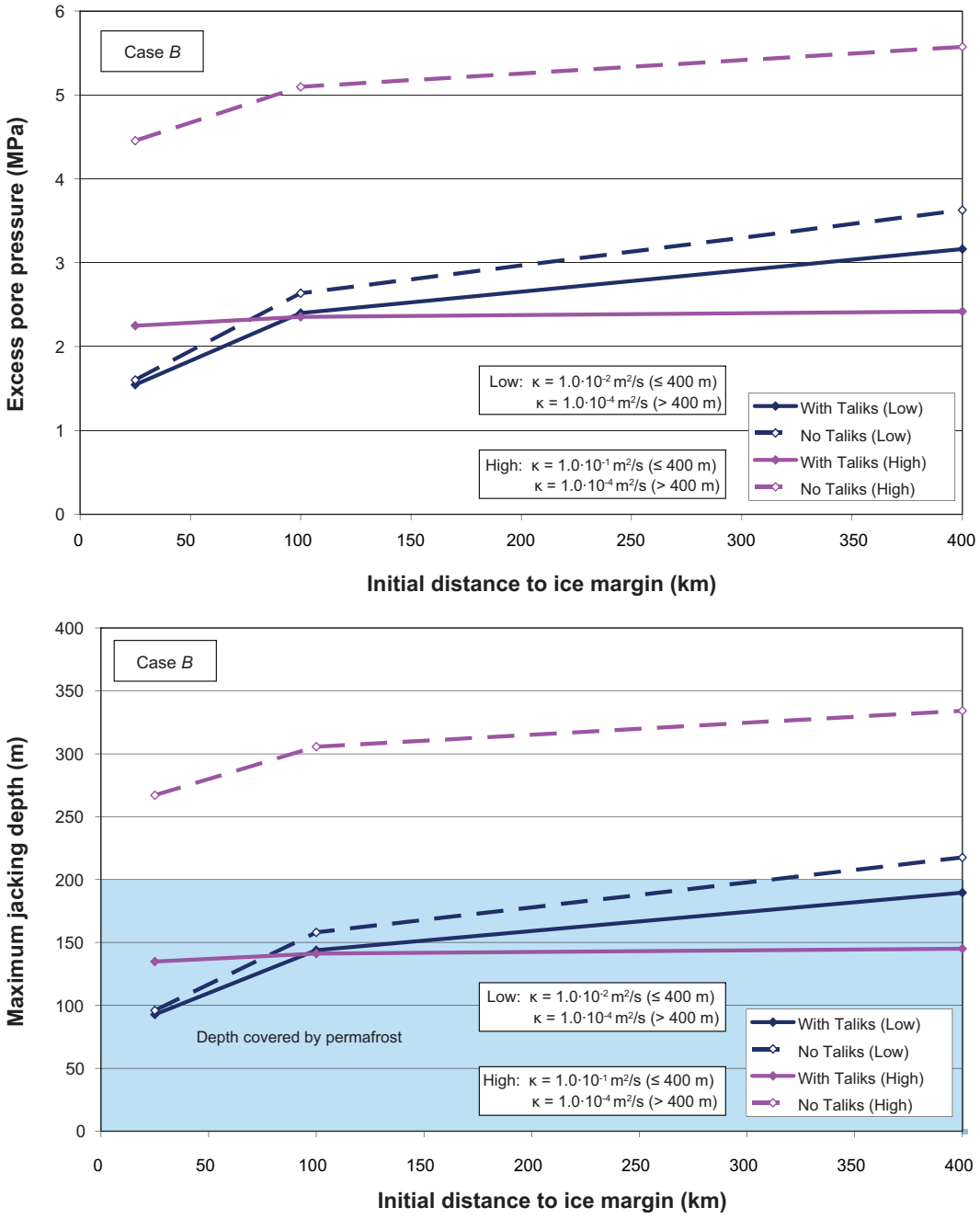

Figure 8-12. *Influence of two taliks positioned 4 and 9 km, respectively, from the repository site as functions of the initial distance to the ice margin. Top: Excess pore pressure at the ice margin beneath the permafrost. Bottom: The corresponding maximum jacking depth are calculated from the excess pore pressures as these do not vary with depth in the high diffusivity upper part of the rock. Blue area represents depth covered by permafrost. Note that jacking can only occur beneath the permafrost region (>200 m).*

8.5 Summary

8.5.1 Continuous permafrost without taliks

The following conclusions can be drawn regarding the issues (cf. Figure 8-2) that were identified as having an impact on the potential for hydraulic jacking and the associated maximum jacking depth (a summary of the maximum jacking depths obtained in this study are given in Table 8-1):

- The maximum jacking depth is greater in rock with high hydraulic diffusivity. In the present study, the hydraulic diffusivity in uppermost 400 m of rock is assumed to be either 10^{-2} m^2/s or 10^{-1} m^2/s and 10^{-4} m^2/s below 400 m.
- The initial thickness of the permafrost does not in itself have an impact on the maximum jacking depth; in the numerical models it is set to 200 m. The pore pressure beneath the permafrost depends on the hydrostatic pressure at the melt zone and on the hydraulic diffusivity of the rock mass.
- The hydrostatic pressure at the melt zone (see Eq. 8-1) is determined by the melting rate of the permafrost, the advance rate of the ice front and the ice sheet profile. The associated maximum jacking depth depends also on the hydraulic diffusivity of the rock.
- A large distance from the repository site to the ice margin at the time when the permafrost layer has first melted at some position behind the advancing ice front increases the maximum jacking depth. All jacking depth estimates made here are based on the assumption that the permafrost layer first melted 10,000 years prior to the ice front arriving at the site. This corresponds to a distance of 400 km.
- Seasonal boundary pressure variations at the permafrost melt zone may reduce the maximum jacking depth by 40–50%.

8.5.2 Influence of taliks

The influence open taliks has on pore pressures and corresponding jacking depths depends on site-specific conditions. For a proper site-specific analysis, this would require that all taliks, *i.e.* not only from one profile as shown in Figure 8-10, were incorporated in the models. Therefore, the reductions in excess pore pressure and estimates of maximum jacking depths presented in this chapter should be seen as giving a generic understanding of the effects of open taliks.

Based on the results presented in Section 8.4, it seems that taliks, in general, are more influential when the hydraulic diffusivity is high. For example, in the models with the higher value of the hydraulic diffusivity (10^{-1} m^2/s) in the upper 400 m of rock, the maximum excess pore pressure is more than halved when the taliks are included, whereas for the lowest value of the hydraulic diffusivity the reduction is only 13%. It should be noted that, as all modelling work has been conducted in 2D, the taliks are represented by infinitely long trenches in the out-of-plane direction, whereas in reality they will be finite in size. Therefore, their influence may be exaggerated. However, no sensitivity analyses have been performed with regard to taliks.

Table 8-1. Summary of maximum jacking depths obtained in this study. Note that these estimates do not include seasonal variations in the boundary hydrostatic pressure or the influence of open taliks. The initial permafrost depth is 200 m.

Melting rate	High diffusivity (10^{-1} m^2/s above 400 m 10^{-4} m^2/s below 400 m)	Low diffusivity (10^{-2} m^2/s above 400 m, 10^{-4} m^2/s below 400 m)
Case A (0.03 m/a during the first 4,300 years and thereafter 2.5 m/a).	No jacking	No jacking
Case B (1 m/a)	330 m	220 m
Case C (0.025 m/a)	No jacking	No jacking
'Worst case' (0.53 m/a for high diffusivity, 1.3 m/a for low diffusivity)	350 m	230 m

9 Conclusions and discussion

9.1 General

The present report comprises results from a generic study of the potential for hydraulic jacking of sub-horizontal fractures with data mainly from the Forsmark site /SKB 2005, 2006c, Follin et al. 2007, SKB 2008/. A summary of the data used in the modelling is presented in Table 9-1. The hydraulic conductivity at Laxemar site is greater in magnitude than at Forsmark, but shows a similar trend of decreasing with depth, cf. Figure 5-3 and Figure 5-7. The estimated specific storage coefficient is of the same magnitude at both sites, cf. subsections 5.1.3 and 5.2.2. However, the differences between the sites are small enough that general conclusions regarding the potential for hydraulic jacking of sub-horizontal fractures can be drawn for both sites.

All results are compiled from 2D-models of the pore pressure distribution/evolution in the rock below an ice sheet or below an impermeable permafrost layer without any attempt to replicate the local topography or fracture configurations at the repository sites. Throughout the study, a generic representation of a theoretical steady-state ice front profile is used /Paterson 1994/, which is assumed to terminate above sea level at all times. This profile is considered to be steep enough to represent an advancing ice at the Forsmark and Laxemar sites and is considerably steeper than expected ice profiles during stationary and retreating phases (Figure 3-3). Based on results from the reference glacial cycle in SR-Can /SKB 2006a/, the maximum ice sheet thickness is set to 3,000 m. Assessments of the potential of hydraulic jacking at different depths are made, assuming that the glacially induced vertical stress is equal to the weight of the ice (cf. Appendix C) and that the hydrostatic pressure at the ice/rock interface corresponds to 90% of the height of the ice (*i.e.* about 98% of the ice load) in all models at all times unless explicitly stated otherwise, cf. Figure 3-4.

Two types of analyses were performed:

- Steady state analyses (the pore pressure distribution due to a stationary ice front can be considered an upper bound estimate of pore pressures due to an advancing ice front). Steady state analyses are conducted in order to investigate the potential for hydraulic jacking in rock with few conductive fractures. Furthermore, steady state pore pressure distributions in homogeneous rock are used as initial conditions during the retreat phase for the transient analyses.
- Transient analyses (the retreat phase and advance phase without and with permafrost conditions). Transient analyses are only conducted for homogeneous rock conditions.

Table 9-1. Summary of hydraulic data for Forsmark used in the modelling work, cf. Section 5.1.

Depth range	Hydraulic conductivity (m/s)	Specific storage coefficient (m^{-1})	Hydraulic diffusivity (m^2/s)
All rock	10^{-9}–10^{-8}	10^{-7}	10^{-2}–10^{-1}
0–400 m	10^{-9}–10^{-8}	10^{-7}	10^{-2}–10^{-1}
> 400 m	10^{-11}	10^{-7}	10^{-4}

9.2 Homogeneous rock model

In uniformly and homogeneously fractured rock, *i.e.* rocks in which the hydrological conditions can be approximated by a uniform bulk hydraulic diffusivity, analytical diffusion expressions (see Section 4.3) have been used to estimate the pore pressure distribution under the ice sheet and the associated maximum jacking depths during the advancement, periods of stationary conditions and subsequent retreat of the ice front. The following can be concluded:

- **Advancing ice front without permafrost conditions.** Steady state analyses can be regarded as an upper bound estimate of the pore pressure distribution during the advancement of an ice sheet. In this case, the maximum jacking depth beneath the ice margin is about 30 m, cf. Figure 6-1 (right).
- **Retreating ice front.** At the Forsmark site the bulk hydraulic diffusivity is assumed to be in the range 10^{-2}–10^{-1} m^2/s (and even higher at Laxemar), cf. Table 9-1. In this diffusivity range, the jacking depths are of the order of 50 m and seem to be practically independent of the retreat speed (200–500 m/a) and duration of preceding periods with a stationary ice front, cf. Figure 6-3 to Figure 6-5.

The analytical expressions used to assess the maximum jacking depths in homogeneously fractured rock cannot account for spatial variations of the hydraulic diffusivity. However, the variations of the hydraulic conductivity with depth (high near the ground surface and decreasing with depth) at the two repository sites investigated by SKB will prevent an upwards transfer of pore pressures from regions with low permeability when the ice retreats, thus allowing for faster pressure reduction in the upper parts of the rock, cf. Appendix D. This will result in a reduced maximum jacking depth.

9.3 Modelling of rock with few conductive fractures

For rock with few conductive fractures, analytical estimates show that fracture lengths of several kilometres are needed for sufficiently high pore pressures to propagate undisturbed to the ice front and thereby initiate hydraulic jacking at large depths. For example, the minimum fracture length needed in order to initiate jacking at 400 m depth is 7.6 km provided that the hydrostatic pressure at the ice/bed interface is 90% of the height of the ice and that the rock is perfectly impermeable everywhere, cf. Figure 7-1 (lower left). When the draining of fractures due to the rock's non-zero permeability is taken into account, the required lengths would be even greater, see Figure 7-5 to Figure 7-11. This observation points to the very specific conditions regarding fractures and background permeability required to initiate jacking at large depths. To the authors' knowledge, no gently dipping fractures of the required length have been observed at either Forsmark or Laxemar, cf. *e.g.* Figure 7-2.

9.4 Permafrost impact

The potential for hydraulic jacking in homogeneously fractured rock during combined glacial and permafrost conditions is studied by use of numerical Code_Bright and *FLAC* models (see Section 4.4). Two scenarios regarding the situation of permafrost in front of the advancing ice sheet are considered. The first scenario relates to the situation with continuous permafrost without taliks and the second one to the influence of open taliks within the permafrost body. In the numerical models the permafrost is represented by an impermeable rectangular region with a thickness of 200 m.

The following can be concluded from the analyses regarding continuous permafrost without taliks:

- The most important parameter that governs the maximum jacking depth is the hydraulic diffusivity of the rock mass. High values of the hydraulic diffusivity result in large jacking depths.
- The initial permafrost thickness in itself does not have an influence on the maximum jacking depth as the pore pressure beneath the permafrost is governed by the hydrostatic pressure at the melt zone and the diffusivity of the rock mass.

- As the permafrost is assumed to melt linearly from below, the distance between the permafrost melt zone and the ice margin (see Figure 8-2 and Figure 8-3) is constant at all times and is determined by the melting rate of the permafrost and the rate at which the ice front is advancing (Eq. 8-1). For high values of the hydraulic diffusivity, a slow melting rate (*i.e.* a large distance between the permafrost melt zone and the ice margin) will result in a larger jacking depth and vice versa, cf. Figure 8-5.
- The time passing between the time when the permafrost layer has first melted at some position behind the advancing ice front and the time when the ice margin arrives at the site has an impact on the maximum jacking depth. If a long time has passed, the pore pressures have had time to build up beneath the permafrost and consequently the maximum jacking depth increases, cf. Figure 8-5 and Figure 8-7.
- Allowing for seasonal variations in the hydrostatic pressure at the melt zone may reduce the maximum jacking depth by 40–50%.

In the most conservative model, the hydraulic diffusivity is set to 10^{-1} m^2/s in the upper 400 m of rock and 10^{-4} m^2/s elsewhere, the permafrost melting rate is 0.53 m/a and the permafrost layer is assumed to have first melted 10,000 years prior to the ice front arriving at the site. For this combination of parameters, the maximum jacking depth is 350 m without considering seasonal variations in the hydrostatic pressure at the melt zone. Accounting for seasonal variations would reduce the maximum jacking depth to about 200 m. For a lower value of the hydraulic diffusivity, *e.g.* 10^{-2} m^2/s in the upper 400 m of rock, hydraulic jacking below the permafrost is unlikely.

The influence open taliks has on pore pressures and corresponding jacking depths depends on site-specific conditions, *e.g.* the diffusivity of the rock, the sizes and numbers of the taliks and their locations in relation to the point being considered. Based on the results from the analyses in Section 8.4, it seems that taliks, in general, are more influential when the diffusivity is high. For example, in the models with the highest value of the hydraulic diffusivity in the upper 400 m of rock, the excess pore pressure beneath the permafrost is more than halved when the taliks are included, whereas for the lowest value of the hydraulic diffusivity the reduction is only 13%, cf. Figure 8-12. However, a proper site-specific analysis would require that all taliks, *i.e.* not only from one profile as shown in Figure 8-10, were incorporated in the models. Therefore, the results presented in Section 8.4 should be seen as giving a generic understanding of the effects of open taliks.

9.5 Relevance of models

9.5.1 Ice sheet thickness and water pressure at the ice/bed interface

The maximum ice sheet thickness, used in the analyses, is set to 3,000 m based on results from the reference glacial cycle in SR-Can in which the maximum height of the ice is 2,900 m at Forsmark and 2,400 m at Laxemar /SKB 2006a/. Results from modelling of the largest Fennoscandian ice sheets during the past 2 million years, the so-called Saalian ice sheet, indicate that the maximum expected ice thickness at Forsmark and Laxemar are about 3,200 m and 2,600 m, respectively /SKB 2006a/. Additional sensitivity analyses for the SR-Can safety assessment indicated that it is unlikely that the ice sheet would ever exceed a thickness of 3,700 m at these sites /SKB 2006a/. Therefore, the ice sheet thickness used in the modelling work appears to be adequate for the Forsmark site and conservative for the Laxemar site.

The hydrostatic pressure at the ice/ground interface is kept at 90% of the height of the ice (*i.e.* approximately 98% of the mechanical ice load) during ice front advance, periods of stationary conditions and ice front retreat, regardless of any possible discharge paths along the ice/ground interface. However, the uncertainties regarding the actual basal pressure variations beneath ice sheets are large and, in reality, the ratio between hydrostatic pressure at the ice/bed interface and mechanical load is unlikely to be uniform along the flow line, cf. Figure 9-1.

If the water pressure at the ice/bed interface is increased, the maximum jacking depth would also increase. In the latter case, the largest drops in effective vertical stress are not necessarily found at the ice margin, but can be located well under the ice sheet. However, it is unlikely that the hydraulic pressures would be higher than ice overburden pressure. When the water pressure at the ice/bed interface increases, the subglacial drainage system rapidly develops to account for the increased amount of water, which in turn results in that the water pressure again falls /*e.g.* Boulton et al. 2001b, Jansson et al. 2007/. For details on present knowledge on the glacial hydrological system, see /Jansson et al. 2007/.

9.5.2 Hydro-mechanical couplings

Model limitations

In the present study, the coupling between fluid pressure and permeability is not considered and the density of water is assumed to be constant.

The analytical results are based on hydro-mechanically un-coupled equations and are governed by diffusion only. However, the hydraulic diffusivity depends on the hydraulic conductivity, the bulk modulus of water, the porosity and the elastic properties of the rock mass.

None of the numerical models account for the possible effects of flexural stresses, *i.e.* reduction of the transmissivity of steeply dipping fractures because of horizontal stress increases under the ice (or corresponding transmissivity increases in the forebulge region outside the ice). This is in keeping with the modelling approach taken by the DECOVALEX and BENCHPAR groups /Chan et al. 2005/. In relation to the importance of the extension and connectivity of highly transmissive horizontal fractures demonstrated here, mechanically induced variations in the transmissivity of steeply dipping fractures are not likely to be important. The following additional limitation is also introduced in the *UDEC* modelling. The code cannot handle hydro-mechanical couplings adequately in models with large variations in fracture apertures, which results in the initially largest apertures remaining fixed during the calculations.

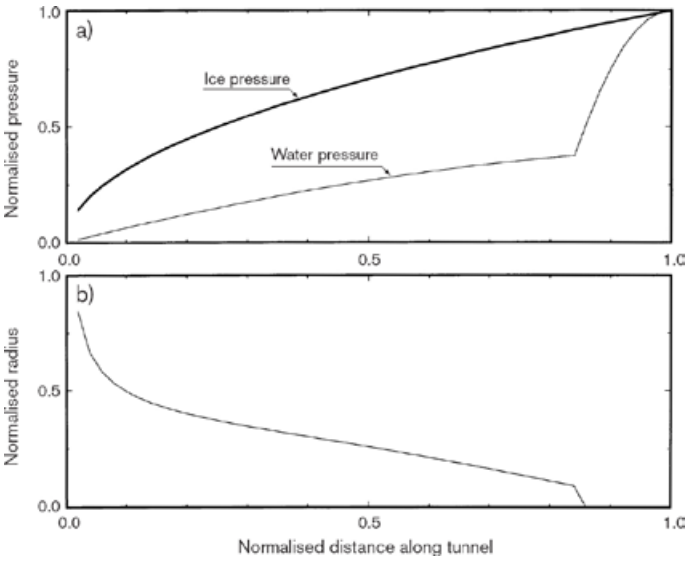

Figure 9-1. *Top: Distribution of normalized water pressure along a subglacial tunnel. Bottom: Corresponding tunnel radius along its length. From /Boulton et al. 2001b/.*

Importance of mechanical load on pore pressures

It is outside the scope of this report to perform fully coupled H-M analyses. However, an indication of the importance of mechanical load on the excess pore pressure can be found by examining solutions to Eq. 4-1 in 1D and accounting for temporal changes in the glacially induced vertical stress, cf. Appendix A. The 1D calculations show that, if changes in the vertical stress are not taken into account, the pore pressure will be underestimated during the advance of the ice sheet. This problem can be overcome by assuming that the pore pressure distribution will have reached steady state before the start of the retreat. During the retreat of the ice front, accounting for changes in the glacially induced vertical stress tends to reduce the pore pressure more quickly. Therefore, it appears that the boundary load term can be conservatively ignored. However, given that the stress state during the glacial cycle is influenced by varying flexural stresses, applying the 1D loading term must be considered a very approximate way of accounting for the mechanical impact on the pore pressure evolution. Accounting for the impact of the flexural stresses induced in the reference glacial scenario /Lund et al. 2009/ on the pore pressure evolution in 1D (see Appendix A) has a similar effect as the 1D loading term. For the purpose of obtaining bounding estimates of the glacially induced pore pressure and associated maximum jacking depth beneath a warm-based ice, it appears that the mechanical impact on the pore pressure evolution can be ignored.

Fracture closure/opening

Load and pressure induced variations of the transport properties of the rock mass and fractures are not considered in the modelling approach (see also subsection on model limitations). Estimates of the variations in relative transmissivity of fractures with different orientations and at different depths during SKB's reference glacial cycle indicate that these variations are typically in the range 50–200% for the most sensitive stress-transmissivity model considered by /Hökmark et al. 2010/ when the temperature reduction due to permafrost is not considered. Given the results by /Hökmark et al. 2010/ and that the range in hydraulic diffusivity considered relevant for the rock at Forsmark spans one or two orders of magnitude, this particular hydro-mechanical coupling is likely to be of subordinate importance.

9.5.3 Material properties

Specific storage coefficient

In the expression used for the one-dimensional specific storage coefficient (Eq. 4-4), it is assumed that the solid grains are incompressible (*i.e.* $K_S \rightarrow \infty$) /Neuzil 2003/ and the elastic properties are taken to be those of the rock mass in fracture domains FFM01 and FFM06 at Forsmark /SKB 2008, Table 7-6/. An expression for the one-dimensional specific storage coefficient that accounts for the compressibility of intact rock is given by /Neuzil 2003/:

$$S_S = \rho g \left[\left(\frac{1}{K} - \frac{1}{K_S} \right) (1-\lambda) + \left(\frac{n}{K_f} - \frac{n}{K_S} \right) \right], \text{ where } \lambda = 2 \left(1 - \frac{K}{K_S} \right) \frac{1-2\nu}{3(1-\nu)}$$

The ratio between Young's modulus of the rock mass and Young's modulus of intact rock at the Forsmark site is around 0.9 /SKB 2008, Tables 7-3 and 7-6/. Inserting typical values of the elastic properties of the rock mass and corresponding properties of intact rock into the expression above results in values of the specific storage coefficient in the range $2.6 \cdot 10^{-8}$–$6.4 \cdot 10^{-8}$ m^{-1} (or 0.16–0.64 of the values assumed in this study, cf. subsection 5.1.3). However, the modelling work conducted here involves larger volumes of rock than the two fracture domains considered for the repository at Forsmark, which implies that the elastic properties of the rock mass have to be considered on a larger scale. Accounting for surrounding rock with lower stiffness and the presence of deformation zones will effectively reduce the deformation modulus of the rock mass. /Mas Ivars and Hakami 2005, Hakami 2006, Glamheden et al. 2007b/ give values of the rock mass deformation modulus in the range 40–45 GPa, which corresponds to about 50–60% of the value given for intact rock at Forsmark /SKB 2008/. Inserting the latter values of the rock mass elastic properties into the expression above results in values of the specific storage coefficient in the range $1.1 \cdot 10^{-7}$–$1.9 \cdot 10^{-7}$ m^{-1} (*i.e.* very similar to the values given in subsection 5.1.3). This discussion points to the inherent uncertainties associated with data on this modelling scale.

Tensile strength

In the present modelling work it is assumed that hydraulic jacking is initiated when the effective vertical stress is zero, *i.e.* assuming that the tensile strength is zero. Including tensile strength in the calculations of the maximum jacking depth, will reduce the depth. Site-specific values of the tensile strength need to be considered in order to determine the actual reduction in maximum jacking depth.

9.6 Maximum jacking depths

Based on the modelling results in Chapters 6, 7 and 8 and the discussion provided above, the following conclusions regarding the maximum jacking depth during the different phases of the glacial phase are drawn, see Table 9-2.

9.7 Final remarks

All models, analytical as well as numerical, examined here are well on the conservative side from many aspects:

- A steep ice sheet profile is used during all stages of glaciation; ice sheet profiles are expected to be less steep during the retreat phase than during steady-state conditions and advances, cf. Figure 3-3. However, spatial variations along the ice front, *e.g.* due to bays and valleys, cannot be modelled in 2D. Provided that the scale of these irregularities along the ice front are smaller than the distances the glacially induced pore pressures can potentially be transferred (approximately a few tens of kilometres), they are unlikely to influence the estimated maximum jacking depths.
- The hydrostatic pressure at the ice/bed interface is assumed to be 90% of the height of the ice at all times and along the entire flow line. Seasonal variations and lateral variations due to *e.g.* subglacial tunnels are not considered. These would reduce the effective boundary pressure.
- The 2D approach does not allow for modelling of vertical fractures that strike normally to the ice front. Such fractures or fracture zones would efficiently contribute to dissipate excess pore pressures in the region around the ice front and are present in the repository region at both the Forsmark and Laxemar sites /SKB 2008, 2009/.
- Jacking at large depths requires that highly transmissive horizontal fractures extend many kilometres into the high pressure region under the ice. The 2D results presented here were obtained implicitly assuming this to be the case uniformly for many tens of kilometres in the out-of-plane direction, *i.e.* along the ice front. In the 3D reality this will not be possible.

The potential for hydraulic jacking is always greatest at shallow depths. Therefore, if jacking occurs at all, it is likely to be a local, near-surface phenomenon. As hydraulic jacking is initiated, the associated increase in fracture transmissivity will tend to reduce the pore pressure and prevent hydraulic jacking from occurring at larger depths. This is not considered in the estimates of the maximum jacking depths provided in Table 9-2, which therefore should be considered conservative estimates.

Table 9-2. Summary of estimated maximum jacking depths during different phases of the glacial phase.

	Analytical solutions (homogeneous rock model)	Numerical solutions (homogeneous rock model)	Numerical solutions (rock with few conductive fractures)
Advancing ice front			
without permafrost	30 m	–	< 200 m
with permafrost	–	200 m	–
Retreating ice front	100 m	–	–

10 References

SKB's (Svensk Kärnbränslehantering AB) publications can be found at www.skb.se/publications.

Bense V F, Person M A, 2008. Transient hydrodynamics within intercratonic sedimentary basins during glacial cycles. Journal of geophysical research, Volume 113, F04005, doi: 10.1029/2007FJ000969.

Boulton G S, Kautsky U, Morén L, Wallroth T, 2001a. Impact of long-term climate change on a deep geological repository for spent nuclear fuel. SKB TR-99-05, Svensk Kärnbränslehantering AB.

Boulton G S, Zatsepin S, Maillot B, 2001b. Analysis of groundwater flow beneath ice sheets. SKB TR-01-06, Svensk Kärnbränslehantering AB.

Carslaw H S, Jaeger J C, 1959. Conduction of Heat in Solids, 2nd ed. Oxford University Press, UK,

Chan T, Christiansson R, Boulton G S, Eriksson L O, Hartikainen J, Jensen M R, Mas Ivars D, Stanchell F W, Vistrand P, Wallroth T, 2005. DECOVALEX III/BENCHPAR PROJECTS. The Thermal-Hydro-Mechanical Responses to a Glacial Cycle and their Potential Implications for Deep Geological Disposal of Nuclear Fuel Waste in a Fractured Crystalline Rock Mass. SKI 2005:28, Strålsäkerhetsmyndigheten (Swedish Radiation Safety Authority), Stockholm, Sweden.

CIMNE (International Center for Numerical Methods in Engineering), 2004. Code_Bright. Version 2.2 users guide. Departemento de Ingenieria del Terreno, Cartográfica y Geofísica. Universidad Politécnica de Cataluña, Spain.

Follin S, Levén J, Hartley L, Jackson P, Yoyce S, Roberts D, Swift B, 2007. Hydrogeological characterisation and modelling of deformation zones and fracture domains, Forsmark modelling stage 2.2. SKB R-07-48, Svensk Kärnbränslehantering AB.

Gascoyne M, 2000. A review of published literature on the effects of permafrost on the hydrogeochemistry of bedrock. SKB R-01-56, Svensk Kärnbränslehantering AB.

Glamheden R, Fredriksson A, Röshoff K, Karlsson J, Hakami H, Christiansson R, 2007a. Rock Mechanics Forsmark. Site descriptive modelling Forsmark stage 2.2. SKB R-07-31, Svensk Kärnbränslehantering AB.

Glamheden R, Maersk Hansen L, Fredriksson A, Bergkvist L, Markström I, Elfström M, 2007b. Mechanical modelling of the Singö deformation zone. Site descriptive modelling Forsmark stage 2.1. SKB R-07-06, Svensk Kärnbränslehantering AB.

Grasby S, Chen Z, 2005. Subglacial recharge into the Western Canadian Sedimentary Basin – Impact of Pleistocene glaciation on basin hydrodynamics. Geological Society of America Bulletin, Volume 117, No. 3–4 pp. 500–514.

Hakami E, Fredriksson A, Lanaro F, Wrafter J, 2008. Rock mechanics Laxemar. Site descriptive modelling. SDM-Site Laxemar. SKB R-08-57, Svensk Kärnbränslehantering AB.

Hakami H, 2006. Numerical studies on spatial variation of the in situ stress field at Forsmark – a further step. Site descriptive modelling Forsmark – stage 2.1. SKB R-06-124, Svensk Kärnbränslehantering AB.

Hartikainen J, Kouhia R, Wallroth T, 2010. Permafrost simulations at Forsmark using a numerical 2D thermo-hydro-chemical model. SKB TR-09-17, Svensk Kärnbränslehantering AB.

Hökmark H, Fälth B, Wallroth T, 2006. T-H-M couplings in rock. Overview of results of importance to the SR-Can safety assessment. SKB R-06-88, Svensk Kärnbränslehantering AB.

Hökmark H, Lönnqvist M, Fälth B, 2010. THM-issues in repository rock. Thermal, mechanical, thermo-mechanical and hydro-mechanical evolution of the rock at the Forsmark and Laxemar sites. SKB TR-10-23, Svensk Kärnbränslehantering AB.

Itasca, 2005a. *FLAC* – Fast Lagrangian Analysis of Continua, User's guide. Itasca Consulting Group, Inc., Minneapolis, Minnesota, USA.

Itasca, 2005b. *UDEC*, Universal Distinct Element Code. Itasca Consulting Group, Inc., Minneapolis, Minnesota, USA.

Jansson P, Näslund J-O, Rodhe L, 2007. Ice sheet hydrology – a review. SKB TR-06-34, Svensk Kärnbränslehantering AB.

Leijon B, 2005. Investigations of superficial fracturing and block displacements at drill site 5. Forsmark site investigation. SKB P-05-199, Svensk Kärnbränslehantering AB.

Lindblom U, 1997. Hydromechanical instability of a crystalline rock mass below a glaciation front. SKB U-97-13, Svensk Kärnbränslehantering AB.

Lund B, Schmidt P, Hieronymus C, 2009. Stress evolution and fault stability during the Weichselian glacial cycle. SKB TR-09-15, Svensk Kärnbränslehantering AB.

Mas Ivars D, Hakami H, 2005. Effect of a sub-horizontal fracture zone and rock mass heterogeneity on the stress field in Forsmark area – a numerical study using 3DEC. Preliminary site description Forsmark area – version 1.2. SKB R-05-59, Svensk Kärnbränslehantering AB.

McEwen T, de Marsily G, 1991. The Potential Significance of Permafrost to the Behaviour of a Deep Radioactive Waste Repository. SKI Report 91:8, Strålsäkerhetsmyndigheten (Swedish Radiation Safety Authority), Stockholm, Sweden.

Moeller C A, Mickelson D M, Anderson M P, Winguth C, 2007. Groundwater flow beneath Late Weichselian glacier ice in Nordfjord, Norway. Journal of glaciology, Volume 53, No. 180, pp. 84–90.

Neuzil C E, 2003. Hydromechanical coupling in geologic processes. Hydrogeology Journal, Vol. 11, No. 1, pp. 41–83.

Olofsson I, Simeonov A, Stephens M, Follin S, Nilsson A-C, Röshoff K, Lindberg U, Lanaro F, Fredriksson A, Persson L, 2007. Site descriptive modelling Forsmark, stage 2.2. A fracture domain concept as a basis for the statistical modelling of fractures and minor deformation zones, and interdisciplinary coordination. SKB R-07-15, Svensk Kärnbränslehantering AB.

Paterson W S B, 1994. The physics of glaciers. Elsevier Science Ltd., Oxford, UK,

Rhén I, Follin S, Hermanson J, 2003. Hydrological Site Descriptive Model – a strategy for its development during Site Investigations. SKB R-03-08, Svensk Kärnbränslehantering AB.

Rhén I, Forsmark T, Hartley L, Jackson P, Roberts D, Swan D, Gylling B, 2008. Hydrogeological conceptualisation and parameterisation. Site descriptive modelling. SDM-Site Laxemar. SKB R-08-78, Svensk Kärnbränslehantering AB.

SKB, 2005. Preliminary site description. Forsmark area – version 1.2. SKB R-05-18, Svensk Kärnbränslehantering AB.

SKB, 2006a. Climate and climate-related issues for the safety assessment SR-Can. SKB TR-06-23, Svensk Kärnbränslehantering AB.

SKB, 2006b. Long-term safety for KBS-3 repositories at Forsmark and Laxemar – a first evaluation. Main report of the SR-Can project. SKB TR-06-09, Svensk Kärnbränslehantering AB.

SKB, 2006c. Site descriptive modelling Forsmark stage 2.1. Feedback for completion of the site investigation including input from safety assessment and repository engineering. SKB R-06-38, Svensk Kärnbränslehantering AB.

SKB, 2008. Site description of Forsmark at completion of the site investigation phase. SDM-Site Forsmark. SKB TR-08-05, Svensk Kärnbränslehantering AB.

SKB, 2009. Site description of Laxemar at completion of the site investigation phase. SDM-Site Laxemar. TR-09-01, Svensk Kärnbränslehantering AB.

SKB, 2010. Climate and climate related issues for the safety assessment SR-Site. SKB TR-10-49, Svensk Kärnbränslehantering AB.

Talbot C J, 1999. Ice ages and nuclear waste isolation. Engineering Geology, Vol. 52, Issues 3–4, pp. 177–192.

Vidstrand P, 2003. Surface and subsurface conditions in permafrost areas – a literature review. SKB TR-03-06, Svensk Kärnbränslehantering AB.

Vidstrand P, Wallroth T, Ericsson L O, 2008. Coupled HM effects in a crystalline rock mass due to glaciation: indicative results from groundwater flow regimes and stresses from an FEM study. Bulletin of Engineering Geology and the Environment, Vol. 67, No. 2, pp. 187–197.

Wahlgren C-H, Curtis P, Hermanson J, Forssberg O, Öhman J, Fox A, La Pointe P, Drake H, Triumf C-A, Mattsson H, Thunehed H, Juhlin C, 2008. Geology Laxemar. Site descriptive modelling. SDM-Site Laxemar. SKB R-08-54, Svensk Kärnbränslehantering AB.

Appendix A

A.1 Importance of overburden stress on pore pressures

During a glacial period, the glacially induced vertical stress changes significantly with time and cannot be ignored. As the transfer of pore pressures can often be assumed to be mostly in the vertical direction /Neuzil 2003/, a 1D analysis will give an indication of the importance of the boundary load term. A qualitative inspection of Figure 6-2 (top) shows that the pressure gradient in the vertical direction is about 15–20 times greater than the horizontal pressure gradient.

Assuming that the density and hydraulic conductivity, k, are constant and that there are no significant changes in elevation with time /Neuzil 2003/, Eq. 4-1 can be rewritten as

$$\nabla^2 P + \zeta \frac{S_S}{k}\frac{\partial \sigma_{zz}}{\partial t} - \frac{S_S}{k}\frac{\partial P}{\partial t} = 0 \text{ with} \qquad \text{A-1}$$

$$\zeta = \frac{\beta(1+\nu)}{3(1-\nu)-2\alpha\beta(1-2\nu)}\text{, where} \qquad \text{A-2}$$

$$\alpha = 1 - \frac{K}{K_S} \text{ and} \qquad \text{A-3}$$

$$\beta = \frac{\frac{1}{K}-\frac{1}{K_s}}{\left(\frac{1}{K}-\frac{1}{K_s}\right)+\left(\frac{n}{K_f}-\frac{n}{K_s}\right)} \qquad \text{A-4}$$

where ζ is the one-dimensional loading efficiency /Neuzil 2003/, α is Biot's coefficient, /Itasca 2005a/, β is the three-dimensional loading efficiency, also known as Skempton's coefficient /Neuzil 2003/, K is the drained bulk modulus, K_S is the bulk modulus of the solids, K_f is the bulk modulus of the pore fluid (water), and n is effective porosity.

Eq. A-1 can be solved analytically in one dimension (cf. Eq. A-5), where σ_{zz} is the glacially induced vertical stress and the boundary pressure is given by the function P_0, κ is hydraulic diffusivity ($\frac{k}{S_s}$)and ζ is the 1D loading efficiency. The boundary conditions are given in Figure A-1, where it is assumed that the boundary pressure is 90% of the height of the ice (or approximately 98% of the mechanical ice load), cf. Eq. A-6. Here, the ice sheet grows to reach its full height in 10,000 years, is stationary at constant height for 15,000 year and retreats back to zero height in about 1,300 years.

$$P(z,t) = \frac{2}{\sqrt{\pi}} \int_{z/\sqrt{4\kappa t}}^{\infty} \left(P_0\left(t - \frac{z^2}{4\kappa\eta^2}\right) - \zeta\sigma_{zz}\left(t - \frac{z^2}{4\kappa\eta^2}\right)\right)\exp\left(-\eta^2\right)d\eta + \zeta\sigma_{zz}(t) \qquad \text{A-5}$$

$$P(z,t) = \frac{2}{\sqrt{\pi}} \int_{z/\sqrt{4\kappa t}}^{\infty} (0.9/0.917 - \zeta)\sigma_{zz}\left(t - \frac{z^2}{4\kappa\eta^2}\right)\exp\left(-\eta^2\right)d\eta + \zeta\sigma_{zz}(t) \qquad \text{A-6}$$

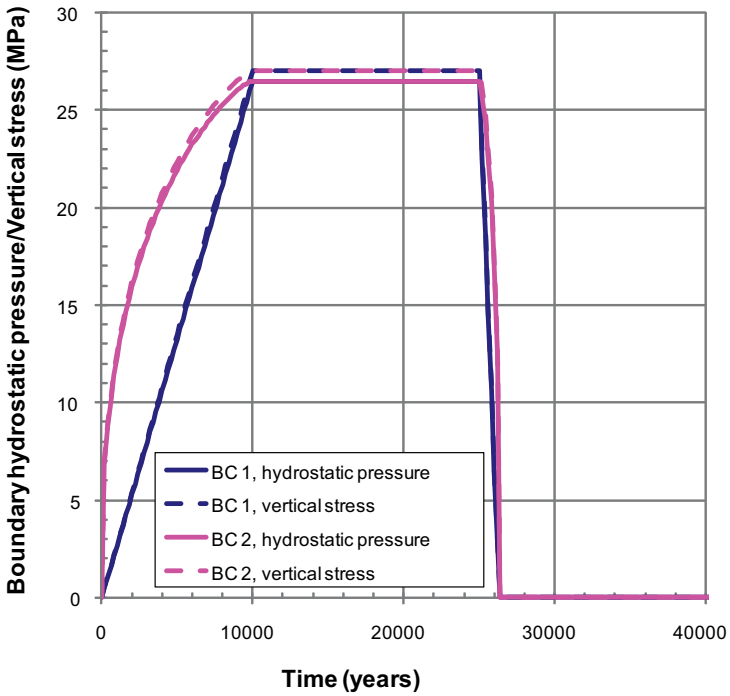

Figure A-1. *Hydrostatic pressure at the ice/bed interface and vertical stress.*

Figure A-2 shows the temporal development of the pore pressures at 500 m depth for two values of the 1D loading coefficient – $\zeta = 0$ and 1. For $\zeta = 0$, Eq. A-6 reduces to the 1D solution /Carslaw and Jaeger 1959/ to the linear diffusion equation (Eq. 4-2). Inserting site specific data for Forsmark /SKB 2008/ into equation A-4 gives a value of the one-dimensional loading coefficient, ζ, of around 0.4 (see above). As seen in the figure, the load term tends to increase the pressure during the advance of ice and reduces the pressure more quickly during the retreat of the ice sheet.

Figure A-3 shows the pore pressure distribution along vertical scan-lines after 15,000 years, 25,500 years and 26,333 years. Here, it is clearly illustrated that the boundary load term makes a noticeable contribution to the pore pressure distribution. However, at repository level (450–500 m), the difference in pore pressure is less than 1 MPa, a difference that decreases with increasing hydraulic diffusivity.

If the boundary load term is not taken into account ($\zeta = 0$), the pore pressure will be underestimated during the advance of the ice sheet. However, this problem can be overcome by assuming that the pore pressure distribution will have reached steady state before the start of the retreat. As the boundary load term tends to reduce the pore pressure more quickly during the retreat of the ice, there will not be any adverse effects on the results by ignoring this term. Instead it will result in more excessive estimates of maximum jacking depth as the pore pressures will be exaggerated.

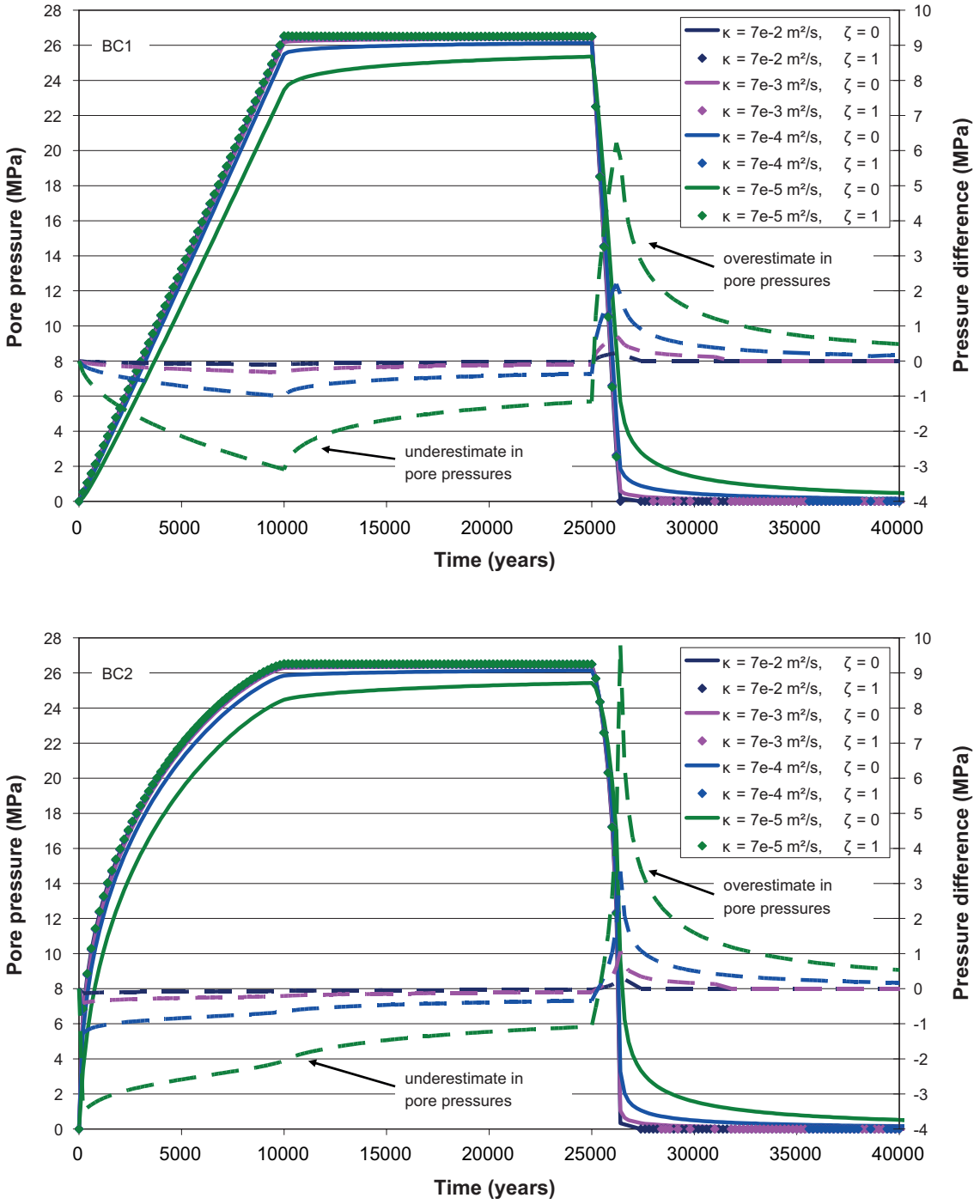

Figure A-2. *Temporal development of the pore pressures at 500 m depth for boundary conditions corresponding to Figure A-1. Solid lines and plot symbols represent pore pressures with ζ = 0 and ζ = 1, respectively. Dashed lines represent the difference between the pore pressure results.*

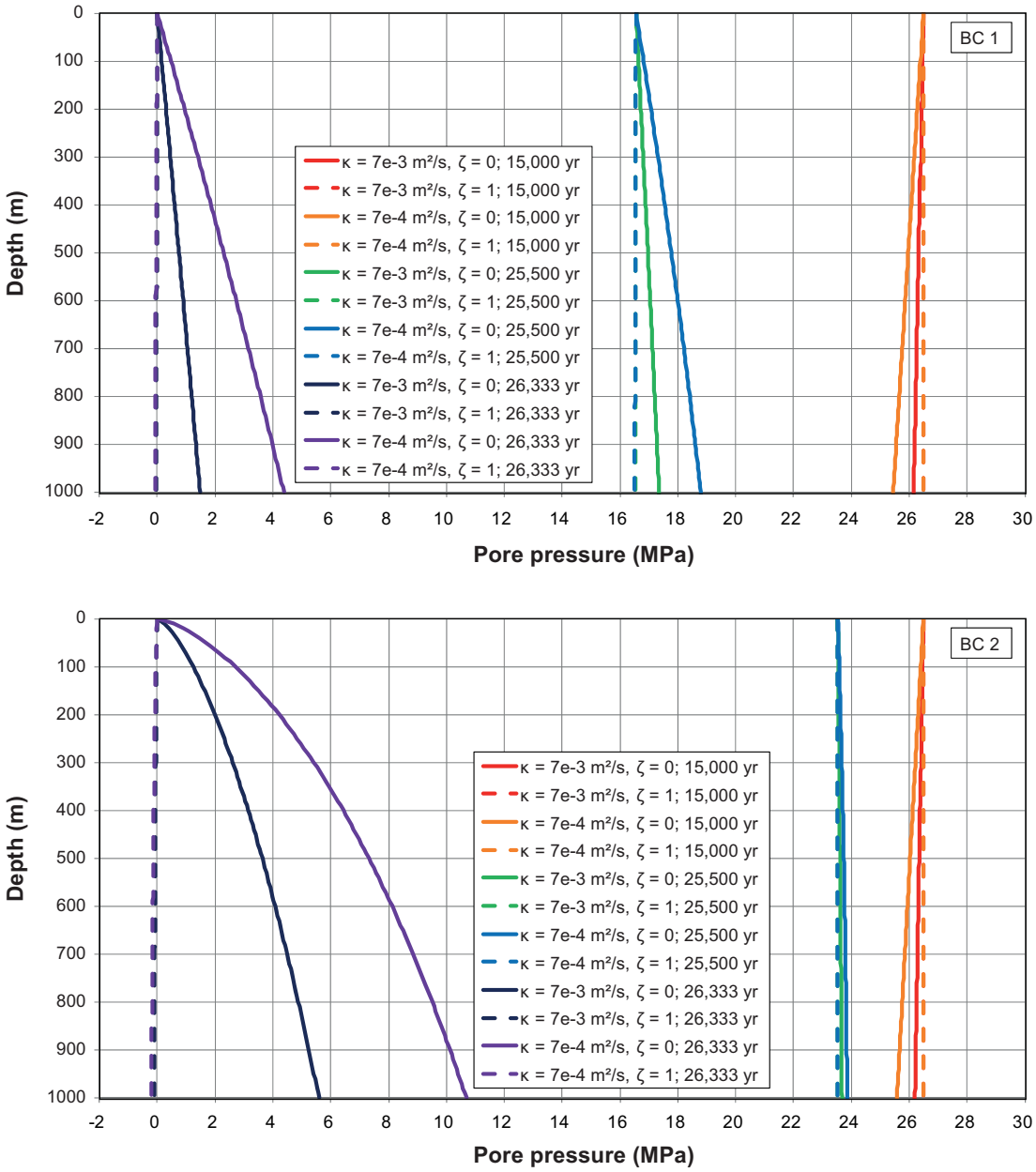

Figure A-3. *Pore pressure distribution along vertical scan-lines for the two different boundary conditions BC1 (top) and BC2 (bottom) presented in Figure A-1.*

A.2 Importance of mean normal stress on pore pressures

In the analyses presented in the previous section, it is assumed that the loading due to the ice sheet does not induce any lateral strain. However, as shown by /Lund et al. 2009/, the bending of the crust due to the ice load induces horizontal stresses that are of the same magnitude or greater than the vertical stress (see Figure 3-2). In the present section, the effects of non-zero lateral strain on the evolution of the glacially induced pore pressure are investigated.

For constant hydraulic conductivity and water density, an equation for pore fluid flow that accounts for non-zero lateral strain is given by /Neuzil 2003/ as

$$\nabla^2 P + \beta \frac{S_{S3}}{k}\frac{\partial \sigma_t}{\partial t} - \frac{S_{S3}}{k}\frac{\partial P}{\partial t} = 0, \qquad \text{A-7}$$

where β is Skempton's coefficient defined in Eq. A-4, S_{S3} is the three-dimensional specific storage coefficient and $\sigma_t = (\sigma_{xx}+\sigma_{yy}+\sigma_{zz})/3$ is the mean normal stress. The effects of a one-way hydro-

mechanical coupling can be found by examining solutions to Eq. A-7 using the mean normal stress calculated from the glacially induced stresses at 500 m depth at Forsmark presented by /Lund et al. 2009/, see Figure A-4. For a fully coupled analysis, Eq. A-7 and equations of stress (see e.g. /Neuzil 2003/) have to be solved in a coupled fashion.

By observing that $S_{S3} = S_S/(1-\lambda\cdot\beta)$ /Neuzil 2003/, the solution to Eq. A-7 in one dimension is given by the following expression (cf. also Eq. A-5),

$$P(z,t) = \frac{2}{\sqrt{\pi}} \int_{z/\sqrt{4(1-\lambda\cdot\beta)\kappa t}}^{\infty} \left(P_0\left(t - \frac{z^2}{4(1-\lambda\cdot\beta)\kappa\eta^2} \right) - \beta\sigma_t\left(t - \frac{z^2}{4(1-\lambda\cdot\beta)\kappa\eta^2} \right) \right) \exp\left(-\eta^2\right) d\eta + \beta\sigma_t(t), \quad \text{A-8}$$

where $P_0(t)$ is the hydrostatic pressure at the ground surface set to be about 98% of the glacially induced vertical stress (see Figure A-4) and $\lambda = 2\alpha(1-2\nu)/3(1-\nu)$. In the following analyses Poisson's ratio (ν) is set to 0.24 (see Table 5-1).

Skempton's coefficient (Eq. A-4) can be written in terms of α (= $1-K/K_S$) as

$$\beta = \frac{\alpha}{\alpha(1+n) + n\left(\frac{K}{K_f} - 1\right)}, \quad \text{A-9}$$

where $K = E/(3(1-2\nu))$, to yield an equation that does not explicitly depend on the bulk modulus of the solid (K_S). For a medium with very low porosity, β approaches 1 for all values of α (cf. Figure A-5, left). The one-dimensional loading efficiency (ζ) can also be written in terms of α by substituting β (Eq. A-9) in Eq. A-2. The relationship between β and ζ for values of α in the range 0 to 1 is shown in Figure A-5 (right).

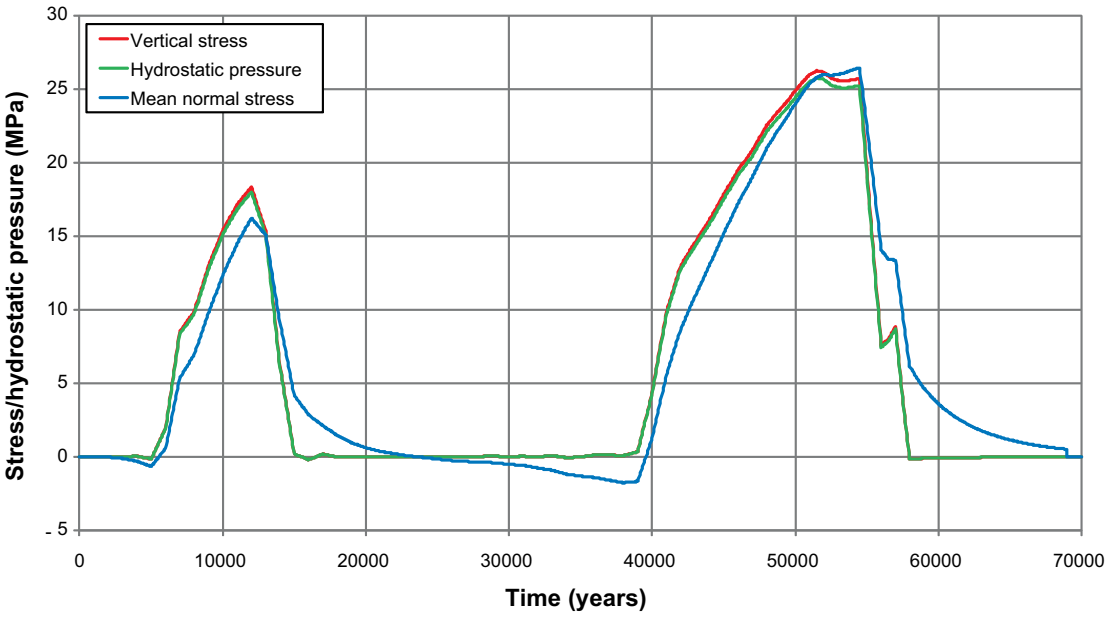

Figure A-4. *Input data to Eqs. A-5 and A-8 based on the reference glacially induced stresses (model T9) by /Lund et al. 2009/. The hydrostatic pressure at the ice/bed interface is assumed to be approximately 98% of the vertical stress.*

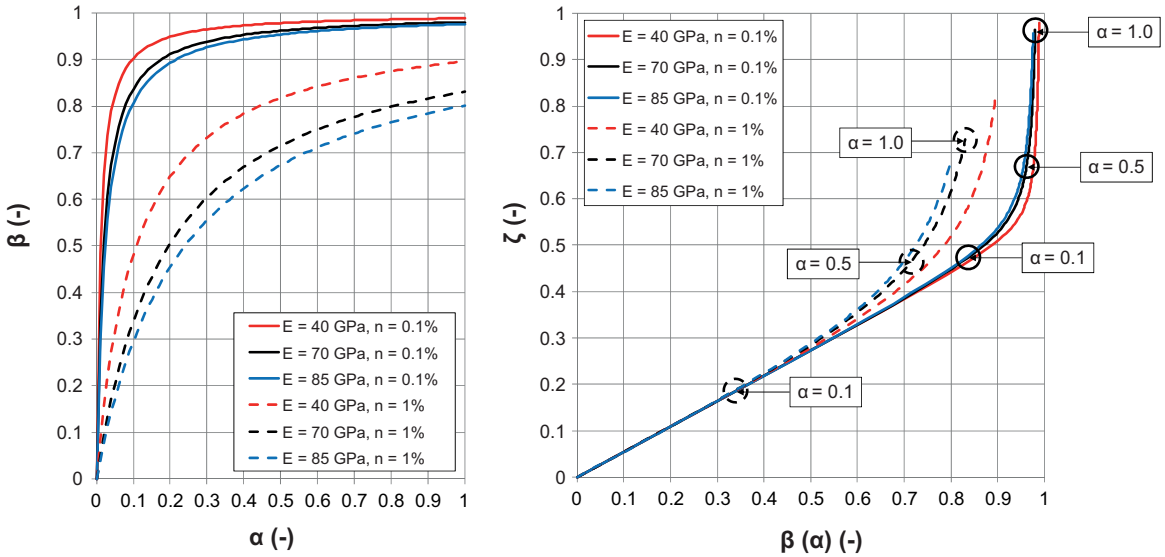

Figure A-5. *Left: Skempton's coefficient (β) as a function of α for values of Young's modulus in the range 40–85 GPa and porosity values in the range 0.1–1%. Right: Corresponding relationship between β and ζ for values of α in the range 0 to 1.*

Figure A-6 shows the temporal evolution of the pore pressures at 500 m and 5 km for three sets of values for the 3D (β) and 1D (ζ) loading efficiencies: $\beta = \zeta = 0$ (equivalent with mechanically uncoupled flow, cf. Eq. 8-2) and the loading efficiencies evaluated for $\alpha = 0.5$, $E = 70$ GPa and porosity either 0.1% ($\beta = 0.96$, $\zeta = 0.67$) or 1% ($\beta = 0.72$, $\zeta = 0.46$), see Figure A-5 (right). Figure A-7 shows the pore pressures as functions of depth as the ice front is advancing (45,000 years), retreating (55,500 years) and after the ice sheet has disappeared (61,000 years).

By comparing results from the three different ways of estimating the pore pressure, it is seen that expressions involving the load term or the mean normal stress tend to increase the pressure more quickly during the advance of ice and reduce the pressure more quickly during the retreat of the ice sheet than if these terms are ignored. For low values of the hydraulic diffusivity and at very large depths, the pore pressure is dominated by the terms $\zeta \cdot \sigma_{zz}$ or $\beta \cdot \sigma_t$ (see Figure A−7, bottom right). However, the potential for hydraulic jacking is greater at shallow depths.

For the purpose of obtaining bounding estimates of the glacially induced pore pressure and associated maximum jacking depth beneath a warm-based ice as the ice front is retreating, it appears that the impact of the flexural stresses induced in the reference glacial scenario /Lund et al. 2009/ can be ignored.

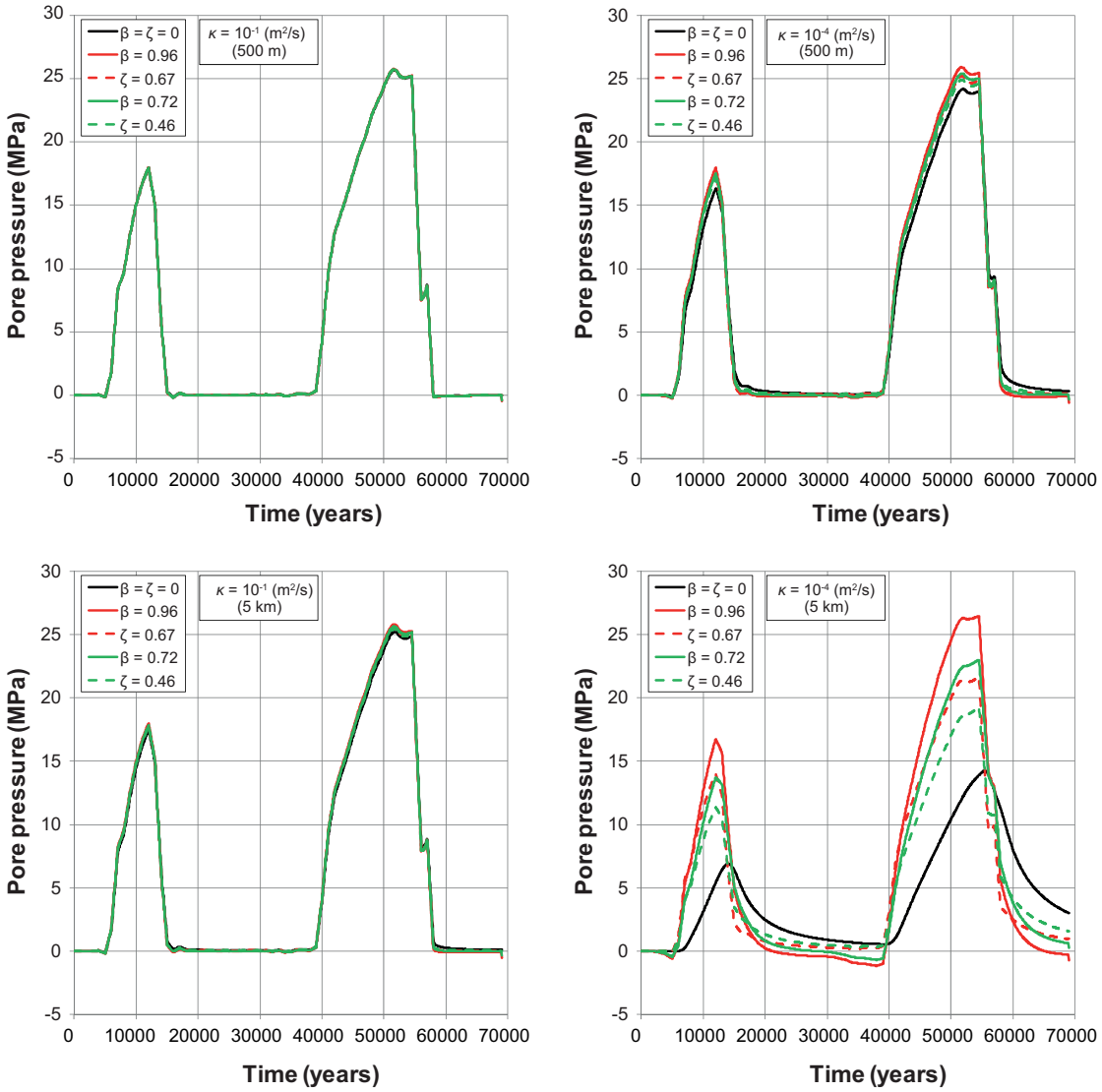

Figure A-6. *Temporal development of the pore pressures at 500 m (top) and 5 km (bottom) depth for different values of the hydraulic diffusivity – 10^{-1} m^2/s (left column) and 10^{-4} m^2/s (right column). $\beta = \zeta = 0$ represents the solution to the ordinary diffusion equation, $\beta = 0.96$ and $\zeta = 0.67$ are given by Eqs. A-8 and A-5, respectively, with loading efficiencies evaluated for $\alpha = 0.5$, $E = 70$ GPa and $n = 0.1\%$, $\beta = 0.72$ and $\zeta = 0.46$ are evaluated for $n = 1\%$.*

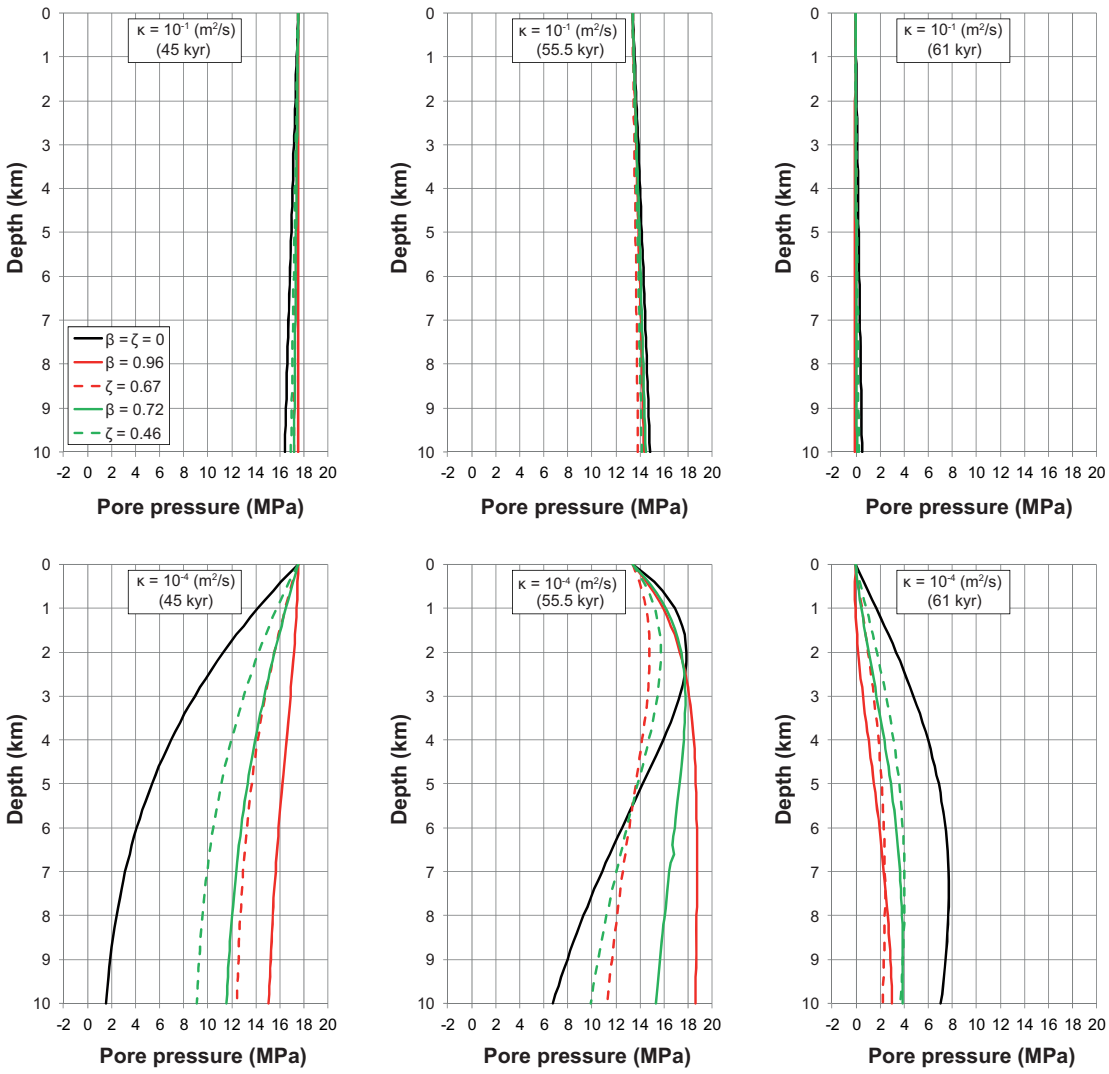

Figure A-7. *Pore pressure as functions of depth at given times for different values of the hydraulic diffusivity – 10^{-1} m²/s (top) and 10^{-4} m²/s (bottom). $\beta = \zeta = 0$ represents the solution to the ordinary diffusion equation, $\beta = 0.96$ and $\zeta = 0.67$ are given by Eqs. A-8 and A-5, respectively, with loading efficiencies evaluated for $\alpha = 0.5$, $E = 70$ GPa and $n = 0.1\%$, $\beta = 0.72$ and $\zeta = 0.46$ are evaluated for $n = 1\%$.*

Appendix B

B.1 Derivations and verifications of analytical expressions

B.1.1 Verification of expression for hydraulic diffusivity

An analytical solution for the pore pressure development in a semi-infinite solid with initial pore pressure P_0 and constant boundary pressure P_1 is given by /Carslaw and Jaeger 1959/:

$$P(x,t) = P_1 + (P_0 - P_1)\,\mathrm{erf}\left(\frac{x}{2\sqrt{\kappa \cdot t}}\right) \qquad \text{B-1}$$

A comparison between a numerical representation of the pore pressure distribution for a one-dimensional case and the analytical solution (Eq. B-1) was made using a fully coupled 1D Code_Bright hydro-mechanical model.

The Code_Bright model was represented as a horizontal slab with dimensions 1x200 m with properties as in Figure B-1. The initial pore pressure was set to 5 MPa and initial stresses were zero. All boundaries were impermeable and mechanically fixed in their normal directions with the exception of the sides at $x = 0$, which was kept constant at 15 MPa and $x = 200$ m and was mechanically free. Isothermal conditions at 20°C were kept throughout the calculation.

In the analytical solution, the hydraulic diffusivity is given by Eq. 4-3, the initial pore pressure, P_0, is 5 MPa and the boundary pressure, P_1, is 15 MPa.

Figure B-1 shows a comparison between the analytical and numerical solutions of the pore pressure at four points in time. It is clearly seen that the agreement between the two solutions is very good. It has thus been verified that the hydraulic diffusivity can be represented as in Eq. 4-3.

B.1.2 2D transient analyses

The solution (Eq. 4-8) to the diffusion equation in the half-plane $-\infty < x < \infty$ and $y > 0$, where the pore pressure distribution is initially zero and the plane at $y = 0$ is kept at a pressure given by the function $f(x, t)$ can be derived using standard techniques of Fourier and Laplace transformations. As the diffusion equation is linear, the principle of superposition applies and the solution where the pore pressure distribution is initially given by a steady state distribution (cf. Eq. 4-9), can be found by using a similar approach. This solution is found by examining functions of the form, see *e.g.* /Carslaw and Jaeger 1959/:

$$u(x, y, t) + v(x, y, t) \qquad \text{B-2}$$

where

- $u(x, y, t)$ is the pore pressure distribution in a solid with initially zero pressure and the plane $y = 0$ (ground surface) is kept at a pressure given by a function $f(x, t)$, cf. Eq.4-8.
- $v(x, y, t)$ is the pore pressure distribution in a solid where the pressure is initially given by the steady state pore pressure distribution, $P_{SS}(x, y)$, due to $f_0(x) = f(x, 0)$ and has zero pressure on the plane $y = 0$.

By introducing a third function, $w = v - P_{SS}$, then $w = 0$ at $t = 0$ and $w = -P_{SS}(x, 0) = -f_0(x)$ at $y = 0$. As P_{SS} is a solution to the diffusion equation, so is w. It is now obvious that w is a special case of Eq. 4-8, where $f(x, t) = f_0(x)$. Substituting for u and v in Eq. B-2 gives Eq. 4-9. Note an arbitrarily chosen initial pore pressure distribution will in general result in a more complicated expression.

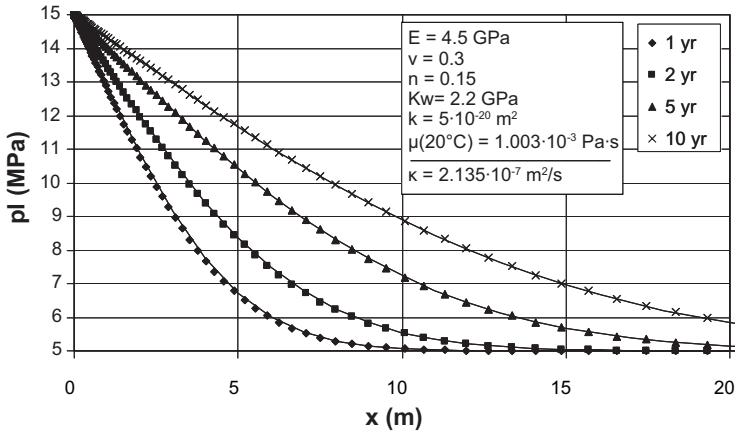

Figure B-1. *Liquid pressure as a function of the distance from the boundary. Lines and symbols represent analytical and numerical solutions, respectively. Note that here, k (m^2) represents the intrinsic permeability.*

The 2D analytical solution (Eq. 4-8) has been tested against the thermal logic in the numerical code *FLAC* /Itasca 2005a/.

In the *FLAC* model, the rock is represented by a rectangular solid 1,600 km wide and 40 km deep. The hydraulic diffusivity is set to $5 \cdot 10^{-4}$ m^2/s. In the code the hydraulic diffusivity, κ, is expressed in terms of thermal conductivity (representing hydraulic conductivity) and heat capacity (representing specific storage coefficient). The pore pressure, at the boundary representing the ground surface, is specified according to Figure 3-4 (left), where the ice is advancing at a speed of 40 m/year, stationary for 5,000 years at full height (3,000 m) and then retreats back to zero with a speed of 300 m/year. All other boundaries are adiabatic.

The temporal development of the pore pressures at 200, 400, 800, 1,200 and 2,000 m depth, given by *FLAC* and the analytical solutions, are compared in Figure B-2. As seen in the figure, the two solutions are in good agreement.

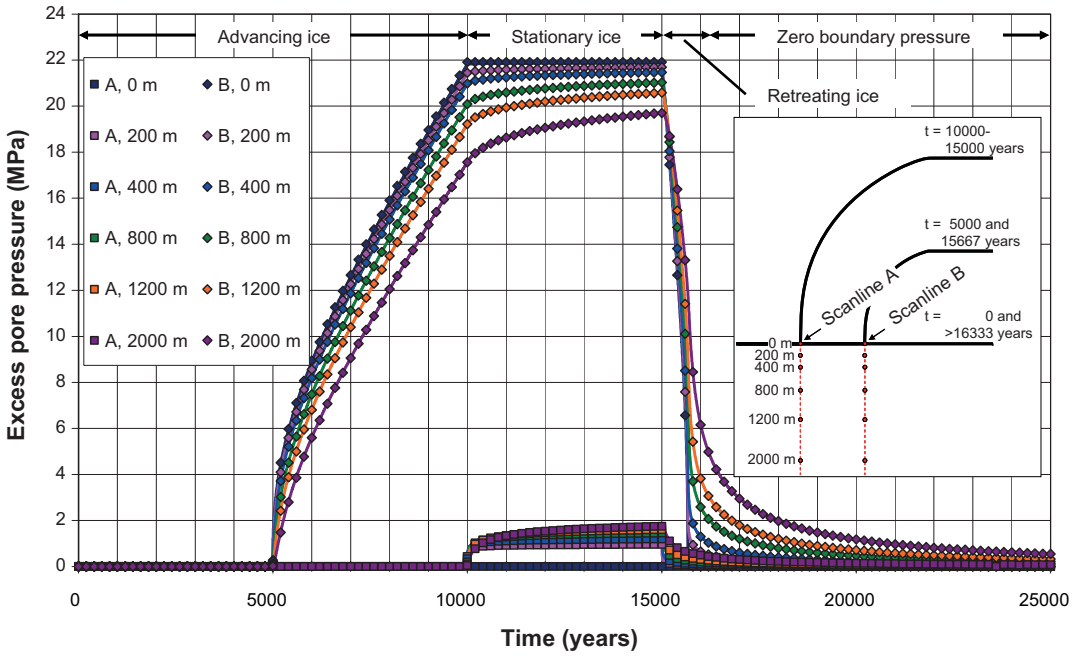

Figure B-2. *Comparison between the temporal development of numerically and analytically obtained excess pore pressures at two horizontal positions and different depths below the ground surface. Lines and symbols represent numerical (FLAC) and analytical solutions, respectively.*

Appendix C

C.1 Vertical stress assumptions

The changes in the vertical stress with time during a glacial period reflect the changes in ice sheet thickness /Lund et al. 2009/. In the modelling work conducted here, it is assumed that the glacially induced vertical stress is equal to the ice load at all depths. To illustrate that this is the case also at positions near the ice margin, Figure C-1 (left) shows numerically calculated vertical stresses due to the ice load (results from the *UDEC* modelling in Chapter 7 with the ice sheet profile shown in Figure 3-3, black curve) along horizontal scan-lines 100 m, 500 m and 1,000 m below the ground surface. The ice load at the boundary representing the ground surface (y = 0 m) is shown alongside the numerically calculated stresses for comparison. The glacially induced vertical stresses are uniformly distributed, but marginally higher than the ice load at positions below the ice front. Beneath the ice sheet, the glacially induced vertical stress is slightly less than the ice load, cf. Figure C-1 (right). However, the difference is small. This shows that setting the glacially induced vertical stress equal to the ice load at all depths is a valid approximation.

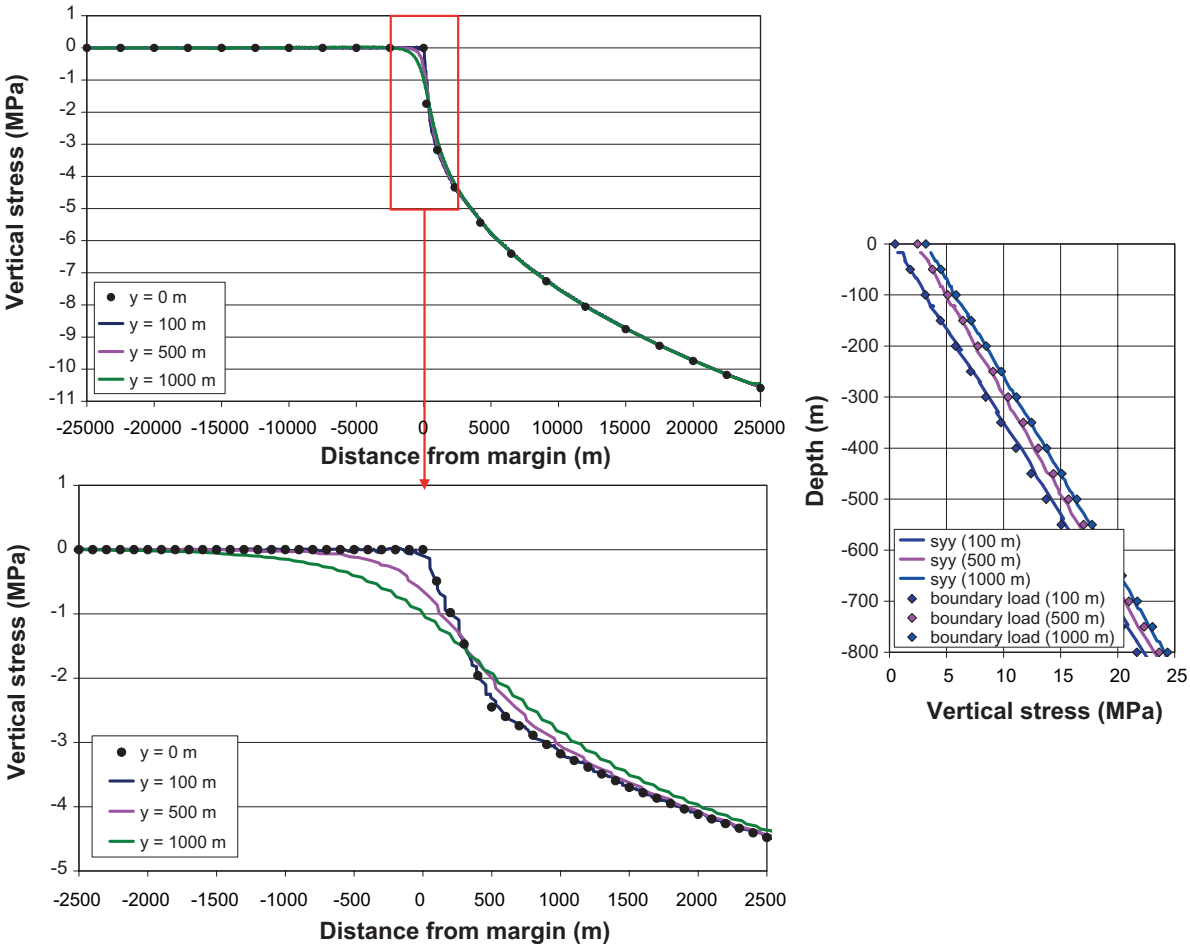

Figure C-1. *Numerically calculated vertical stress component due to the ice load at 100 m, 500 m and 1,000 m depth compared with the ice load applied at the boundary representing the ground surface (left). Vertical stress component due to the ice load at positions (horizontal distance) under the ice sheet compared with the ice load applied at the boundary at all depths added to the in situ vertical stress component (right).*

Appendix D

D.1 Effects of depth-dependent hydraulic conductivity

Inhomogeneous hydraulic properties cannot be handled by use of the analytical solutions described in Chapter 4. At the Forsmark site, typical bulk conductivity values at repository depth are in the range $5 \cdot 10^{-10}$–$1 \cdot 10^{-8}$ m/s, cf. Figure 5-3. In this conductivity range, the jacking depths are of the order of 50 m and seem to be practically independent of the retreat speed and duration of stationary ice, cf. Figure 6-3 to Figure 6-5. However, at larger depths the rock has a much lower hydraulic conductivity.

To illustrate the effects of variations in hydraulic conductivity with depth, the pore pressures are calculated using the finite difference code *FLAC* /Itasca 2005a/, cf. Section 4.4. In the models, the initial pore pressure is given by an approximated steady state distribution and the pressure on all boundaries is zero, cf. Figure D-1. Material properties (as input to the code) are given as diffusivities, where the values of the hydraulic conductivity are presented below and the specific storage coefficient is $1.5 \cdot 10^{-7}$ m^{-1}. Three cases are studied:

- Uniform hydraulic conductivity at all depths: $5 \cdot 10^{-9}$ m/s,
- Depth-dependent hydraulic conductivity: $5 \cdot 10^{-9}$ m/s (0–200 m), $5 \cdot 10^{-10}$ m/s (200–400 m) and $6 \cdot 10^{-11}$ m/s (below 400 m),
- Uniform hydraulic conductivity at all depths: $6 \cdot 10^{-11}$ m/s.

The resulting pore pressures are presented in Figure D-2 as functions of depth at four horizontal positions (0 m represents the position of the initial ice margin) under the ice 100 years after the disappearance of the ice. In the case with a variation in hydraulic conductivity, the pore pressures above 400 m are smaller than the in the case with uniform (constant high) hydraulic conductivity everywhere. The low permeability at larger depths will prevent a vertical transfer of pore pressures upwards and thus contribute to a more effective drainage of the upper part of the system. Below 400 m, the pore pressures will remain rather high due to the low hydraulic conductivity.

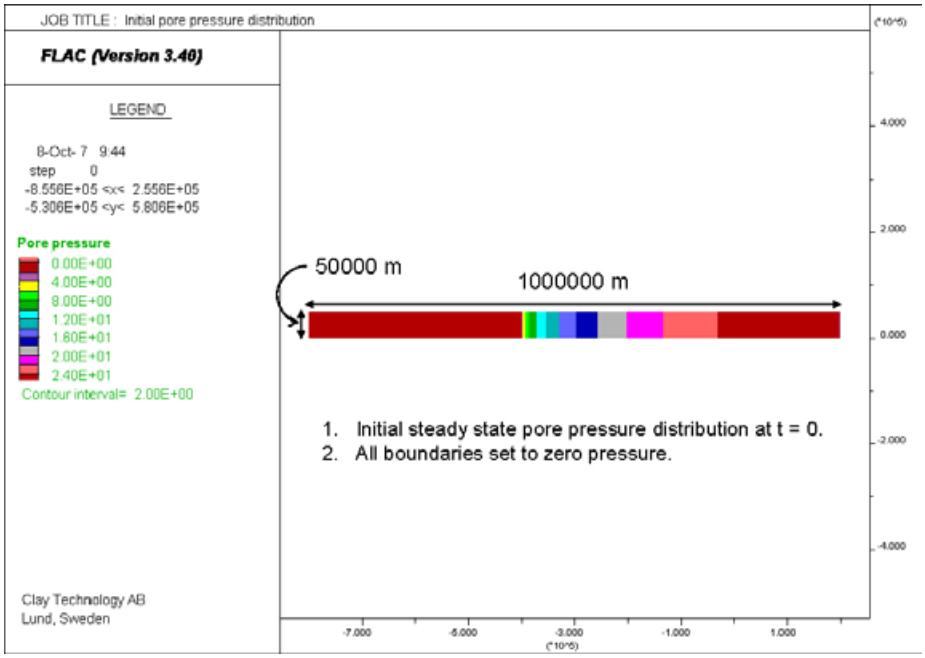

Figure D-1. *Numerical FLAC model geometry with initial pore pressure distribution and boundary conditions.*

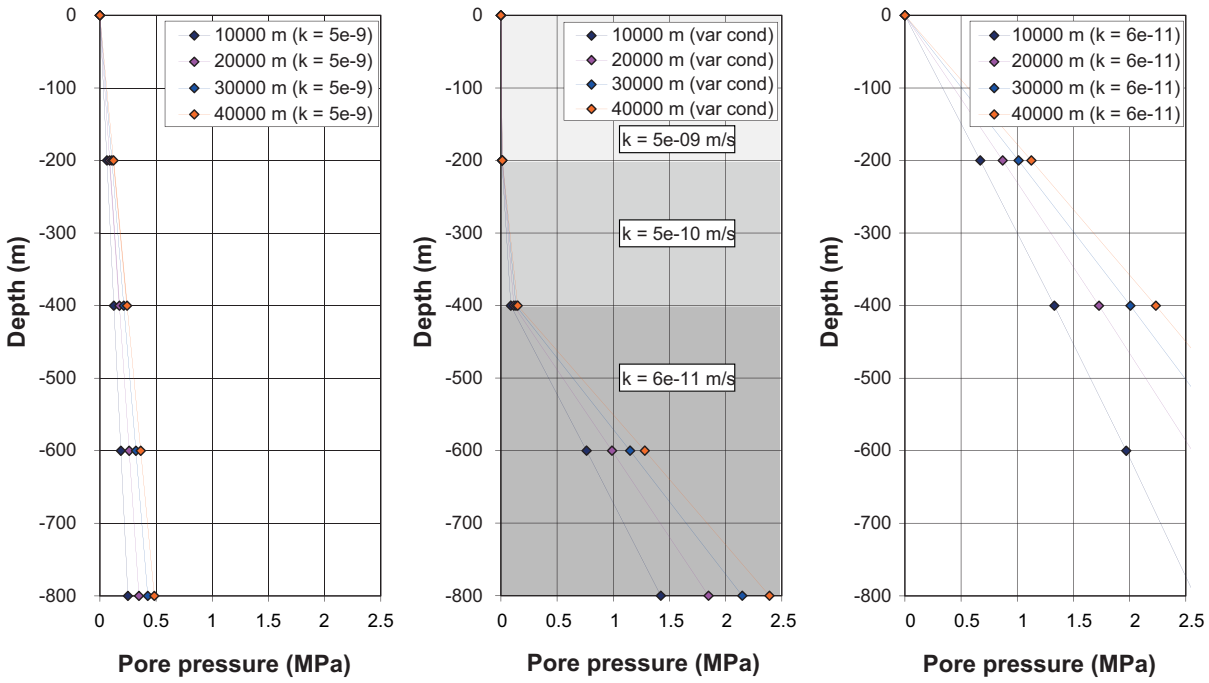

Figure D-2. *Resulting excess pore pressures at given horizontal positions after 100 years as functions of depth. The initial excess pore pressure distribution is given by an approximate steady state pressure distribution (same as the boundary pressure at all depths). At time t = 0, the pressure drops instantaneously to zero at the boundary (y = 0). Left: Uniform hydraulic conductivity corresponding to that of the upper part of the rock. Middle: Depth-dependent hydraulic conductivity. Right: Uniform hydraulic conductivity corresponding to that of the lower part of the rock.*

E.2 1D estimates of pore pressures during combined glacial and permafrost conditions

Permafrost can be considered to be a more or less impermeable layer /*e.g.* Vidstrand 2003/, which considerably reduces or prevents vertical and lateral flow of groundwater. If the permeability in the near-surface parts of the rock is considerably higher than below, the propagation of pore pressures in this layer can be approximated by a 1D expression. Although the 1D approach will overestimate the excess pore pressures (and corresponding maximum jacking depths) as in reality the flow will not be purely horizontal, it allows for the possibility to quickly determine the importance of certain combinations of parameters (*i.e.* diffusivity and permafrost melting rates) without having to rely on extensive and time consuming numerical work. The pressure at the permafrost melt zone (P_1, which depends on the distance from the ice margin) will completely dominate the maximum pressure beneath the permafrost and the pore pressure is given as a function of the lateral distance, x, from the melt zone by /Carslaw and Jaeger 1959/, see Eq. E-1.

$$P(x,t) = P_1\left(1 - \mathrm{erf}\left(\frac{x}{2\sqrt{\kappa \cdot t}}\right)\right) \qquad \text{E-1}$$

Figure E-1 shows the excess pore pressure along a horizontal scan-line from the permafrost melt zone after 100 years, 1,000 years, 5,000 years and 10,000 years. The following conclusions can be drawn by studying the figure.

Case A (melting rate 0.03 m/a for the first 4,300 years, thereafter 2.5 m/a for 30 years): If the hydraulic diffusivity in the upper 400 m is at most $1.0 \cdot 10^{-2}$ m^2/s, the maximum jacking depth after 10,000 years is around 40 m. Increasing the diffusivity in the upper parts of the crust by one order of magnitude to $1.0 \cdot 10^{-1}$ m^2/s, the corresponding maximum jacking depth after 10,000 years is just over 600 m.

Case B (melting rate 1 m/a): The maximum jacking depth after 10,000 years is around 400 m if the hydraulic diffusivity in the upper parts of the crust is in the range $1.0 \cdot 10^{-2}$–$1.0 \cdot 10^{-1}$ m^2/s.

Case C (melting rate 0.025 m/a): If the hydraulic diffusivity in the upper 400 m is at most $1.0 \cdot 10^{-2}$ m^2/s, the pressure pulse will not reach the ice margin within 10,000 years and consequently jacking will not occur at any depth. Increasing the diffusivity in the upper parts of the crust by one order of magnitude to $1.0 \cdot 10^{-1}$ m^2/s, the corresponding maximum jacking depth after 10,000 years is just over 300 m.

It can be concluded that, provided that the hydraulic diffusivity in the upper part of the rock is at most $1.0 \cdot 10^{-2}$ m^2/s, hydraulic jacking below a depth of 40 m in Cases A and C can be completely ruled out. It should be noted that all the above estimated maximum jacking depths are overestimates because of the 1D representation. Additional factors that will tend to reduce the maximum jacking depth are open taliks or seasonal variations in hydrostatic pressure at the ice/bed interface, which are not accounted for here. Two-dimensional analyses of combined glacial and permafrost conditions are conducted in Chapter 8.

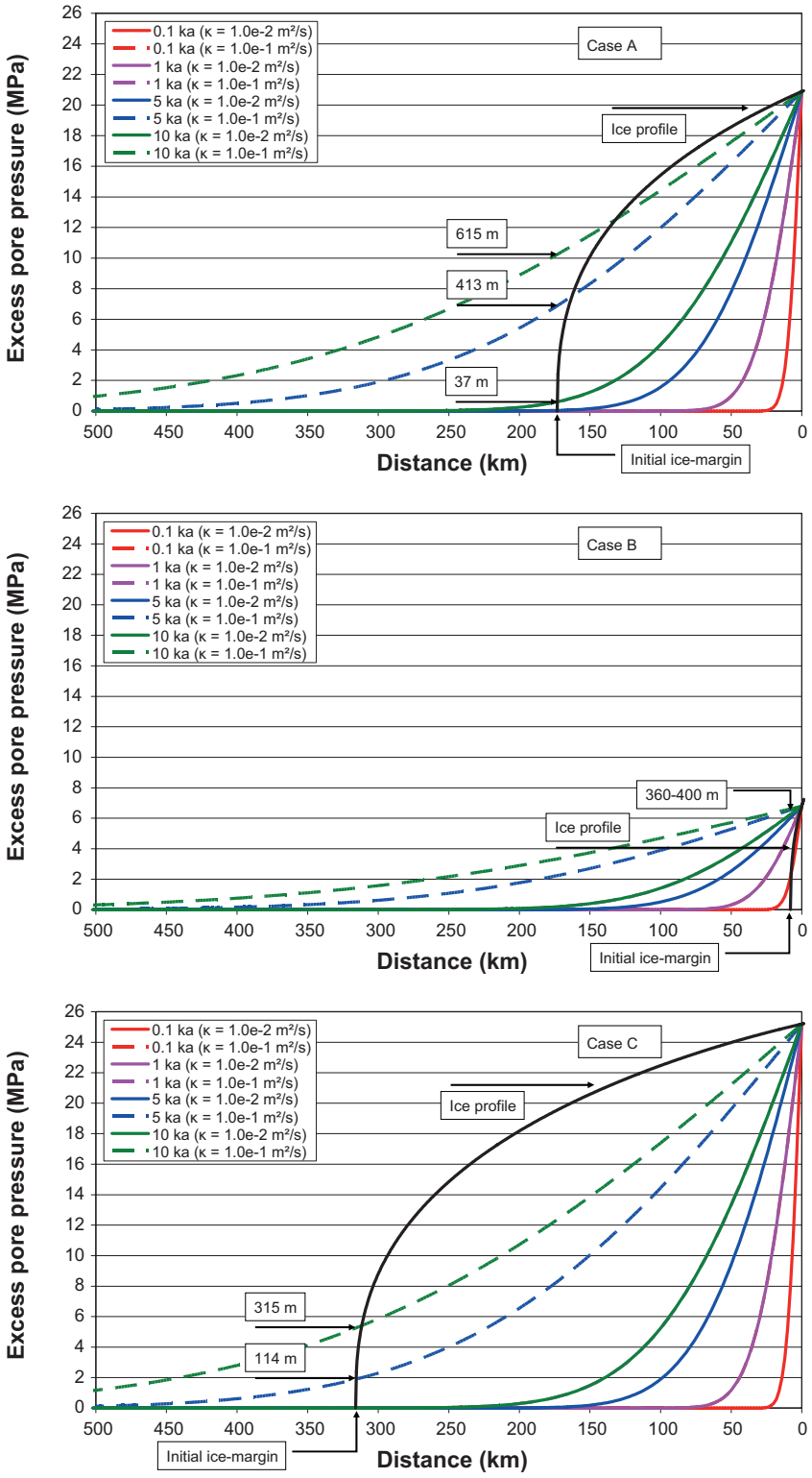

Figure E-1. *1D estimates of the excess pore pressure beneath the permafrost and corresponding maximum jacking depths as functions of the lateral distance from the permafrost melt zone. Note that the excess pore pressure and corresponding jacking depth are exaggerated compared with 2D analyses.*